Islamic University of Gaza

Deanery of Higher Studies

Faculty of Science

Department of Physics

Dye-sensitized Solar Cell Using Natural Dyes "DSSCs"

الخلايا الصبغية باستخدام الصبغات الطبيعية

By

Mahmoud B. M. Abuiriban

B.Sc. in Physics/Electronics, Alazhar University of Gaza

Supervisors

Dr. Sofyan A. Taya — **Associate professor of physics**

Dr. Taher M. El-Agez — **Associate professor of physics**

Submitted to the Faculty of Science as a Partial Fulfillment of the Master of Science (M. Sc.) in Physics

1435 - 2013

Dedication

To my father's soul, my mother, my wife, my children, my brothers, and my sisters.

To everyone, who works hard to develop our country "Palestine".

Mahmoud B. M. Abuiriban

Acknowledgments

In the name of Allah to whom whelmed me all power to continue my life with all challenges to arrive to this point. I would like to thank all those who helped me to complete this thesis, by advice and efforts.

I am indebted to my supervisors Dr. Sofyan A. Taya and Dr. Taher M. El-Agez for their support and help for performing and writing this work, and Hatem S. El-Ghamri, who explained to me the full image of experimental work. Also, I would like to express my thanks to Dr. Hassan S. Ashour who helped me a lot during my undergraduate study.

Abstract

In this thesis, many dye sensitized solar cells were fabricated using TiO_2 as a semiconducting layer and natural dyes as photosensitizers. Thin layers of nanocrystalline TiO_2 were prepared on transparent fluorine doped tin oxide (FTO) conductive glass. Doctor blade method was used in the coating process. Twenty seven natural dyes were tried such as Bougainvillea, Passion Fruit, Clove, Carob, Black tea, Green tea, Basil flower, Mint flower, Henna tree, onions Peel, Royal Poinciana, Schinus Terebinthifolius, Eggplant Peel, Eggplant pulp, and others. The absorption spectra of these dyes were performed. The I-V characteristic curves of all fabricated cells were measured, plotted, and analyzed at different incident light intensities. The parameters related to the solar cell performance were presented such as the maximum absorption peak (λ_{Max}), short circuit current (J_{SC}), open circuit voltage (V_{OC}),maximum power point (P_{Max}), fill factor (*FF*), and efficiency (η), where the absorption spectra of all dyes and the J-V characteristic curves of the fabricated cells were presented. The output power was calculated and plotted for each case. Also, short circuit current, open circuit voltage, maximum absorption wavelength, maximum power, fill factor, and power conversion efficiency were presented. Moreover, the impedance spectroscopy of the fabricated cells was investigated, more of the treatment on cells were studied, such as the effect of mordant, and using another semiconductor material with the three best dyes (fig leaves, schinus terebinthifolius leaves, and zizyphus leaves) and Ru complexcis-dicyano-bis(2,2'-bipyridyl-4,4'-dicarboxylic acid) ruthenium(II), Ruthenizer 505, (Solaronix, Switzerland).

The results revealed that the extract of plants leaves have the highest efficiency. The schinus terebinthifolius leaves is the best natural dye were used, has efficiency value of 0.78%, the mixture of $ZnAl_2O_4$ with TiO_2 can increases the efficiency of cells.

نبذة

في هذا البحث تم إعداد عدد من الخلايا الشمسية الصبغية باستخدام TiO_2 كطبقة شبه موصله وتم صبغها باستخدام سبعة وعشرون صبغة طبيعية. هذه الصبغات استخرجت من عينات من الطبيعة كأوراق الشجر والزهور واللحاء والجزر ومنها زهرة الجهنمية و زهرة النعناع و زهرة الريحان و أوراق شجر الزيتون والتين والسدر والعوسج و كذلك الشاي الأسود والأخضر وبعض العينات الأخرى , وتم قياس منطقة امتصاص الضوء لجميع الصبغات.

اعدت طبقة شبه الموصل على زجاج موصل للكهرباء FTO باستخدام Doctor blade method, وسخنت لدرجة حرارة 450 ومن ثم تركت لتبرد وبعد ذلك وضعت في الصبغة. وبعد إتمام عملية تجهيز الخلايا, تم قياس خصائص الخلايا: ومن أهم هذه الخصائص فرق جهد القطع وشدة تيار التوصيل السلكي و كذلك تم حساب القدرة والكفاءة لجميع هذه الخلايا عن ثلاث قوة ضوئية مختلفة. وتبين في نهاية الدراسة أن الصبغات المستخرجة من أوراق الشجر أفضل من الصبغات المستخرجة من باقي أجزاء الشجرة.

وتم أيضا دراسة استخدام محفذات الصبغ على صبغ الخلايا ولكنها لم تعطي نتائج أفضل من ناحية الخصائص ولكنها عملت على زيادة تثبيت الصبغات في الخلايا.

كذلك استخدم مادة شبه موصله أخري $ZnAl_2O_4$ مع TiO_2 بشكل خليط بين المادتين وقد أعطت نتائج أعلى مما أعطته باستخدام TiO_2 بمفرده.

List of Figures

Chapter One

Chapter Two

Chapter Three

Chapter Four

List of Tables

Chapter One

Chapter Three

Chapter Four

Contents

Chapter 1

Introduction

1.1 Energy Sources

Energy is the greatest challenge facing mankind in this century. Energy sources are classified into two types, nonrenewable and renewable sources. Nonrenewable sources such as fossil fuels (coal, petroleum, and natural gas) have been the energy sources for human society for a long time. Fossil fuel is being rapidly depleted by excessive exploration, and its burning has caused and is still causing damage to the earth environment. Alternative or renewable energy sources (Biomass, Geothermal, Hydropower, Solar, wind) are the other resources for human, and the best renewable energy source available to human is solar energy, but only a few of the accessible solar radiation is used. The average power density of solar radiation of the sun is 1200 W/m^2, generally it is known as the solar constant. The power of solar radiation reaching to the earth is

$$\text{Solar power} = 1200 \times 2\pi \times (6371 \times 10^3)^2 \cong 30.5 \times 10^{16} \text{ W.} \tag{1.1}$$

Provided that the radius of the earth is 6371 Km [1].

Each day has 86400 sec, and each year has 365 day, then yearly solar energy is

$$\text{yearly solar energy} = 30.5 \times 10^{16} \times 86400 \times 365 \cong 9.6 \times 10^{24} \ J \cong 9600000 \text{ EJ,} \tag{1.2}$$

where $EJ = 10^{18} \ J$

An image of how much energy that is, the yearly energy use of the entire world is about $500\,EJ$. Simply, 0.01% of the yearly solar energy reaching the earth can take place of the energy needed by the entire world. But not all solar radiation reaches the surface of the earth can be used, even if only 10% of total solar radiation is in working condition, then 0.1% of it is able to power the entire world [1].

It is interesting to match up the yearly solar energy that reaches the earth to the proved total store of fossil fuels; see Table 1.1. The numbers confirm that the total proved resources of fossil fuel is more or less 1.4% of the solar energy that reaches the surface of the earth each year. Fossil fuels are solar energy stored as concentrated biomass over many millions of years [1].

Table 1.1. Proved resources of various fossil fuels

Item	Quantity	Unit Energy	Energy (EJ)
Crude oil	1.65×10^{11} *tons*	4.2×10^{10} J/ton	6,930
Natural gas	1.81×10^{14} m^3	3.6×10^{7} J/m^3	6,500
High-quality coal	4.9×10^{11} *tons*	3.1×10^{10} J/ton	15,000
Low-quality coal	4.3×10^{11} *tons*	1.9×10^{10} J/ton	8,200
Total			36,600

If the current level of spending of fossil fuel continues, the internal fossil energy will be depleted in about 1000 years. At this time, the operation of renewable energy is still a small percentage of total energy use; see Table 1.2. The use of solar energy through photovoltaic technology only accounts for 0.07% of total energy spending. But, internationally, solar photovoltaic energy is the greatest growing energy source. Solar photovoltaic will soon become the main source of energy [1].

Table 1.2. Renewable energy resources

Type	Resource ($EJ/year$)	Implemented ($EJ/year$)	Percentage Explored
Solar	9,600,000	0.31	0.0012%
Wind	2,500	4.0	0.16%
Geothermal	1,000	1.2	0.10%
Hydro	52	9.3	18%

Like many countries, Palestine especially Gaza strip is facing an energy crisis that is close to rising into a full humanitarian crisis as the only power station was forced to shut

down due to the lack of fuel. Due to this international problem the research of the renewable energy sources must be carried out.

1.2 History of Solar Cells

In 1953, Bell Labs was started a research project for devices to provide energy source to remote parts of the world where no grid power was available [2]. Darryl Chapin suggested using solar cells. At that time, the photovoltaic effect in selenium, discovered in the 1870s, has already commercialized as a device for the measurement of light intensity in photography. Figure 1.1(a) is a diagram showing a selenium solar cell which consists of; a layer of Se applied on a copper substrate, and then covered by a semitransparent film of gold. When the device is exposed to visible light, a voltage is generated, which in turn generates a current. The generated current depends on the intensity of light. It has been a standard instrument in the first half of the twentieth century for photographers to measure light conditions. This device is much more strong and handy than photo resistors because there are no moving parts and no battery is necessary.

Chapin started with selenium photocells with efficiency of 0.5%, which is low to produce power for communication applications. Next, Calvin Fuller and Gerald Pearson joined Chapin in using the silicon technology for solar cells; a solar cell with 5.7% efficiency was invented [2].

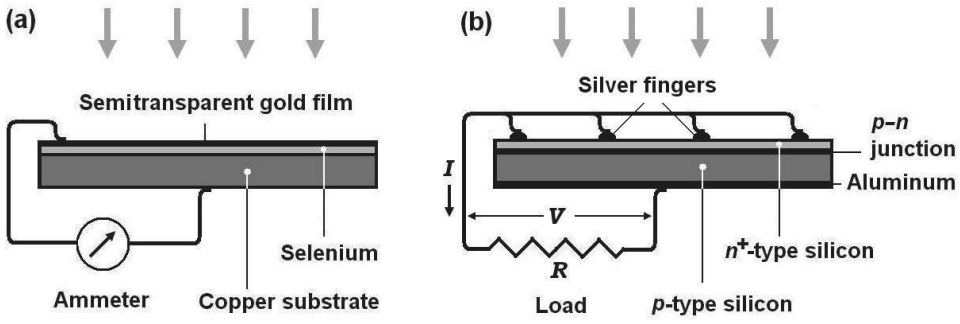

Fig. 1.1 Selenium solar cell (a) and silicon solar cell (b).

A schematic of silicon solar cell is shown in Figure 1.1(b). The silicon solar cell is made from a single crystal of silicon. By controlling the doping profile, a p–n junction is formed. The n-side of the junction is very thin and highly doped to allow light to come to the p–n junction with very little attenuation, but the lateral electric conduction is high enough to collect the current to the front contact through an array of silver fingers. The back side of the silicon is covered with a metal film, typically aluminum. The basic structure of the silicon solar cell has remained almost unchanged until now [2].

In 1958, the first attempt for using Photovoltage (PV) cell to power a satellite was carried out. By 1972, more or less than 1000 satellites were working by solar power. But PV cells were still too expensive for the use on the earth. In 1971, the cost of PV power was 200 times the cost of normal electricity. Researchers began to find ways to make cheaper PV cells. In 1973, the cost of oil became high. This gave scientists strong reason to try to find ways to improve PV cells. By the mid-1970s, PV cells were being used for power in remote places. They were used to give power to radio, satellite, telephone systems, and railway track warning lights. PV cells were also used at sea to give power to buoys, lighthouses, and fog horns [2].

For many years PV cells were expensive because they were made of thin films of pure silicon crystals, so new types of silicon were invented, such as thin ribbons and sheets of silicon. In 1976, scientists began to make silicon PV cells using silicon made from lots of small crystals joined together, called amorphous silicon. These types of PV cells are not as expensive as single silicon crystals, but they can create lower amounts of electricity. In the 1980s, PV cells were also being made from other materials apart from silicon, such as gallium arsenide, copper sulphide and cadmium sulphide, and in the 1990s, PV cells were built by using flexible plastic sheets [2].

Since 1996, many buildings have walls, windows and roofings covered with PV panels. As a new technology is developed, PV cells continue to become cheaper, more durable and better at generating electricity. In recent years new PV technology is now more efficient than ever at generating electricity from sunlight. Some super-thin PV cells are now over 30 times as efficient as the first selenium cells [2].

Dye-sensitized solar cell (DSSC) was proposed by O'Regan and Grätzel in 1991[3]. It is known as "Grätzel Cell". DSSC is classified as the third generation of photovoltaic devices for the conversion of visible light into electric energy [4]. In this cell the sensitization is formed by the dye absorption of part of the visible light spectrum. Light is absorbed in single layer of dye molecules that is adsorbed on a layer of titanium dioxide (TiO_2) particles that is spread on a conductive transparent glass. After light excitation, the dye molecule injects an electron into TiO_2 film. The electron is transported to the conductive glass where it is collected and transferred through a load. The positive charge is transferred from the dye to an electrolyte. Opposite of the TiO_2 film is the counter electrode, where the electrolyte is reduced into its original state by the electron collected at TiO_2 side of the cell.

1.3 Comparison between DSSC and Silicon Solar Cell

Current commercial solar electricity technology lies firmly on silicon based solar cells. The energy conversion in solar cells is based on charge separation. In silicon cells, an absorbed photon makes a free electron-hole pair, and the charge separation is calculated by an electric potential difference. To stay away from early recombination of these charges, the silicon must be of high purity. In addition of being expensive, silicon based cells require high illumination in order to be efficient.

DSSC has many advantages over silicon solar cell. It is cheaper, there is no need for clean room technology, and the cell can be operated under low light situations and under full sun light. The technology of DSSC is not yet mature and a lot of research is still needed [5].

The use of natural dyes extracted from trees, fruits, and vegetables as sensitizers for the conversion of solar energy into electricity is very interesting because they improve the economical aspect and make important profit by decreasing the pollution of environmental [6 – 8].

The early reviews in the field of DSSC described the device and the research challenges that must be continued in DSSC technology. These challenges are improving

efficiency, stability, and manufacturability. Efficiency improvements depend on the development of new combinations of dyes, electrolytes, and counter electrodes.

1.4 Terms and Concepts of Solar Cells.

1.4.1 Normal Light Setting

The efficiency and the output power of a solar cell are usually tested under the following standard test conditions (STC) means an irradiation of 1000 W/m^2 with air mass spectra (AM 1.5) at 25° C.

1.4.2 Some Parameters of a photovoltage cell

The open-circuit voltage V_{OC} is the voltage between the terminals of a solar cell under standard light conditions, when the current is zero. The short-circuit current I_{SC} is the current of a solar cell under standard light conditions, when the voltage across the load is zero. By using a resistive load R, the voltage V will be less than V_{OC}, and the current I is less than I_{SC}. The output power P=IV.

Figure 1.2 shows the relation among these parameters. The point of maximum power is characterized by I_{MP} and V_{MP}, where $P_{Max} = I_{MP}V_{MP}$.

The fill factor of a solar cell (FF) is defined

$$FF = \frac{P_{Max}}{I_{SC}V_{OC}} = \frac{I_{MP}V_{MP}}{I_{SC}V_{OC}}, \tag{1.3}$$

where, P_{Max} is the output maximum power, I_{MP} is the current of maximum output power, and V_{MP} is the voltage of maximum output power.

The classic value of the FF for silicon cells is between 0.8 and 0.9 [9], and for DSSCs is between 0.6 and 0.8.

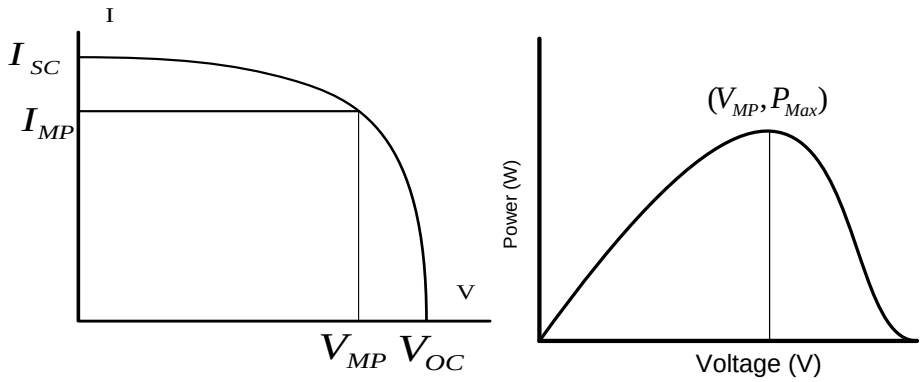

Fig. 1.2. Fill factor and maximum power point.

1.4.3 Efficiency

The efficiency (η) of a solar cell is defined as the ratio of the output power at the maximum power point over the input solar radiation under standard light conditions.

$$\eta = \frac{P_{out}}{P_{in}} \times 100\% . \tag{1.4}$$

where P_{out} is out put power, and P_{in} is incident light power.

1.5 State of the Art

Since Grätzel developed his first dye-sensitized solar cell in 1991, the field of DSSCs has attracted attention due to their advantages. By far, the highest efficiency of DSSCs sensitized by Ru-containing compounds reached 11–12%. On the other hand, organic dyes have been reported to reach efficiency as high as 9.8%. Natural dyes can be found in flowers, leaves, and fruits, and can be extracted by simple processes. As a result of their efficiency, non-toxicity, and complete biodegradation, natural dyes for DSSCs have been a popular subject of research. Several natural dyes have been used as sensitizers in DSSCs, such as cyanin [6-8, 10-19], carotene [20, 21], tannin [22], and chlorophyll [23]. Calogero and Marco obtained an efficiency of 0.66% using red Sicilian orange juice dye as sensitizer [7]. Wongcharee et al. used rosella as a sensitizer

in DSSC, which achieved a conversion efficiency of 0.70% [6]. Roy et al. used Rose Bengal dye as sensitizer, the J_{SC} and V_{OC} of their DSSC reached 3.22 mA/cm^2 and 0.89 V, respectively, and 2.09% efficiency [15], Wang et al. used the coumarin dye as a sensitizer in DSSC and the efficiency was 7.6% [24–27], Zhou et al. worked on twenty natural dyes and got a highest efficiency of 1.17%[28]. Another researchers in same university studied DSSCs were prepared using Zinc oxide (ZnO) as a semiconducting layer with eight natural and eight chemical dyes and got that the extract of safflower and Eosin Y corresponds to the highest efficiency [29], and other for DSSCs were prepared using TiO_2 as a semiconducting layer with twenty natural and eight chemical dyes, and got efficiency of 1.032% for Ziziphus jujuba for natural dye he used [30].

1.6 Aim of this Work

In this thesis, many dye sensitized solar cells were fabricated using TiO_2 as a semiconducting layer and dyed with natural dye. Thin layers of nanocrystalline TiO_2 will be prepared on transparent fluorine doped tin oxide (FTO) conductive glass of dimension $1cm \times 1cm$ with sheet resistance of $15\Omega/cm^2$ and transmission $\geq 80\%$ (Xingyan Tech. Ltd, Hong Kong). Doctor blade method was used in the coating process. Many natural dyes were used such as Bougainvillea, Passion Fruit, Clove grain, Carob fruit, Black tea, Green tea leaves, Basil flower, Mint flower, Henna leaves, onions Peel, Royal Poinciana, Schinus Terebinthifolius, Eggplant Peel, Eggplant pulp, and others. The absorption spectra of these dyes were performed. The I-V characteristic curves of all fabricated cells were measured, plotted, and analyzed at different incident light intensities. Many of the DSSC parameters such as I_{SC}, V_{OC}, P, λ_{Max}, η, and FF were calculated, and study their impedance spectroscopy.

Chapter 2

Dye-Sensitized Solar Cells

Dye sensitized solar cells (DSSCs) have received an increasing attention for the following advantages: low cost, simple manufacturing, and good response to low light density compared to the *p–n* junction devices [3, 24, 31, 32].

2.1 The Components of a Dye-Sensitized Solar Cell (DSSC)

A DSSC consists of sensitizing dye, semiconducting porous film (anode electrode), electrolyte and back electrode (cathode electrode) [31] as shown in figure 2.1. The efficiency of the charge injection process is highly dependent on the bonding structure of the dye adsorbed on the semiconductor. The electron transfer in a DSSC is powerfully influenced by electrostatic and chemical connections between semiconducting porous film surface and the adsorbed dye molecules [34, 35].

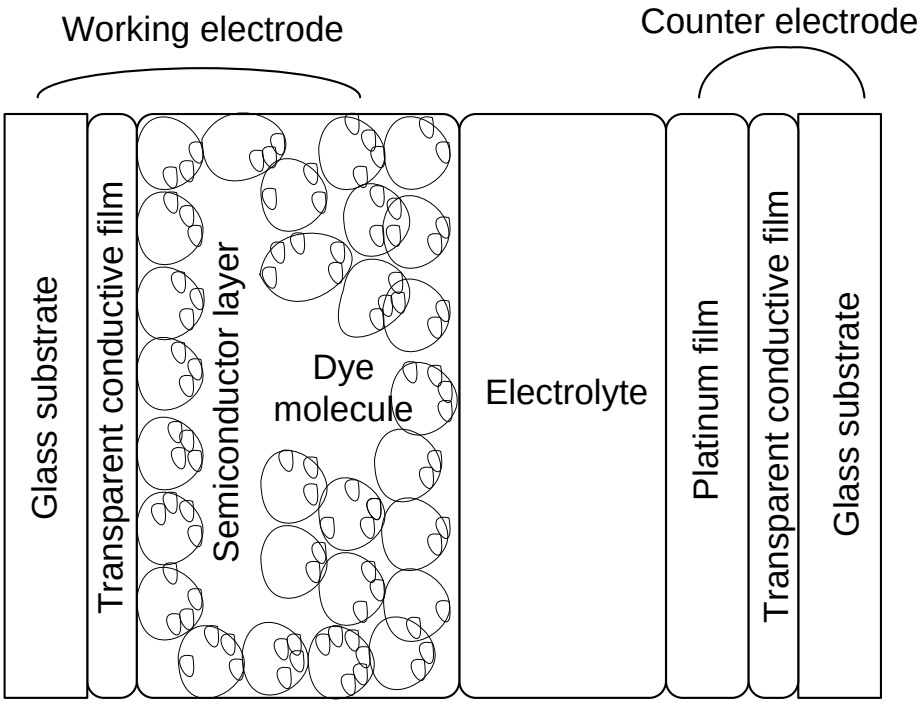

Fig. 2.1. A schematic diagram showing the components of DSSC.

2.1.1 Working Electrode

It is the region that creates electrons, and it consists of a transparent conductive film deposited on glass substrate, a semiconducting layer, and a dye.

2.1.1.1 Transparent Conductive Film

Transparent conducting films (TCFs) are optically transparent and electrically conductive thin layers. TCFs for photovoltaic applications are prepared from both inorganic and organic materials. Inorganic films usually contain layers of transparent conducting oxide (TCO), normally made of indium tin oxide (ITO), fluorine doped tin oxide (FTO), or doped zinc oxide. Organic films usually use carbon nano-tube network and graphene, which can be good transparent to the infrared light [36].

2.1.1.2 Semiconductor Layer

The necessary element of a DSSC is a semiconductor nanostructure material, like titanium dioxide nanoparticles which is known as titanium (IV) oxide or titania. It has the chemical formula TiO_2. When used as a pigment, it is called titanium white, or CI 77891. It is generally obtained in three forms ilmenite, rutile, and anatase. It is well connected to other materials. TiO_2 is a perfect material with its surface is greatly resistant to the continued electron transfer. The energy band gap of TiO_2 (≈ 3 eV) allows it to absorb the solar radiation in the UV region.

2.1.1.3 Dye Molecules

Molecular sensitizers (dye molecules) attached to the semiconductor surface are used to absorption the solar radiation. In general, the main dye molecule usually consists of one metal atom and a large organic structure that provides the required properties (wide absorption range, fast electron injection, and stability). The dye should be sensitive to the visible light which creates excitation in the dye yielding a highly energetic electron, which is rapidly, injected to the TiO_2 particles.

2.1.2 Electrolyte (redox)

The ionic liquid of iodide melts used in DSSCs is a major component because high concentrations of iodide are required to intercept quantitatively the recombination between the electrons injected by the photo-excited sensitizer in the nanocrystalline TiO_2 film and its oxidized form [37]. The viscosity of the iodide solution must be low enough to in order to keep away of mass transport.

2.1.3 Counter Electrode

Fluorine-doped tin oxide (FTO) coated glass substrate covered with a thin layer of platinum is widely used as the counter electrode because of its high catalytic activity with iodide/triiodide redox reaction [38]. On the other hand, its sheet resistance must be low enough to increase the efficiency of the DSSC.

2.2 Working Principle

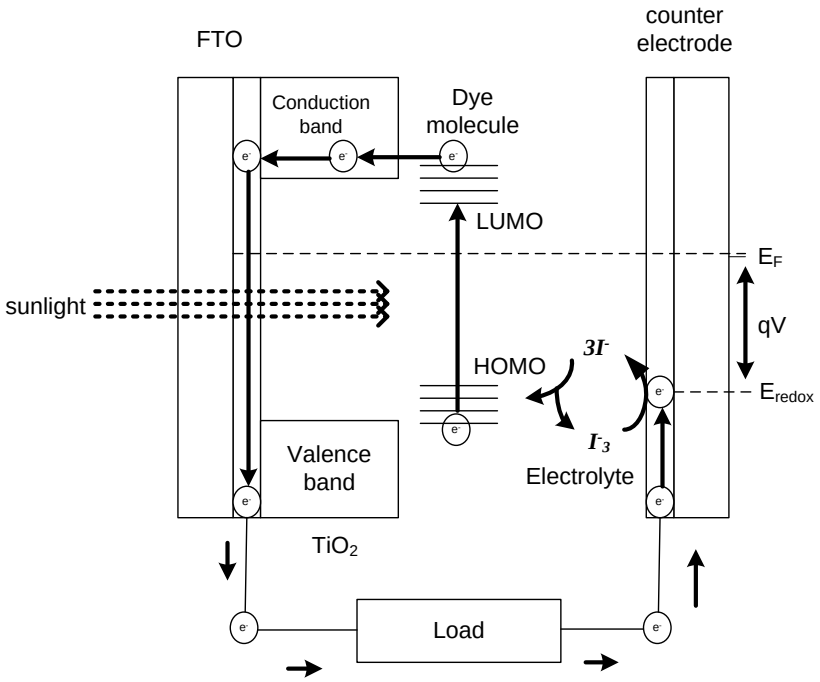

Fig. 2.2. The working principle of a dye-sensitized cell.

Figure 2.2 shows the energy digram and operating principle of a DSSC. A layer of nanostructure TiO_2 is deposited on FTO (photo-electrode) to provide the surface area where dye molecules get adsorbed on it. Upon absorption of sun light, dye molecules get excited from the highest occupied molecular orbital (HOMO) to the lowest unoccupied molecular orbital (LUMO) according to Eq.(2.1). When an electron arrives to the conduction band of TiO_2 film, the dye molecule (photo-sensitizer) becomes oxidized as show in Eq.(2.2). The electron is transported through the TiO_2 and gets to a load as shown in Eq.(2.3). To transport electrons from the photo-electrode to the counter electrode, the electrolyte containing I^-/I^-_3 redox ions are used to fill the cell. Finally, the oxidized dye molecules are regenerated by getting electrons from the I^- ion redox that will be oxidized to I^-_3 (Tri-iodide ions) according to Eq.(2.4). The I^-_3 with electron from the external load is regenerated to I^- ion according to Eq.(2.5). So, the generation of electric current in DSSC causes no permanent chemical change or transformation.

$$D + h\nu \rightarrow D^* \quad (2.1)$$

$$D^* + TiO_2 \rightarrow D^+ + e^-(TiO_2) \quad (2.2)$$

$$e^-(TiO_2) + Load \rightarrow TiO_2 + e^-(Load) + Current \quad (2.3)$$

$$2D^+ + 3I^- \rightarrow 2D + I^-_3 \quad (2.4)$$

$$2e^-(Load) + I^-_3 \rightarrow I^- \quad (2.5)$$

Theoretically, the maximum potential produced by the cell is determined by the energy difference between the electrolyte potential (E_{redox}) and the Fermi level of the TiO_2 (E_f). The small energy separation between the HOMO and LUMO of the dye facilitates absorption of low energy photons in the solar radiation. This is similar to inorganic semiconductors band gap energy E_g. Actually, effective electron injection into the conduction band of TiO_2 can be enhanced with the increase of energy difference of the dye LUMO and the TiO_2 conduction band [39].

2.3 The Cell Parameters

The improvement of solar cells is based on understanding the physical mechanisms which manage its operation. For a DSSC, the main parameters which affect

the device performance are: internal resistance, open circuit voltage, short circuit current, ideality factor, power, fill factor, and efficiency.

2.3.1 Internal Resistance

Three internal impedances have been found in DSSCs [40, 41], namely Z_1, Z_2 and Z_3. Z_1 is related to charge transport at the Pt counter electrode in the high frequency (KHz range) region. Z_2 is the impedance of a diode [39] observed in middle frequency (10-100 Hz) region at TiO_2 / dye/ electrolyte interface. Impedance Z_3 due to Nernstian diffusion is prominent in low frequency (m Hz) region [40].

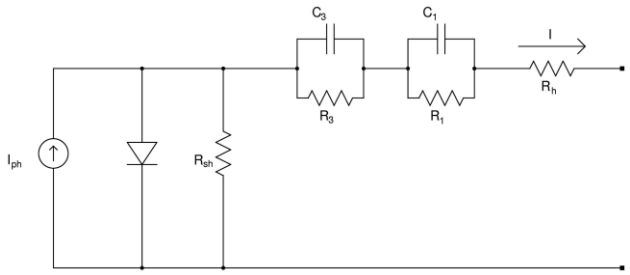

Fig.2.3. Equivalent circuit of actual dye sensitized solar cell (DSSC).

Hence it can be concluded that the actual DSSC model consists of series, shunt resistive and capacitive parts as shown in figure 2.3. Z_1 is the parallel combination of R_1 and C_1, and Z_3 is the parallel combination of R_3 and C_3 as shown in figure 2.3. The real part of Z_1 is related to charge –transfer process occurring at the Pt counter electrode denoted by R_1 and the imaginary part C_1 is the capacitance of Helmholtz double layer at the electrodes. Similarly R_2, the real part of Z_2, corresponds to diode like behavior in the DSSC. Resistance R_3 of Z_3 is proportional to the distance between FTO and Pt counter electrode and is related to diffusion of iodide and trioxide within the electrolyte. If we neglect the effect of capacitance, the series resistance R_s can be written as

$$R_s = R_h + R_1 + R_3, \tag{2.6}$$

where R_h is the sheet resistance of FTO glass substrate.

The shunt resistance R_{sh} is attributed to slow back electron transfer rate from TiO_2 to electrolyte in TiO_2 / dye/ electrolyte interface. Dynamic resistances R_{s0} and R_{sh0} are tangential values at current and voltage axes of I-V curves of cell. These values have been used by several people for determining solar cell parameters [42]. Mathematically they are evaluated as:

$$R_{S0} = (\partial V / \partial I)_{V=V_{OC}} \tag{2.7}$$

$$R_{Sh0} = (\partial V / \partial I)_{I=I_{SC}} \tag{2.8}$$

Usually, RS0 and RSh0 are obtained from the I-V curve by simple linear fit.

2.3.2 Open Circuit Voltage

A logical study of open circuit voltage (V_{OC}) rules the possible power from the device which is the maximum voltage that a device can create. V_{OC} depends on many factors for example temperature, light intensity, electrode thickness and ideality factor that tells us about the physical method of the device operation.

Dependence of V_{OC} on light intensity is an important phenomenon. The light intensity increases charge generation and the temperature increases, it increases the diffusion of charges, and so charge mobility increases, this increases V_{OC} [43,44]. The V_{OC} not only depends on temperature and light intensity but also on electrode thickness. The thickness dependence can be explained by electron intensity effect. As the thickness of electrode increases, the light transmittance decreases, absorption of light decreases, this causes decrease in charge density and V_{OC} [45], such that

$$V_{OC} \propto \frac{K_B T}{q} \ln(\lambda), \tag{2.9}$$

where q is the elementary charge, K_B is the Boltezman constant, T is the temperature, λ is the wavelength of light.

2.3.3 Short Circuit Current

Short circuit current (I_{SC}) is another important parameter in determining the efficiency of any solar cell. Different ways can be conducted to develop the I_{SC}: one way is to develop a dye which can absorb light of longer wavelengths. For Si solar cell, I_{SC} increases with increasing temperature, but it does not in DSSC type [46-48].

Another factor affecting I_{SC} is the thickness of electrode. As the thickness of electrode increases I_{SC} first increases, then it reaches a peak value, then itstarts decreasing. This is due to the fact that thicker electrode can absorb more photons and hence higher I_{SC}, after attaining thickness greater than penetration depth, photons will not be able to generate electrons leading to saturation in I_{SC}. Then due to the increase in recombination, the number of electrons decreases and hence I_{SC} decreases [45]. The optimal thickness is found 12~15μm in case of TiO_2 semiconducting layer.

2.3.4 Ideality Factor

The ideality factor (n) (also called the emissivity factor) is a measure of how closely the diode follows the ideal diode equation, there are second order effects so that the diode does not follow the ideal diode equation and the ideality factor provides a way of describing them. The ideal diode equation assumes that all the recombination occurs via band to band or recombination via traps in the bulk areas from the device (i.e. not in the junction). However recombination does occur in other ways and in other areas of the device. These recombinations produce ideality factors that deviate from the ideal.

Most solar cells, which are somewhat large compared to conventional diodes, well approximate an infinite plane and will usually be near-ideal behavior under standard test condition ($n \approx 1$). Under certain operating conditions, however, the device operation may be subject to recombination in the space-charge region. This is

characterized by a significant increase in ideality factor to n ≈ 2. The latter tends to increase solar cell output voltage while the former takes action to decay it. The net effect, therefore, is a combination of the increase in voltage shown for increasing n [49].

The ideality factor can be defined in the DSSC as the actions similar to that predicted by theory, which assumes the p-n junction of the diode is an infinite plane and no recombination takes place within the space-charge region. A perfect match to theory is achieved when n = 1. When recombination in the space-charge region dominate other recombination, however, n = 2. The effect of changing ideality factor is independently of all other parameters.

2.3.5 Power Density

The output power of a DSSC is given by

$$P = I\ V, \tag{2.10}$$

where I and V are the direct current and the voltage values at output terminals. The output power of a DSSC increases with the increase in value of voltage and current, reaches a maximum value at best value of voltage /current and then starts to decreas, reaches zero value at open circuit voltage/short circuit current density. The maximum power point can be obtained by determining the maximum of output power (P_{Max}) where P_{Max} is equal to [41, 47]

$$P_{Max} = I_{MP} V_{MP}, \tag{2.11}$$

where, P_{Max} is the output maximum power, I_{MP} is the current of maximum output power, V_{MP} is the voltage of maximum output power.

2.3.6 Fill Factor

Fill Factor (*FF*) which is a measurement of the quadratic nature of I-V characteristic curve is another crucial parameter of DSSCs. Typically *FF* for a DSSC varies from 0.6 to 0.8 and decreases with increasing light intensity [42]. It is given by

$$FF = \frac{P_{Max}}{I_{SC}V_{OC}} = \frac{I_{MP}V_{MP}}{I_{SC}V_{OC}} \tag{2.12}$$

2.3.7 Efficiency

Efficiency is the most important parameter used to characterize any type of solar cells. Expressing the ratio between the output electrical power and the input optical power as a percentage, gives what is known as the solar conversion efficiency. Electrical power is the product of current and voltage, so the maximum values for these measurements are important as well, J_{SC} and V_{OC} respectively. The conversion efficiency is given by

$$\eta = \frac{P_{out}(electrical)}{P_{in}} \times 100\% = \frac{P_{\max}(electrical)}{incident\ \ light\ \ power} \times 100\% \tag{2.13}$$

The incident photon-to-current conversion efficiency (IPCE) of DSSC, which is a measure of the quantum efficiency. The IPCE is used to compare the chance that one photon (of a solar power) will create one electron [50] , it is given by

$$\text{IPCE} = \frac{hcJ_{SC}}{e\lambda P_{in}}, \tag{2.14}$$

where λ, e, h and c are the incident wavelength, elementary charge, Planck constant and speed of light, respectively, J_{SC} is the short circuit current density.

2.4 Electrochemical Impedance Spectroscopy (EIS)

Impedance Spectroscopy (sometimes called Dielectric Spectroscopy), also known as Electrochemical Impedance Spectroscopy (EIS), measure the dielectric properties of a medium as a function of frequency. It depends on the interaction between the external fields with the electric dipole moment of the cell. EIS is a method to measure the system impedance on a range of frequencies, and thus shows the frequency response of the system, including energy storage and dissipation properties. Impedance is the opposition to the flow of alternating current (AC) in a complex

system. The system consists of dissipative power (resistor) and energy storage (capacitor) elements. If the system is purely resistive, then opposition to AC or direct current (DC) is simply resistance. In many cases, the data obtained by the EIS are expressed graphically in a Nyquist plot or a Bode plot. On the Nyquist Plot, the impedance can be represented as a vector of length |Z|. The angle between this vector and the X-axis is commonly called the "phase angle", and a Bode plot determines the phase angle as a function of frequency.

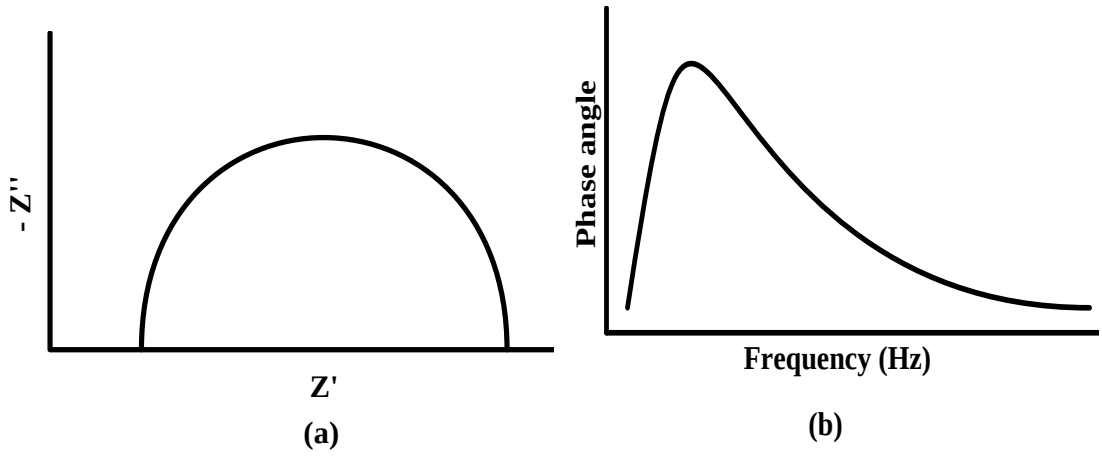

Fig.2.4. Electrochemical Impedance spectroscopy (EIS) output (a) Nyquist plot. (b) Bode plot.

Almost, any system of physical and chemical properties, such as electrochemical cells, has the energy storage and dissipation properties. EIS can examine these systems. This technique has grown significantly over the past few years, and is now being employed extensively in a wide variety of scientific fields, such as testing fuel cells, biomolecular interactions, and characterization of microstructures [51].

2.5 Mordants

A mordant is a substance used to set dyes on fabrics or tissue sections by forming a coordination complex with the dye which then attached to the fabric or tissue. It can be used for dyeing DSSCs, or for intensifying stains in the cell. Mordant term comes from the present participle of French mordre, "to bite." In the past, it was thought a mordant helped the dye on the fiber so that hold during washing. A mordant often have polyvalent metal ions. Coordination compound resulting from the dye and ion is colloidal and can be either acidic or alkaline. Mordants include tannic acid, alum, urine,

chrome alum, sodium chloride, and certain salts of aluminium, chromium, copper, iron, iodine, potassium, sodium, and tin. The three methods used for mordanting:

- Pre-mordanting (onchrome): First the mordant and then the dye.
- Meta-mordanting (metachrome): The mordant with the dye.
- Post-mordanting (afterchrome): First the dye and then the mordant.

The type of mordant used changes the shade obtained after dyeing and also affects the fastness property of the dye. The application of mordant, either pre-, meta- or post-mordant methods, is influenced by:

- The action of the mordant on the substrate: if the mordant and dye methods are harsh (e.g. an acidic mordant with an acidic dye), pre- or post- mordanting limits the potential for damage to the substrate.
- The stability of the mordant and/or dye lake: the formation of a stable dye lake means that the mordant can be added in the dye without risk of losing the dye properties (meta-mordanting).

Dye results can also rely on the mordant chosen as the introduction of the mordant into the dye will have a marked effect on the final color. Each dye can have different reactions to each mordant [52].

Chapter 3

Experimental Work

3.1 Collecting Dyes

In this work, only natural dyes will be used because they are available, cheap, and easy to collect. Twenty seven natural dyes have been collected, 5 dyes are taken from plant flowers (Bougainvillea, Mint flower, Basil flower, Royal Poinciana, and Lycium shawii flower), 8 dyes are taken from plant leaves (Black tea, Green tea, Henna, Olive leaves, Fig leaves, Schinus terebinthifolius, Lycium shawii leaves, and Zizyphus leaves), 3 dyes are extracted from plant bark (Olive bark, Lycium shawii bark, and Zizyphus bark), 3 dyes are extracted from plant root (Olive root, Lycium shawii root, and Zizyphus root), 3 dyes are taken from plant peel (Passion peel, Onion peel, and Eggplant peel), and 5 dyes are extracted from other natural sources (Carob fruit, Clove grain, Eggplant pulp, Olive grain, and Fig leave with the ratio 1: 7Olive leaves by weight). Each dyes is given a code as listed in table 3.1 which shows the Latin and Arabic names of the dyes as well as their codes.

Table 3.1. Latin and Arabic names of chosen dyes

Code	Sample		Code	Sample		Code	Sample	
ND1	جهنمية	Bougainvillea	ND10	تمرحنه	Henna leaves	ND19	ورق العوسج	Lycium shawii leaves
ND2	زهر نعناع	Mint flower	ND11	قشر البسفلورا	Passion peel	ND20	ورق السدر	Zizyphus leaves
ND3	زهر ريحان	Basil flower	ND12	قشر البصل	Onion peel	ND21	لحاء الزيتون	Olive bark
ND4	زهر الظل	Royal poinciana	ND13	قشر الباذنجان	Eggplant peel	ND22	لحاء العوسج	Lycium shawii bark
ND5	زهر العوسج	Lycium shawii flower	ND14	لب الباذنجان	Eggplant pulp	ND23	لحاء السدر	Zizyphus bark
ND6	شاي اسود	Black tea leaves	ND15	حب الزيتون	Olive grain	ND24	جذر الزيتون	Olive root
ND7	شاي اخضر	Green tea leaves	ND16	ورق الزيتون	Olive leaves	ND25	جذر العوسج	Lycium shawii root
ND8	خروب	Carob fruit	ND17	ورق التين	Fig leaves	ND26	جذر السدر	Zizyphus root
ND9	قرنفل	Clove grain	ND18	ورق الظل	Schinus terebinthifolius	ND27	ورق تين1 : 7ورق زيتون	Fig 1: Olive7

3.2 Extracting the Dye

The natural materials were washed with distilled water and left to dry at room temperature for at lest 3 days. After drying and crushing into fine powder using a mixer, they were immersed in ethanol at room temperature in the darkness for 24 hrs. to extract the dyes. We have used $5\,mL$ of alcohol and $200\,mg$ of the sample [29]. The extracts were filtered out to remove the remaining solids of the powder.

The absorption spectra of all extracts have been carried out using a UV-VIS spectrophotometer (Thermoline Genesys 6) in the spectral range from $400\,nm$ to $750\,nm$.

3.3 Preparation of TiO_2 Paste and DSSC Assembly

FTO conductive glass sheet from Xingyan Tech. Ltd, Hong Kong were first cleaned in a detergent solution using an ultrasonic bath for 9 min, rinsed with water and ethanol, and then dried. TiO_2 paste was prepared by adding 50mg of TiO_2 nanopowder to 100mg of polyethylene glycol then grinding the mixture for half an hour until a homogeneous paste was obtained. The paste was deposited on the FTO conductive glass sheet by doctor-blade method in order to obtain a TiO_2 layer of 0.25 cm^2 area using standard scotch tape. The TiO_2 layer was sintered at 450 °C for 40 min [29]. After cooling down to 60 °C, the thickness was measured using Olypus Polarizing Microscope BX53-P with DP73 camera, and found to be $22 \pm 1\,\mu m$. The samples were then immersed in the natural dye extracts for 24 h at 60 °C [6].

The cells are then assembled by fixing the working electrode and the counter electrode by paper clips with a spacer between the electrodes as shown in fig 3.1. The redox electrolyte solution is filled between the sensitized TiO_2 film and the counter electrode composed of a conductive glass sheet plated with platinum (Pt) layer. The electrolyte solution is composed of $2\,mL$ acetonitrile (ACN), $8\,mL$ propylene carbonate (p-carbonate), $0.668\,mg$ potassium iodide (KI), and $0.0634\,mg$ iodine (I_2**)**. The cell is now ready to use, and its charactaristics can be studied.

Fig.3.1. Steps of the DSSC assembly.

3.4 The J-V Characteristic Curves.

The J-V characteristic curves were conducted under simulated sunlight using National Instruments data acquisition card (USB NI 6251) in combination of a Labview program. A computer program OriginPro 7.5 was used to draw the curves. The J-V measurements have been conducted under the illumination of three intensities; 800 W/m^2 , 1000 W/m^2 , and 1200 W/m^2 , which determined by lightmeter (TES 1333 solar power meter, Taiwan).

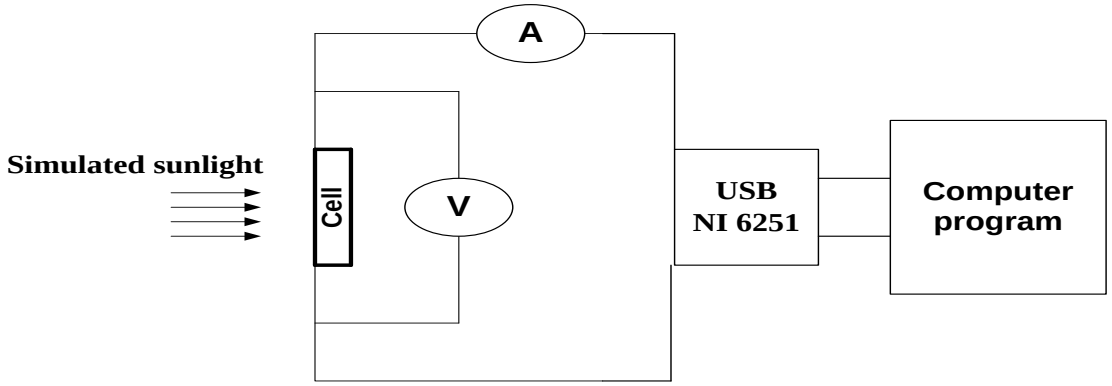

Fig.3.2. Schematic experimental diagram for J-V measurment.

3.5 Electrochemical Impedance Spectroscopy

Impedance spectroscopy was conducted to investigate the electronic and ionic processes. A theoretical model was developed to explain the frequency response of the device. If the measurements are made in the dark, the method is called electrochemical impedance spectroscopy (EIS). If the cell is illuminated during impedance measurements, the method is called photoelectrochemical impedance spectroscopy (PEIS) [5]. Electrochemical Impedance spectroscopy were done by using a Potentiostat-galvanostat Autolab PGSTAT-30N with FRA32M module. Impedance measurements where performed at frequencies between 0 and 100 KHz with an ac signal of 0.6 V amplitude at room light and without temperature add.

An equivalent circuit has been derived from the rate of electron transfer and lifetime of the electron in the film, which are consistent with the values derived from the transient photocurrent and photovoltage measurements [53].

3.6 Mordants

In this work, ferrous sulphate ($FeSO_4.7H_2O$) and copper sulphate ($CuSO_4.5H_2O$) are used as mordants. First a solution of 0.1M of each mordant is prepared by mixing 1.39g of $FeSO_4.7H_2O$ and 0.1mL of H_2SO_4 with 50mL of distilled water, and mixing 2.48g of $CuSO_4.5H_2O$ and 0.1mL of H_2SO_4 with 50mL of distilled water. The use of mordants will be restricted to DSSCs that exhibit the best performance i.e. DSSCs dyed with fig leaves (ND17), schinus terebinthifolius (ND18), and zizyphus leaves (ND20). Pre-mordanting with $CuSO_4.5H_2O$ and $FeSO_4.7H_2O$ is first examined, next, post-mordanting. Then, meta-mordanting with $CuSO_4.5H_2O$ is examined.

3.7 Gahnite

In this work, the use of Gahnite ($ZnAl_2O_4$) as an alternative to TiO_2 will be studied, $ZnAl_2O_4$ has a higher band gap (3.9 eV) than that of TiO_2 (3.2 eV). It belongs

to the spinel group, and it is formed of octahedral crystals, that may be green, blue, yellow, brown or gray. It was named by the Swedish chemist, Johan Gottlieb Gahn, the discoverer of the element manganese. It is sometimes called spinel zinc [54]. The band gap of $ZnAl_2O_4$, calculated using density functional theory is 4.25 eV but the experimental value is 3.8–3.9 eV [55].

DSSCs fabricated by use $ZnAl_2O_4$ as a semiconducting layer were not study, because the $ZnAl_2O_4$ was not stable on FTO. Thus, a mixture of TiO_2 and $ZnAl_2O_4$ is investigated to prepare the paste.

Chapter 4

Results and Discussion

The cell parameters of interest are wavelength at the maximum absorption peak (λ_{Max}), short circuit current (J_{SC}), open circuit voltage (V_{OC}),maximum power point (P_{Max}), fill factor (*FF*), and efficiency (η). In this chapter, the absorption spectra of all dyes and the J-V characteristic curves of the fabricated cells were presented. The output power was calculated and plotted for each case. Also, short circuit current, open circuit voltage, maximum absorption wavelength, maximum power, fill factor, and power conversion efficiency were presented.

4.1 Absorption Spectra of the Dyes

The absorption peak can be explained by the chemical structure and color of the dye. Physically, it can be explained by the difference between energy levels of the materials. Generally, all dyes may be used in DSSCs, but we need to find the appropriate dyes that give a high efficiency when used in DSSCs. These dyes can classified in groups as: flowers (ND1, ND2, ND3, ND4, ND5), peels (ND11, ND12, ND13), leaves two groups (ND6, ND7, ND10, ND17, ND18) and (ND16, ND19, ND20), barks (ND21, ND22, ND23), roots (ND24, ND25, ND26), and others (ND8, ND9, ND14, ND15, ND27). The spectra of all dyes are plotted in Fig. 4.1 through Fig. 4.7. The following observations have been found:

Figure 4.1 shows the absorption spectra for the extracts of Bougainvillea flower (ND1), Mint flower (ND2), Basil flower (ND3), Royal Poinciana flower (ND4), and Lycium shawii flower (ND5). The figure reveals that: the extract of Bougainvillea flower has absorption peak at 666 nm, the absorption spectra of the extract of Mint flower has peak at 664 nm, the extract of Basil flower exhibits an absorption peak at 664 nm, the absorption spectra of the extract of Royal Poinciana flower has absorption peak at 448 nm, and absorption peak for the extract of Lycium shawii flower at 662 nm. The absorption spectra of the extracts of Passion peel (ND11), Onion peel (ND12), and Eggplant peel (ND13) can be seen in figure 4.2. The figure also shows that: the extracts

of Passion peel has an absorption peak at 666 nm, also shows no absorption peaks at this region for the extract of Onion peel, and absorption peaks at 416 nm and 664 nm for the extract of Eggplant peel. Figure 4.3 illustrates the absorption spectra for the extracts of Black tea leaves (ND6), Green tea leaves (ND7), Henna leaves (ND10), Fig leaves (ND17), and Schinus terebinthifolius leaves (ND18). The figure reveals that: the extract of Black tea leaves has an absorption peak of 666 nm, the extract of Green tea leaves has absorption peaks at 410 nm and 666 nm, absorption peaks at 410 nm and 666 nm for the extract of Henna leaves, also shows that there are absorption peaks at 432 nm and 666 nm for the extract of Fig leaves, and absorption peaks at 414 nm and 666 nm for the extract of Schinus terebinthifolius leaves. The absorption spectra for the extracts of Olive leaves (ND16), Lycium shawii leaves (ND19), and Zizyphus leaves (ND20) can be seen at figure 4.4. It is clear that: the extract of Olive leaves has absorption peaks at 432 nm and 664 nm, there are absorption peaks at 412 nm and 664 nm for the extract of Lycium shawii leaves, and for the extract of Zizyphus leaves, there are absorption peaks at 416 nm and 662 nm. Figure 4.5 shows the absorption spectra for the extracts of Olive bark (ND21), Lycium shawii bark (ND22), Zizyphus bark (ND23). The figure shows that: an absorption peak at 662 nm for the extract of Olive bark, the extract of Lycium shawii bark has peaks at 434 nm and 662 nm, and the extract of Zizyphus bark has an absorption peak at 662 nm. Figure 4.6 illustrates the absorption spectra of the extracts of Olive root (ND24), Lycium shawii root (ND25), and Zizyphus root (ND26). The figure reveals that: the extract of Olive root has absorption peak at 636 nm, there is an absorption peak at 662 nm for the extract of Lycium shawii root, and an absorption peak at 664 nm for the extract of Zizyphus root. The absorption spectra of the extracts of Carob (ND8), Clove (ND9), Eggplant pulp (ND14), Olive grain (ND15), and the mixture Fig leaves 1: Olive leaves 7 by weight (ND27) can be shown in figure 4.7. The figure illustrates that: there is an absorption peak at 662 nm for the extract of Carob, an absorption peak at 666 nm for the extract of Clove, absorption peak of 668 nm for the extract of Eggplant pulp, the extract of Olive grain has an absorption peak at 666 nm, and for the extract of the mixture Fig leaves 1: Olive leaves 7 by weight, there are absorption peaks at 432 nm and 664 nm.

Apparently their light absorption is different. This differences in the absorption characteristics can be attributed to the different types of pigment and colors of the extracts. Pigment obtained from leaves is chlorophyll and it is green, while that extracted from flowers is a kind of anthocyanin. Anthocyanin shows the color in the range of visible light from red to blue, it is prospected to become a high efficient sensitizer for wide bandgap semiconductors.

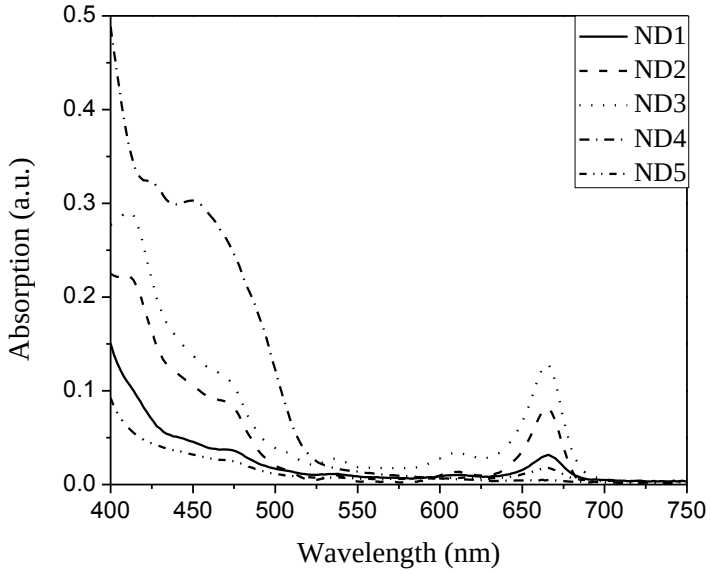

Fig.4.1. The absorption spectrum of ND1, ND2, ND3, ND4, and ND5 using ethanol as a solvent.

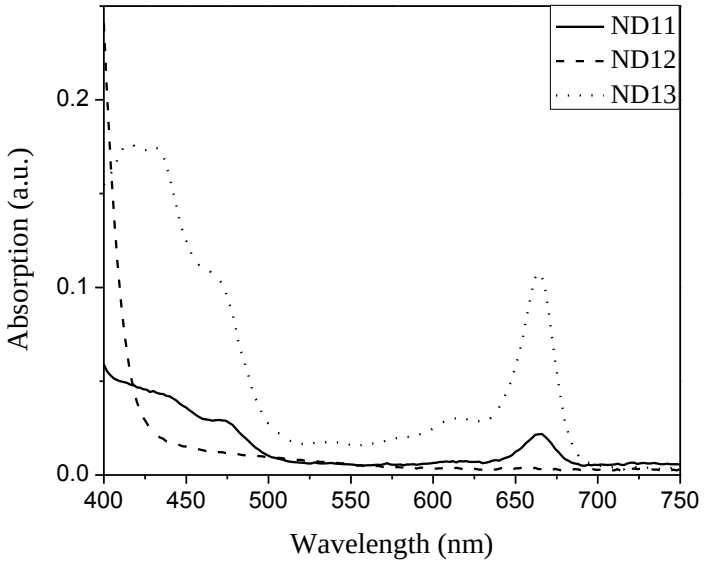

Fig.4.2. The absorption spectrum of ND11, ND12, and ND13 using ethanol as a solvent.

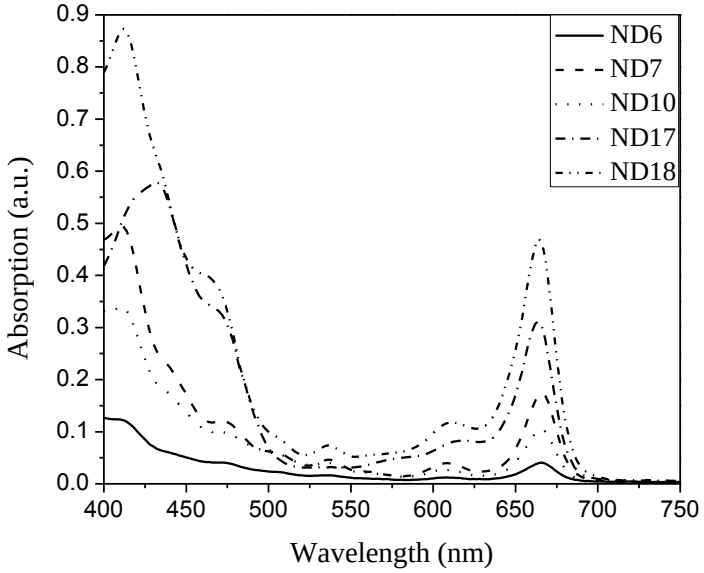

Fig.4.3. The absorption spectrum of ND6, ND7, ND10, ND17, and ND18 using ethanol as a solvent.

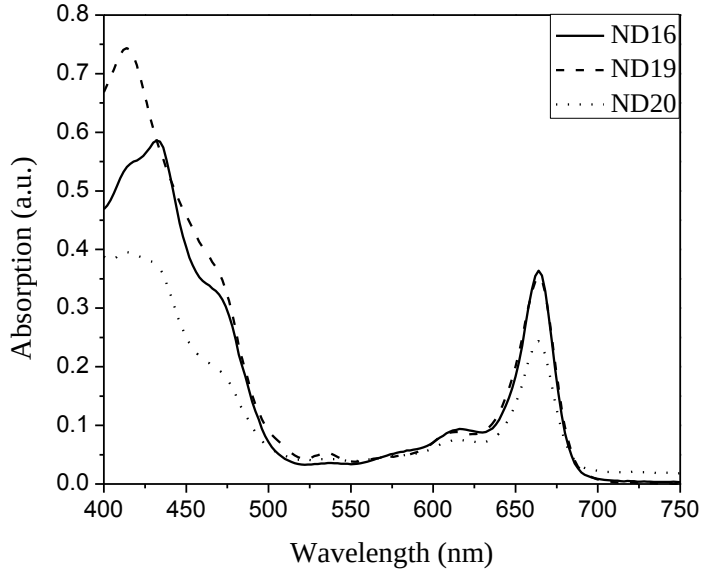

Fig.4.4. The absorption spectrum of ND16, ND19, and ND20 using ethanol as a solvent.

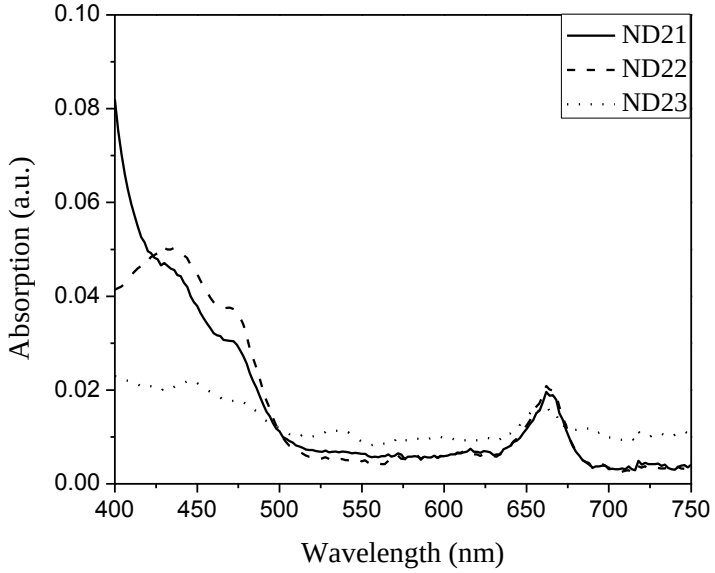

Fig.4.5. The absorption spectrum of ND21, ND22, and ND23 using ethanol as a solvent.

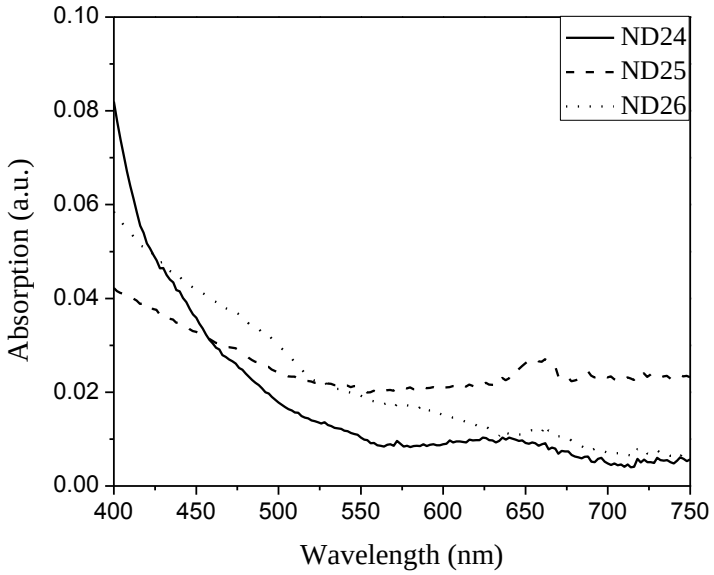

Fig.4.6. The absorption spectrum of ND24, ND25, and ND26 using ethanol as a solvent.

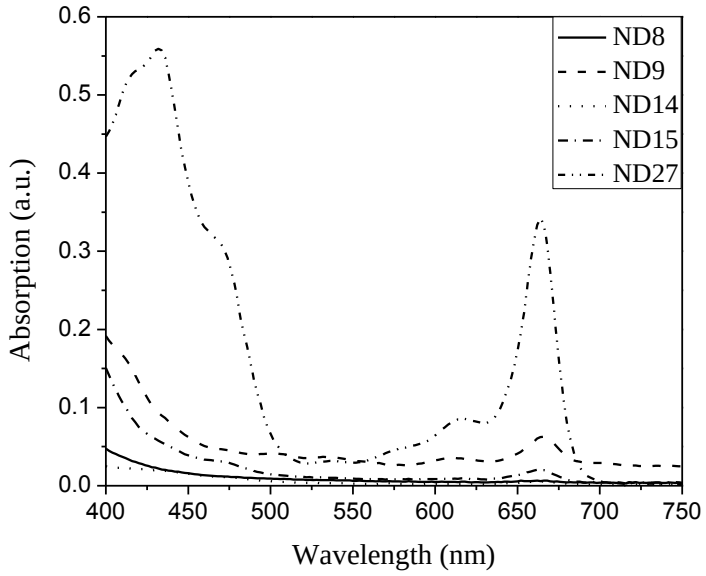

Fig.4.7. The absorption spectrum of ND8, ND9, ND14, ND15, and ND27 using ethanol as a solvent.

4.2 Measuring the J-V Curves

The J-V characteristic curves of all samples are shown in Figs. 4.8-4.34. As can be seen from figures, the short circuit current varies from 0.14 mA/cm^2 to 2.60 mA/cm^2. The highest short circuit current is obtained for the DSSC sensitized with Schinus terebinthifolius (ND18), figure 4.25, and the lowest short circuit current is obtained for the DSSC sensitized with Lycium shawii root (ND25), figure 4.32. Generally, the DSSCs sensitized with plant leaves (Olive leaves, Fig leaves, Schinus terebinthifolius, Lycium shawii leaves, and Zizyphus leaves) gave high values for the short circuit current. The DSSCs sensitized with plant root and bark of Lycium shawii exhibit low values of the short circuit current. These values for the J_{SC} are relatively comparable to the values obtained in reference [11] in which natural dyes extracted from black rice, capsicum, erythrina variegata flower, rosa xanthina, and kelp are used as sensitizers. The J_{SC} has values from 0.225 mA to 1.142 mA. In reference [28], the J_{SC} has values from 0.14 mA to 2.69 mA for DSSCs sensitized with Begonia, Yellow rose, and Mangosteen pericarp. The figures also reveal that J_{SC} increases with increasing the light intensity for all cells.

The open circuit voltage varies from 0.40V to 0.69V. The highest open circuit voltage is obtaind for the DSSC sensitized with Schinus terebinthifolius (ND18), figure 4.25, and the lowest open circuit voltage is obtaind for the DSSC sensitized with Lycium shawii root (ND25), figure 4.32. The DSSCs sensitized with plant leaves (Fig leaves, Schinus terebinthifolius, and Zizyphus leaves) gave high values for the open circuit voltage. The DSSCs sensitized with the root and the bark of Lycium shawii gave low values of the open circuit voltage. These values of the V_{OC} are relatively comparable to the values obtaind in refferance [11], in which the V_{OC} has values from 0.412 V to 0.551 V, and in reference [28], the V_{OC} has values from 0.337 V to 0.689 V. The figures also reveal that the V_{OC} increases with increasing the intensity for all cells.

Figure 4.8 shows the J-V characteristic curves of DSSC sensitized with Bougainvillea at different intensities of illumination (800 W/m^2, 1000 W/m^2, and

$1200\,W/m^2$). Figure 4.9 shows the variation of the current with the voltage at the same different intensities of illumination mentioned above for the DSSC sensitized with the extract of Mint flower. The J-V characteristic curves at the same different intensities of illumination for the DSSC sensitized with the extract of Basil flower is shown in figure 4.10. Figure 4.11 illustrates the variation of the current with the voltage for the DSSC sensitized with the extract of Royal Poinciana. The variation of the current with the voltage for the DSSC sensitized with extract of Lycium shawii flower at different intensities of illumination is shown in figure 4.12. Figure 4.13 shows the J-V characteristic curves of DSSC sensitized with Black tea at the same different intensities of illumination mentioned above. Figure 4.14 shows the variation of the current with the voltage at the same different intensities of illumination mentioned above for the DSSC sensitized with the extract of Green tea. The J-V characteristic curves at the same different intensities of illumination for the DSSC sensitized with the extract of Carob is shown in figure 4.15. Figure 4.16 illustrates the variation of the current with the voltage for the DSSC sensitized with the extract of Clove. The variation of the current with the voltage for the DSSC sensitized with extract of Henna at different intensities of illumination is shown in figure 4.17. Figure 4.18 shows the J-V characteristic curves of DSSC sensitized with Passion peel at the same different intensities of illumination mentioned above. Figure 4.19 shows the variation of the current with the voltage at the same different intensities of illumination mentioned above for the DSSC sensitized with the extract of Onion peel. The J-V characteristic curves at the same different intensities of illumination for the DSSC sensitized with the extract of Eggplant peel is shown in figure 4.20. Figure 4.21 illustrates the variation of the current with the voltage for the DSSC sensitized with the extract of Eggplant pulp. The variation of the current with the voltage for the DSSC sensitized with extract of Olive at different intensities of illumination is shown in figure 4.22. Figure 4.23 shows the J-V characteristic curves of DSSC sensitized with Olive leaves at the same different intensities of illumination mentioned above. Figure 4.24 shows the variation of the current with the voltage at the same different intensities of illumination mentioned above for the DSSC sensitized with the extract of Fig leaves. The J-V characteristic curves at the same different intensities of illumination for the DSSC sensitized with the extract of Schinus terebinthifolius is shown in figure 4.25. Figure 4.26 illustrates the variation of the current with the voltage

for the DSSC sensitized with the extract of Lycium shawii leaves. The variation of the current with the voltage for the DSSC sensitized with extract of Zizyphus leaves at different intensities of illumination is shown in figure 4.27. Figure 4.28 shows the J-V characteristic curves of DSSC sensitized with Olive bark at the same different intensities of illumination mentioned above. Figure 4.29 shows the variation of the current with the voltage at the same different intensities of illumination mentioned above for the DSSC sensitized with the extract of Lycium shawii bark. The J-V characteristic curves at the same different intensities of illumination for the DSSC sensitized with the extract of Zizyphus bark is shown in figure 4.30. Figure 4.31 illustrates the variation of the current with the voltage for the DSSC sensitized with the extract of Olive root. The variation of the current with the voltage for the DSSC sensitized with extract of Lycium shawii root at different intensities of illumination is shown in figure 4.32. Figure 4.33 shows the J-V characteristic curves of DSSC sensitized with Zizyphus root at the same different intensities of illumination mentioned above. Figure 4.34 shows the variation of the current with the voltage at the same different intensities of illumination mentioned above for the DSSC sensitized with the extract of the mixture of Fig and Olive at ratio 1:7.

It is well known that the photon-to-current efficiency depends on the intensity and range of the light absorption of the dye on TiO_2, and the interaction between TiO_2 and the dye. Moreover, a distance between the dye skeleton and the point connected to TiO_2 surface facilitate an electron transfer. Due to the two factors, the photon-to-current efficiency for the extracts of natural dyes absorbed on TiO_2 film and sensitizing effect to TiO_2 film is low [6].

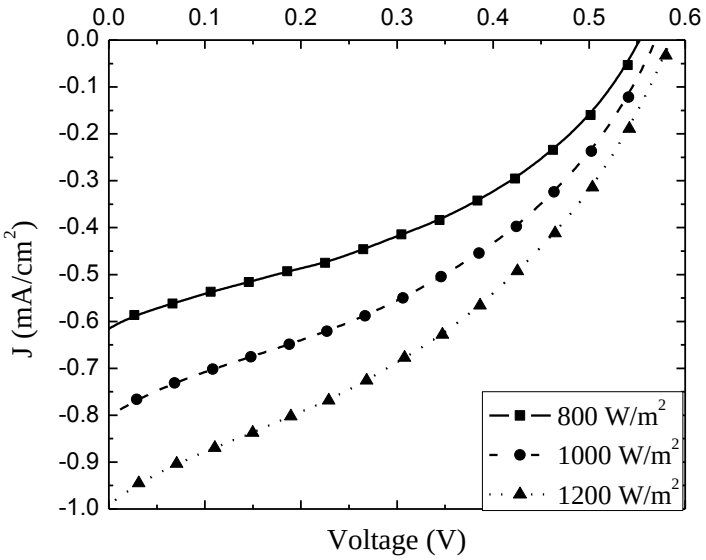

Fig. 4.8. J-V characteristic curves of the DSSC sensitized with Bougainvillea (ND1) at three different light intensities.

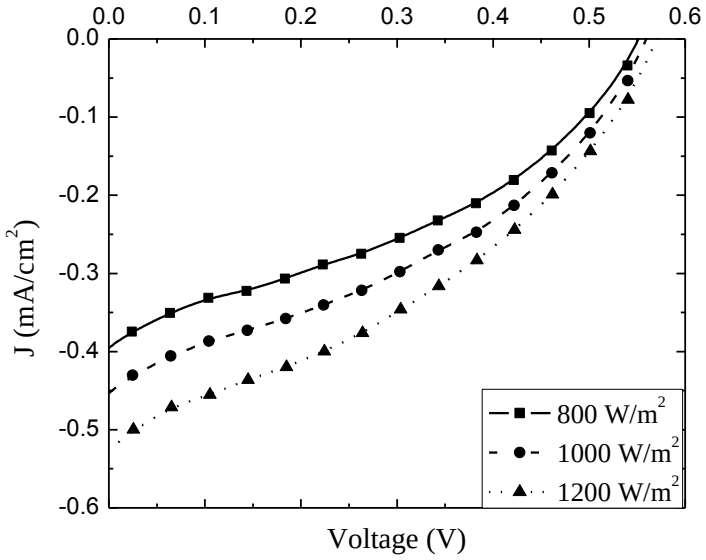

Fig. 4.9. J-V characteristic curves of the DSSC sensitized with Mint flower (ND2) at three different light intensities.

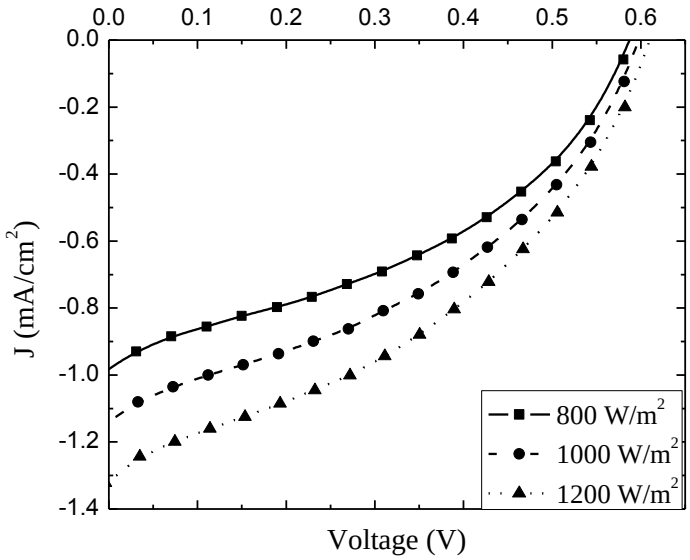

Fig. 4.10. I J-V characteristic curves of the DSSC sensitized with Basil flower (ND3) at three different light intensities.

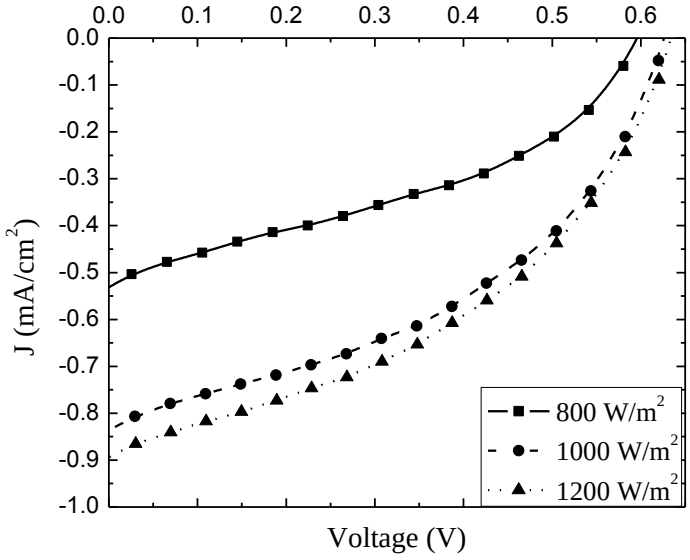

Fig. 4.11. J-V characteristic curves of the DSSC sensitized with Royal poinciana (ND4) at three different light intensities.

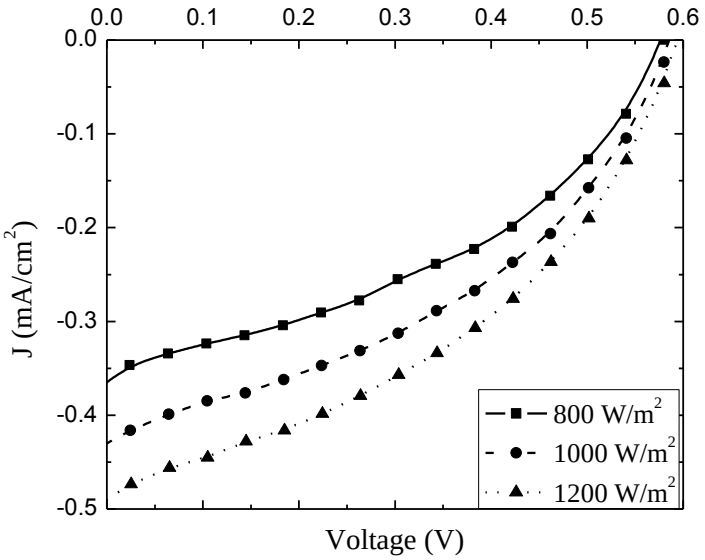

Fig. 4.12. J-V characteristic curves of the DSSC sensitized with Lycium shawii flower (ND5) at three different light intensities.

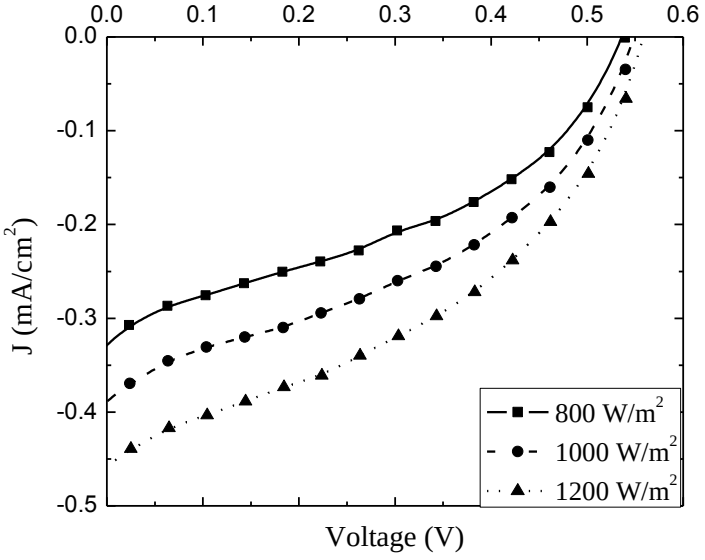

Fig. 4.13. J-V characteristic curves of the DSSC sensitized with Black tea (ND6) at three different light intensities.

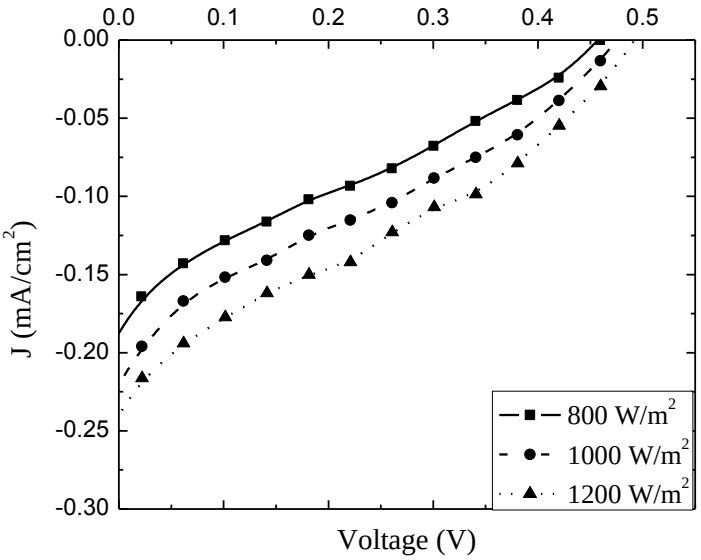

Fig. 4.14. J-V characteristic curves of the DSSC sensitized with Green tea (ND7) at three different light intensities.

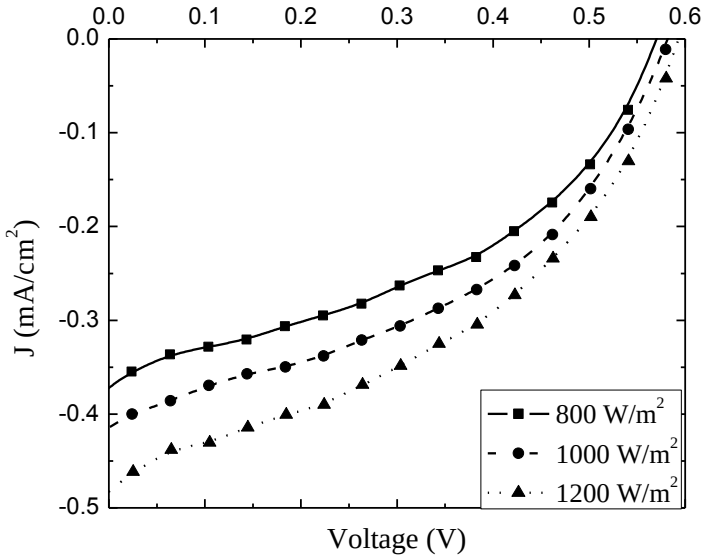

Fig. 4.15. J-V characteristic curves of the DSSC sensitized with Carob (ND8) at three different light intensities.

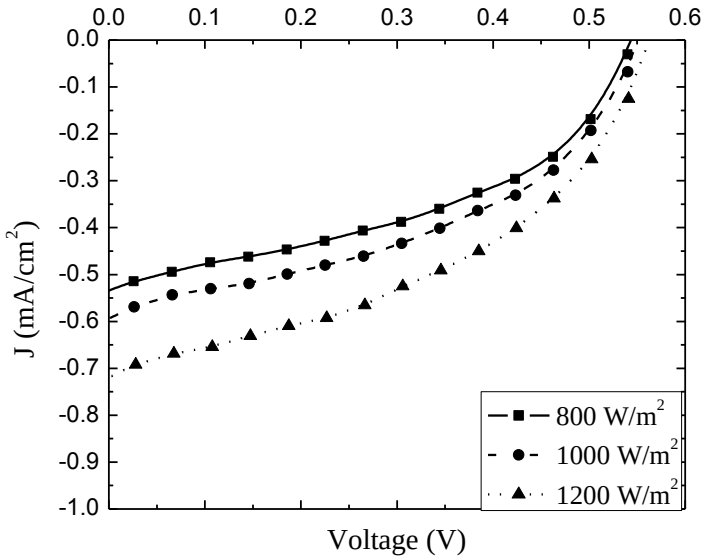

Fig. 4.16. J-V characteristic curves of the DSSC sensitized with Clove (ND9) at three different light intensities.

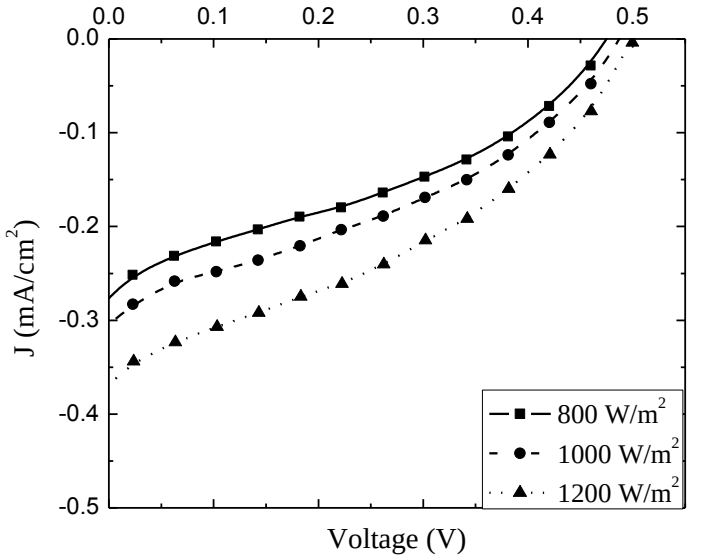

Fig. 4.17. J-V characteristic curves of the DSSC sensitized with Henna (ND10) at three different light intensities.

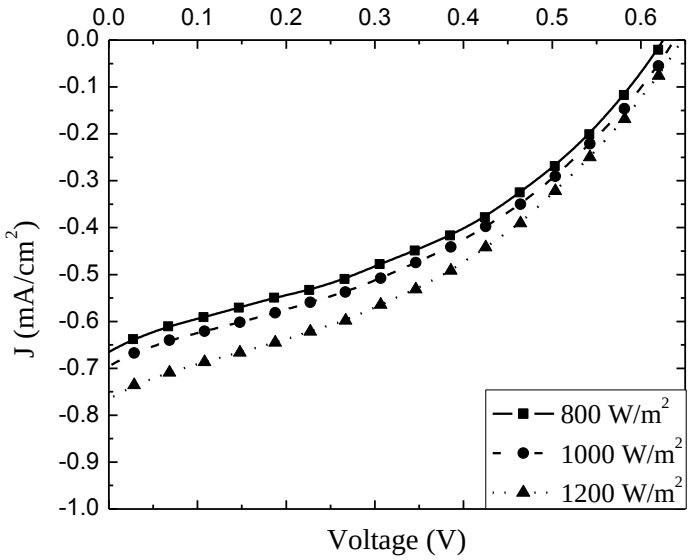

Fig. 4.18. J-V characteristic curves of the DSSC sensitized with Passion peel (ND11) at three different light intensities.

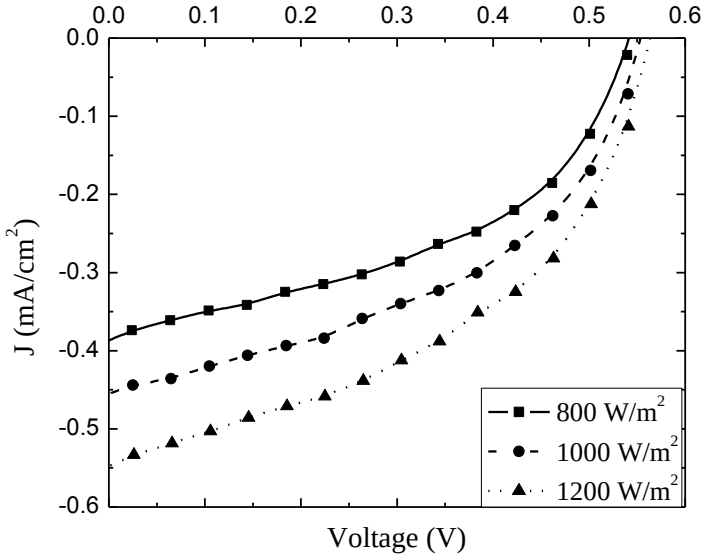

Fig. 4.19. J-V characteristic curves of the DSSC sensitized with Onion peel (ND12) at three different light intensities.

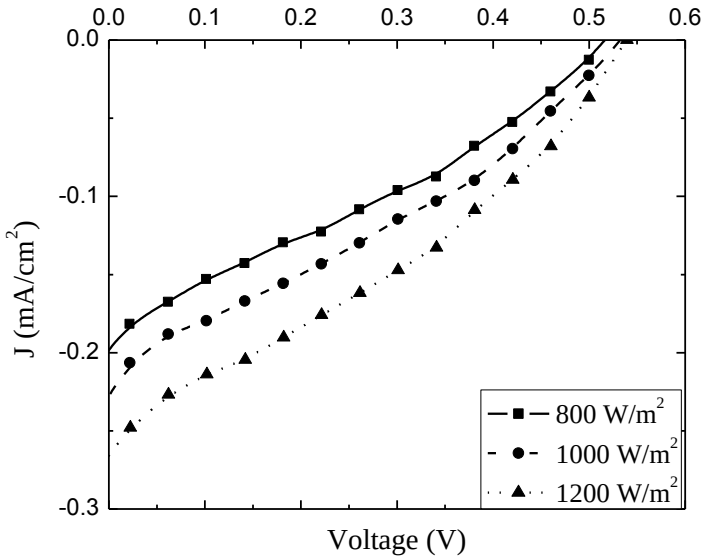

Fig. 4.20. J-V characteristic curves of the DSSC sensitized with Eggplant peel (ND13) at three different light intensities.

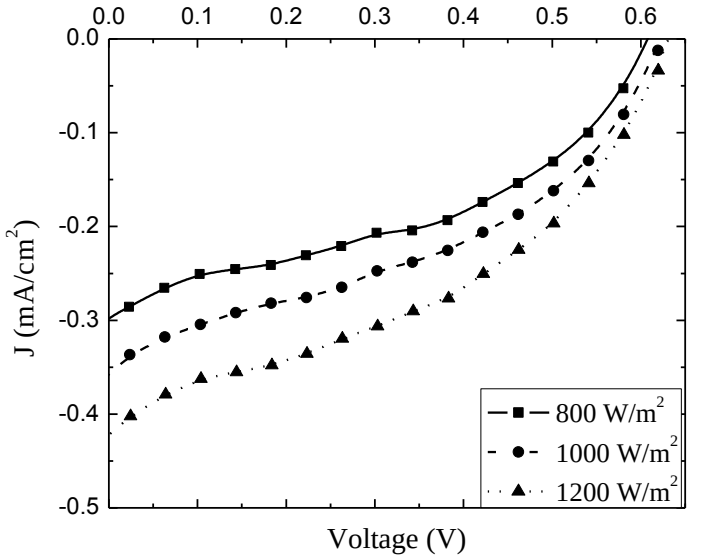

Fig. 4.21. J-V characteristic curves of the DSSC sensitized with Eggplant pulp (ND14) at three different light intensities.

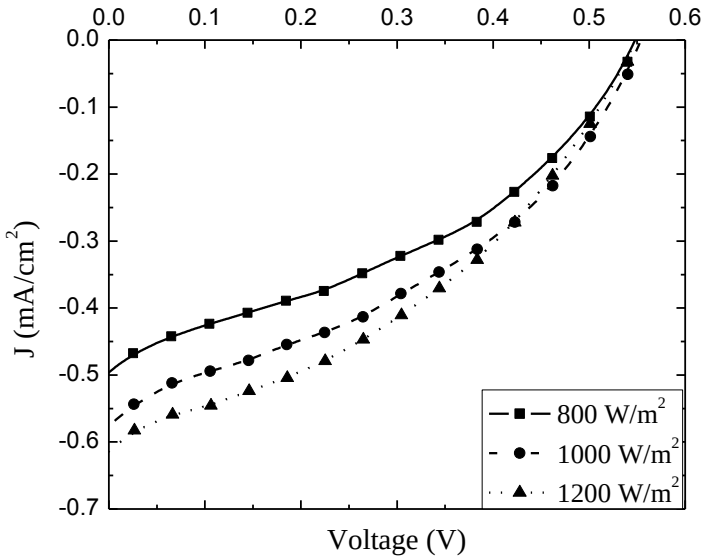

Fig. 4.22. J-V characteristic curves of the DSSC sensitized with Olive (ND15) at three different light intensities.

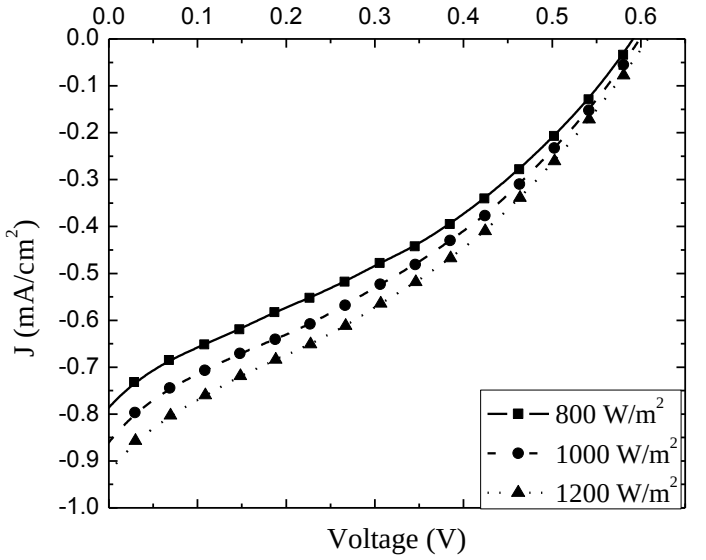

Fig. 4.23. J-V characteristic curves of the DSSC sensitized with Olive leaves (ND16) at three different light intensities.

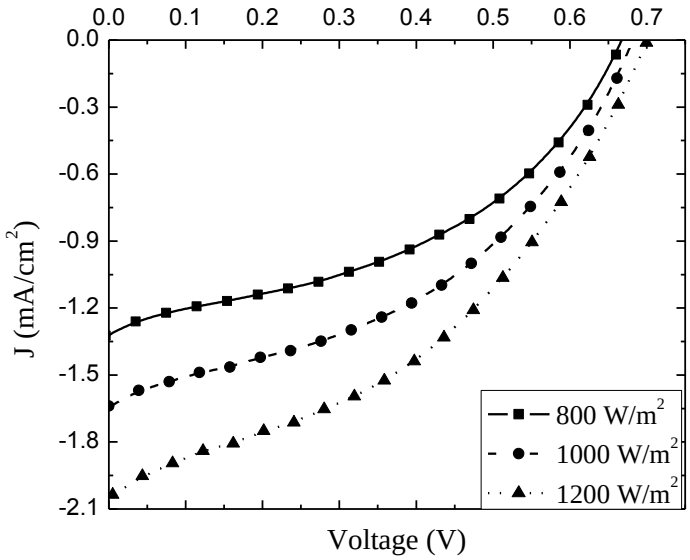

Fig. 4.24. J-V characteristic curves of the DSSC sensitized with Fig leaves (ND17) at three different light intensities.

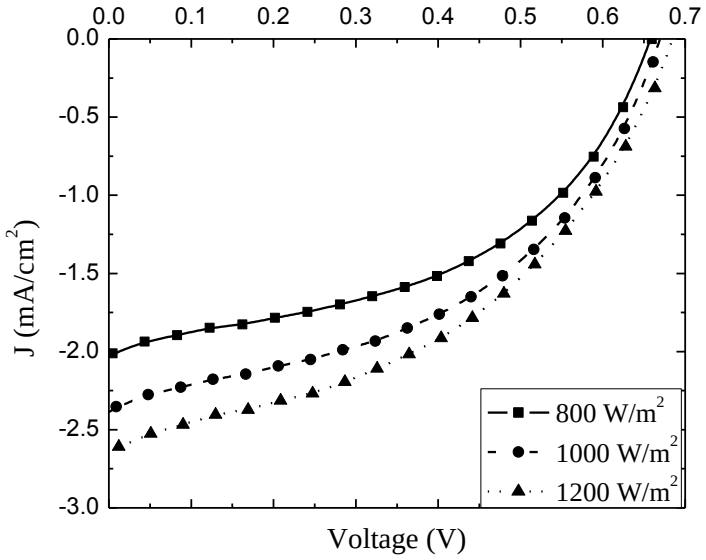

Fig. 4.25. J-V characteristic curves of the DSSC sensitized with Schinus terebinthifolius (ND18) at three different light intensities.

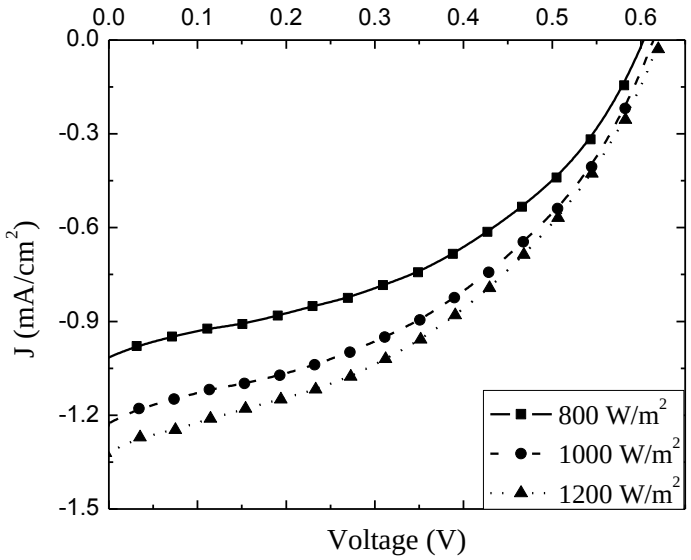

Fig. 4.26. J-V characteristic curves of the DSSC sensitized with Lycium shawii leaves (ND19) at three different light intensities.

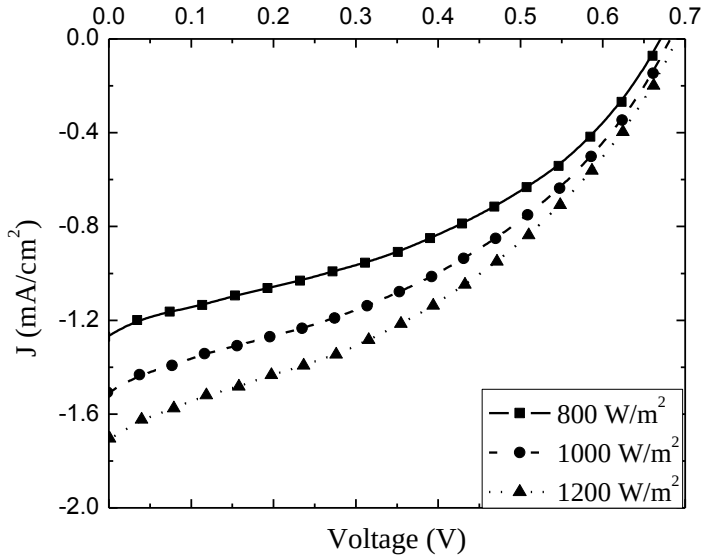

Fig. 4.27. J-V characteristic curves of the DSSC sensitized with Zizyphus leaves (ND20) at three different light intensities.

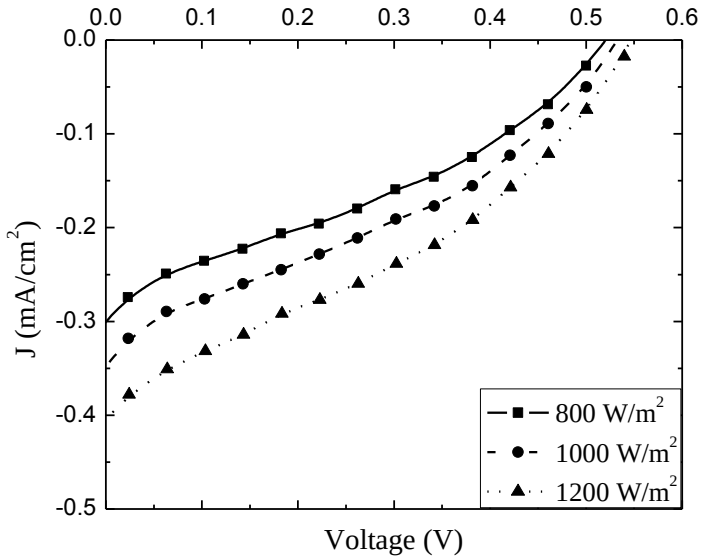

Fig. 4.28. J-V characteristic curves of the DSSC sensitized with Olive bark (ND21) at three different light intensities.

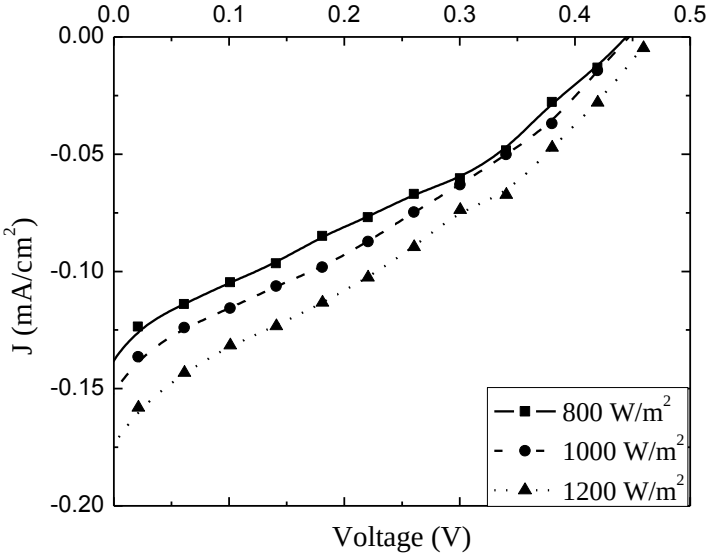

Fig. 4.29. J-V characteristic curves of the DSSC sensitized with Lycium shawii bark (ND22) at three different light intensities.

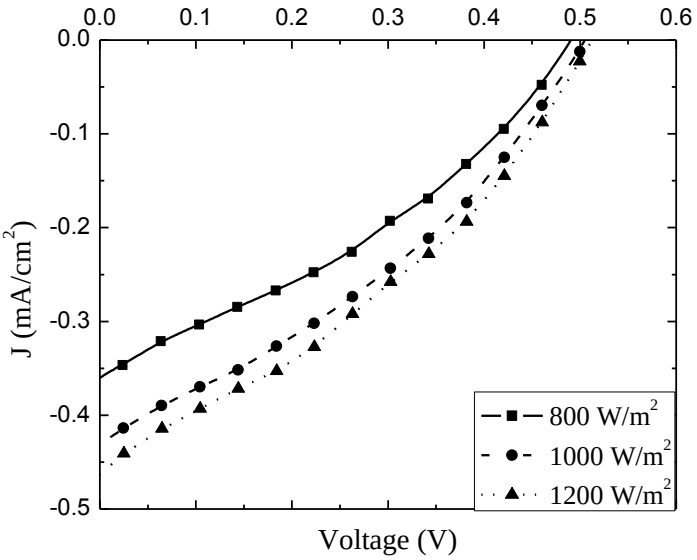

Fig. 4.30. J-V characteristic curves of the DSSC sensitized with Zizyphus bark (ND23) at three different light intensities.

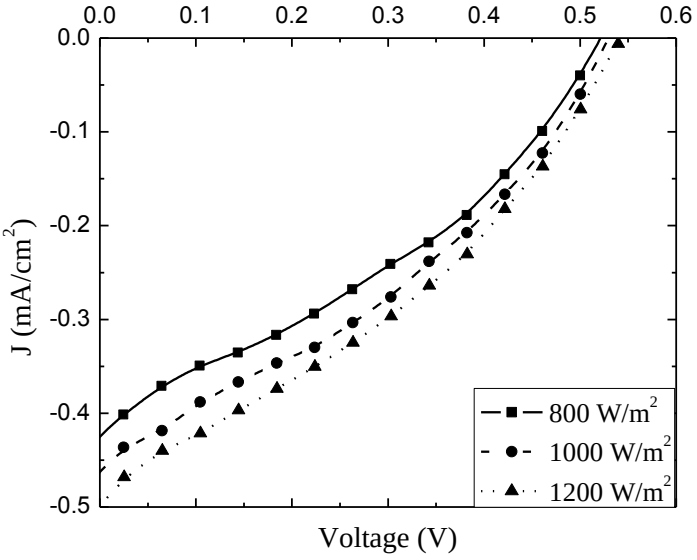

Fig. 4.31. J-V characteristic curves of the DSSC sensitized with Olive root (ND24) at three different light intensities.

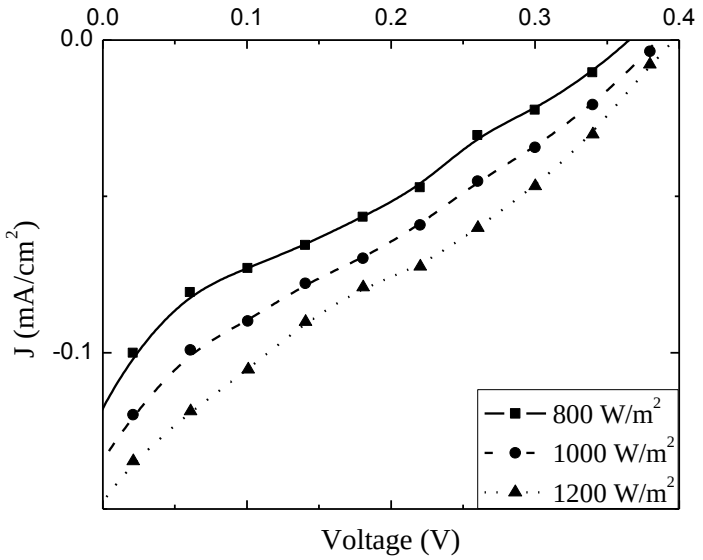

Fig. 4.32. J-V characteristic curves of the DSSC sensitized with Lycium shawii root (ND25) at three different light intensities.

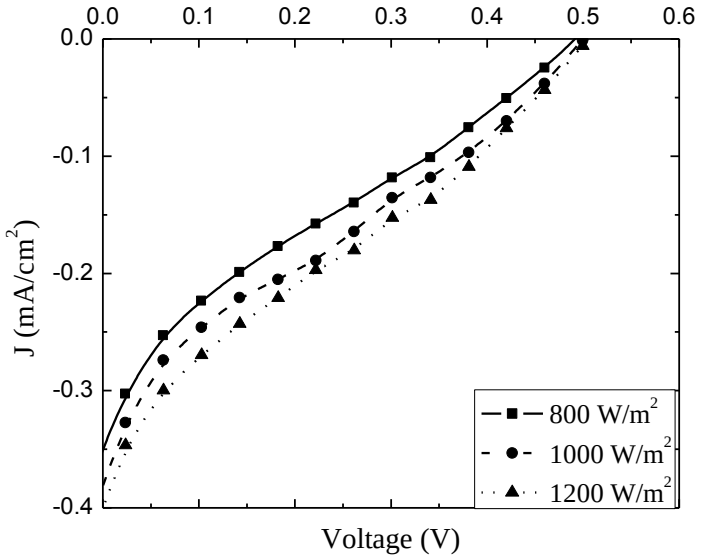

Fig. 4.33. J-V characteristic curves of the DSSC sensitized with Zizyphus root (ND26) at three different light intensities.

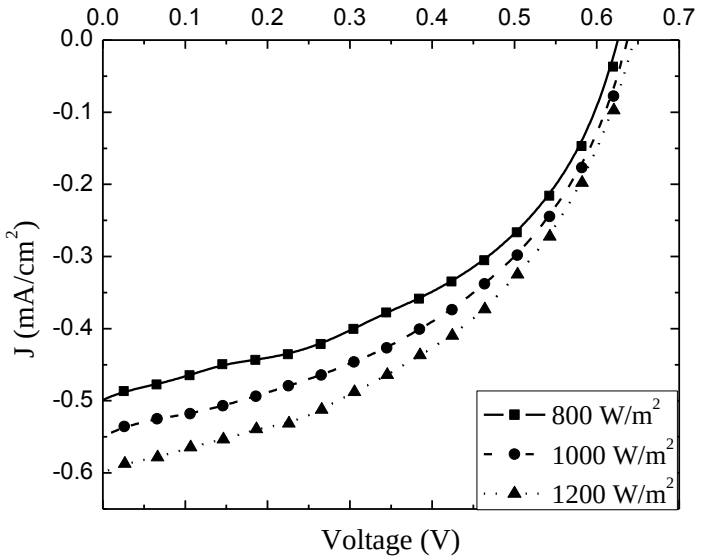

Fig. 4.34. J-V characteristic curves of the DSSC sensitized with Fig 1: Olive7 (ND27) at three different light intensities.

4.3 Power Curves

The power is calculated for each experimental point by multiplying the current density and voltage at each point. The power density curves of all samples are shown in Figs. 4.35-4.61. The power curve of each cell is also shown at three different intensities; 800 W/m^2, 1000 W/m^2, and 1200 W/m^2. As can be seen from figures, the power varies from 0.01 mW/cm^2 to 0.79 mW/cm^2. The highest power is obtained for the DSSC sensitized with Schinus terebinthifolius (ND18), figure 4.52, and the lowest power is obtained for the DSSC sensitized with Lycium shawii root (ND25), figure 4.59 . The DSSCs sensitized with plant leaves (Fig leaves, and Schinus terebinthifolius) gave high values for the power. The DSSCs sensitized with the root and the bark of Lycium shawii exhibit low values of the power. The figures also reveal that the power increases with increasing the light intensity.

Figure 4.35 shows the variation of the power density with the voltage for the DSSC sensitized with the extract of Bougainvillea for three different light intensities. As can be seen from the figure, the maximum output power obtained for the cell is 0.22

mW. Figure 4.36 shows the same for the DSSC sensitized with the extract of Mint flower with the maximum output power of 0.11 mW. The P-V curves of the DSSC sensitized with the extract of Basil flower shown in figure 4.37. The figure shows a maximum power of 0.31 mW. Figure 4.38 shows the variation of the power density with the voltage for the DSSC sensitized with the extract of Royal poinciana for three different light intensities. As can be seen from the figure, the maximum output power obtained for the cell is 0.24 mW. Figure 4.39 shows the same for the DSSC sensitized with the extract of Lycium shawii flower with the maximum output power of 0.12 mW. The P-V curves of the DSSC sensitized with the extract of Black tea shown in figure 4.40. The figure shows a maximum power of 0.10 mW. Figure 4.41 shows the variation of the power density with the voltage for the DSSC sensitized with the extract of Green tea for three different light intensities. As can be seen from the figure, the maximum output power obtained for the cell is 0.03 mW. Figure 4.42 shows the same for the DSSC sensitized with the extract of Carob with the maximum output power of 0.12 mW. The P-V curves of the DSSC sensitized with the extract of Clove shown in figure 4.43. The figure shows a maximum power of 0.17 mW. Figure 4.44 shows the variation of the power density with the voltage for the DSSC sensitized with the extract of Henna for three different light intensities. As can be seen from the figure, the maximum output power obtained for the cell is 0.07 mW. Figure 4.45 shows the same for the DSSC sensitized with the extract of Passion peel with the maximum output power of 0.19 mW. The P-V curves of the DSSC sensitized with the extract of Onion peel shown in figure 4.46. The figure shows a maximum power of 0.14 mW. Figure 4.47 shows the variation of the power density with the voltage for the DSSC sensitized with the extract of Eggplant peel for three different light intensities. As can be seen from the figure, the maximum output power obtained for the cell is 0.05 mW. Figure 4.48 shows the same for the DSSC sensitized with the extract of Eggplant pulp with the maximum output power of 0.11 mW. The P-V curves of the DSSC sensitized with the extract of Olive shown in figure 4.49. The figure shows a maximum power of 0.13 mW. Figure 4.50 shows the variation of the power density with the voltage for the DSSC sensitized with the extract of Olive leaves for three different light intensities. As can be seen from the figure, the maximum output power obtained for the cell is 0.18 mW. Figure 4.51 shows the same for the DSSC sensitized with the extract of Fig leaves with the maximum

output power of 0.58 mW. The P-V curves of the DSSC sensitized with the extract of Schinus terebinthifolius shown in figure 4.52. The figure shows a maximum power of 0.79 mW. Figure 4.53 shows the variation of the power density with the voltage for the DSSC sensitized with the extract of Lycium shawii leaves for three different light intensities. As can be seen from the figure, the maximum output power obtained for the cell is 0.34 mW. Figure 4.54 shows the same for the DSSC sensitized with the extract of Zizyphus leaves with the maximum output power of 0.45 mW. The P-V curves of the DSSC sensitized with the extract of Olive bark shown in figure 4.55. The figure shows a maximum power of 0.07 mW. Figure 4.56 shows the variation of the power density with the voltage for the DSSC sensitized with the extract of Lycium shawii bark for three different light intensities. As can be seen from the figure, the maximum output power obtained for the cell is 0.02 mW. Figure 4.57 shows the same for the DSSC sensitized with the extract of Zizyphus bark with the maximum output power of 0.08 mW. The P-V curves of the DSSC sensitized with the extract of Olive root shown in figure 4.58. The figure shows a maximum power of 0.09 mW. Figure 4.59 shows the variation of the power density with the voltage for the DSSC sensitized with the extract of Lycium shawii root for three different light intensities. As can be seen from the figure, the maximum output power obtained for the cell is 0.01 mW. Figure 4.60 shows the same for the DSSC sensitized with the extract of Zizyphus root with the maximum output power of 0.05 mW. The P-V curves of the DSSC sensitized with the extract of mixture of Fig and Olive by ratio 1:7 shown in figure 4.61. The figure shows a maximum power of 0.41 mW.

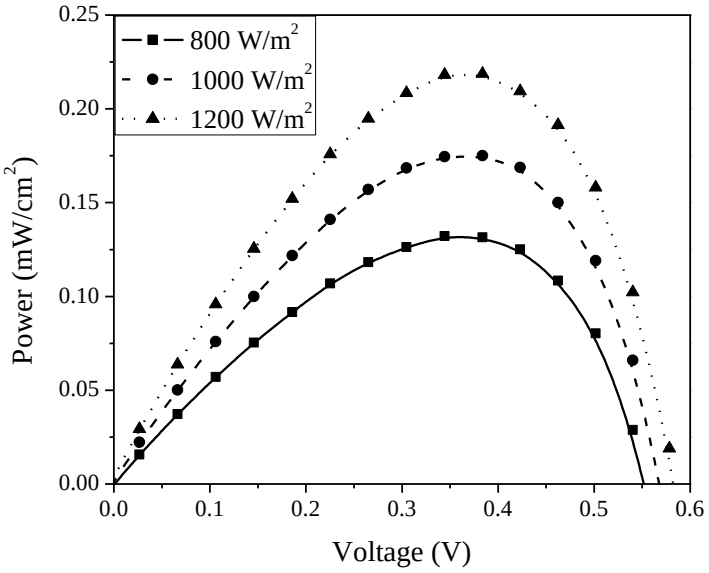

Fig. 4.35. Power versus voltage of the DSSC sensitized with Bougainvillea (ND1) at three different light intensities.

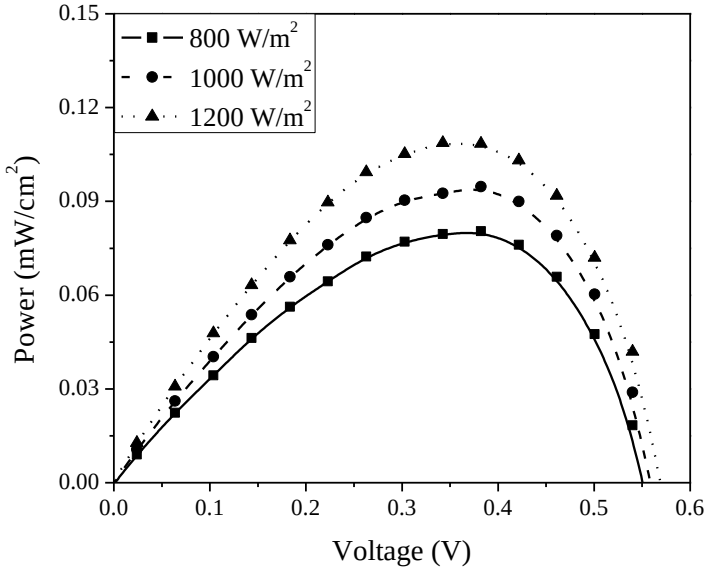

Fig. 4.36. Power versus voltage of the DSSC sensitized with Mint flower (ND2) at three different light intensities.

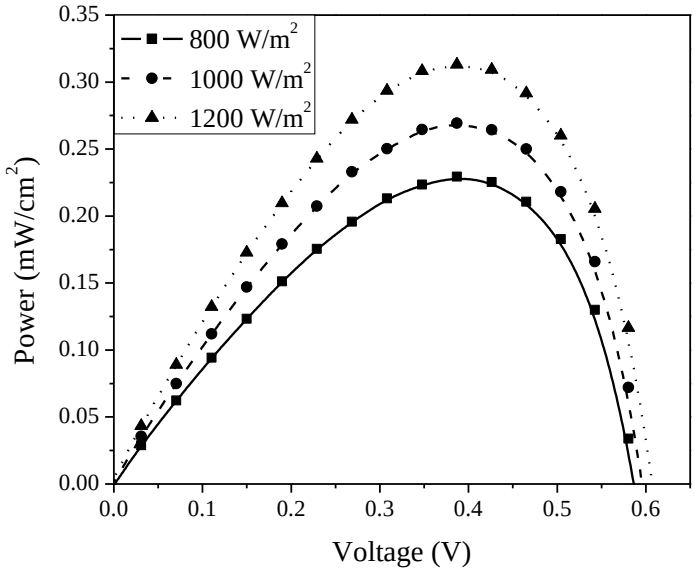

Fig. 4.37. Power versus voltage of the DSSC sensitized with Basil flower (ND3) at three different light intensities.

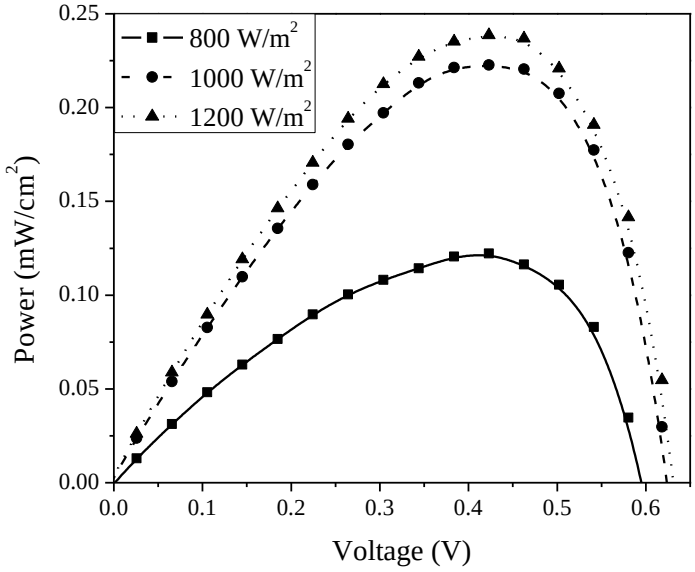

Fig. 4.38. Power versus voltage of the DSSC sensitized with Royal poinciana (ND4) at three different light intensities.

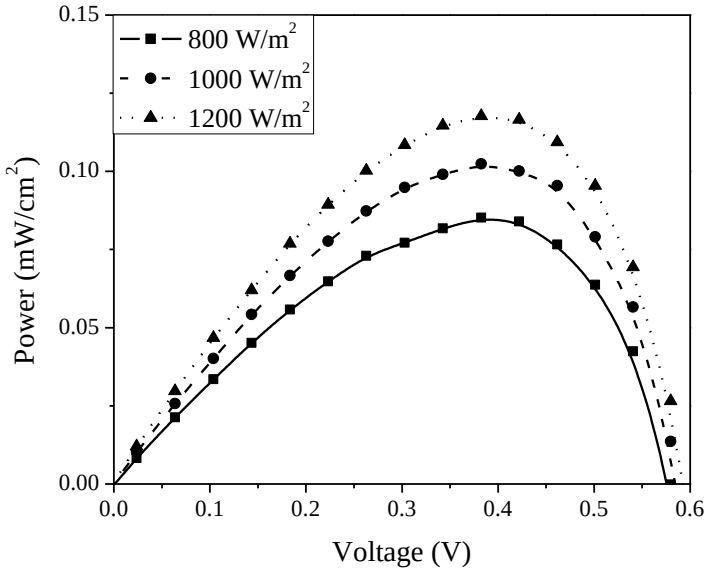

Fig. 4.39. Power versus voltage of the DSSC sensitized with Lycium shawii flower (ND5) at three different light intensities.

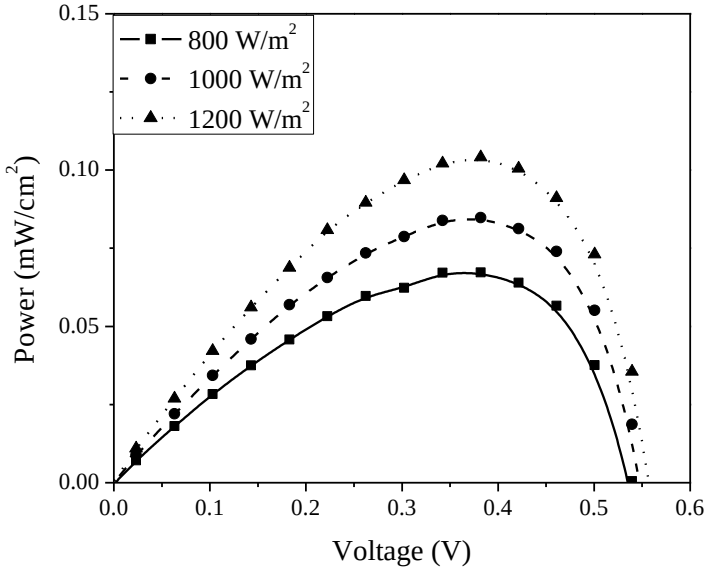

Fig. 4.40. Power versus voltage of the DSSC sensitized with Black tea (ND6) at three different light intensities.

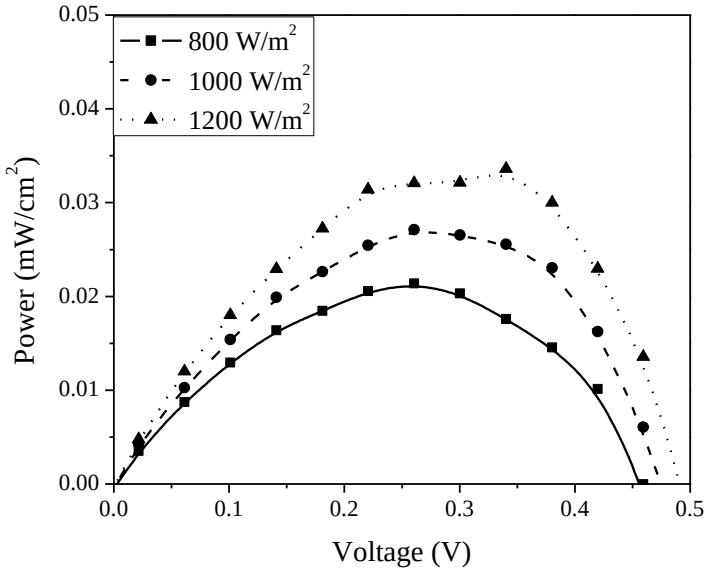

Fig. 4.41. Power versus voltage of the DSSC sensitized with Green tea (ND7) at three different light intensities.

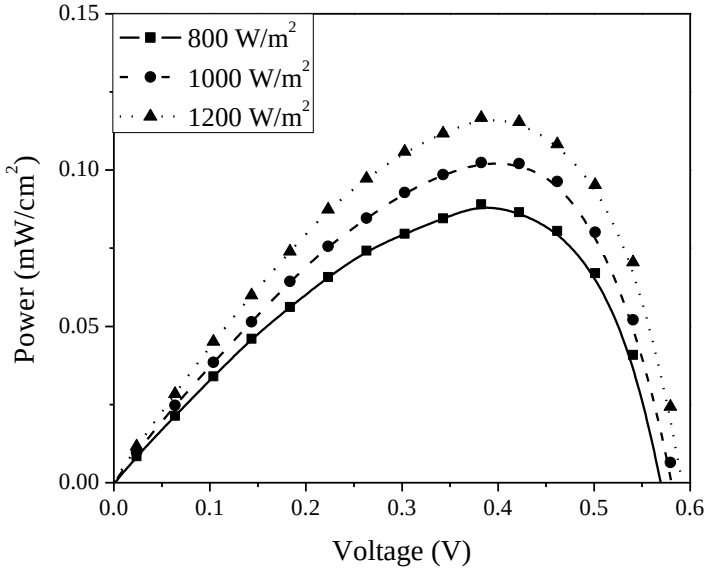

Fig. 4.42. Power versus voltage of the DSSC sensitized with Carob (ND8) at three different light intensities.

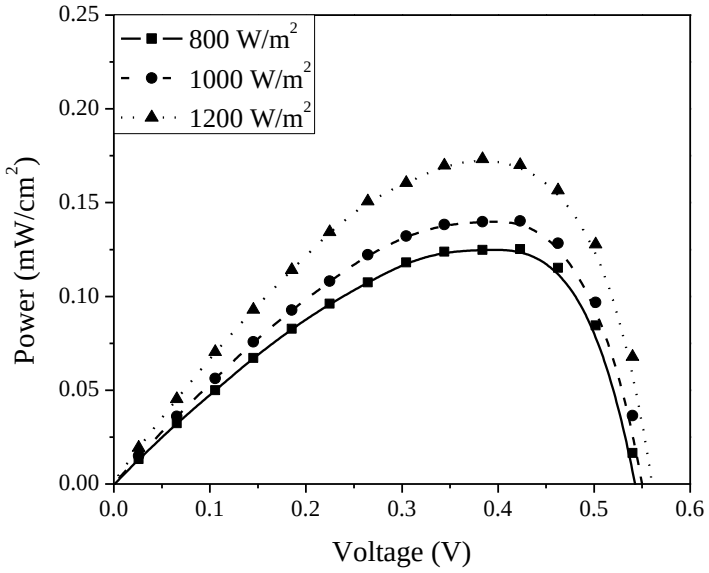

Fig. 4.43. Power versus voltage of the DSSC sensitized with Clove (ND9) at three different light intensities.

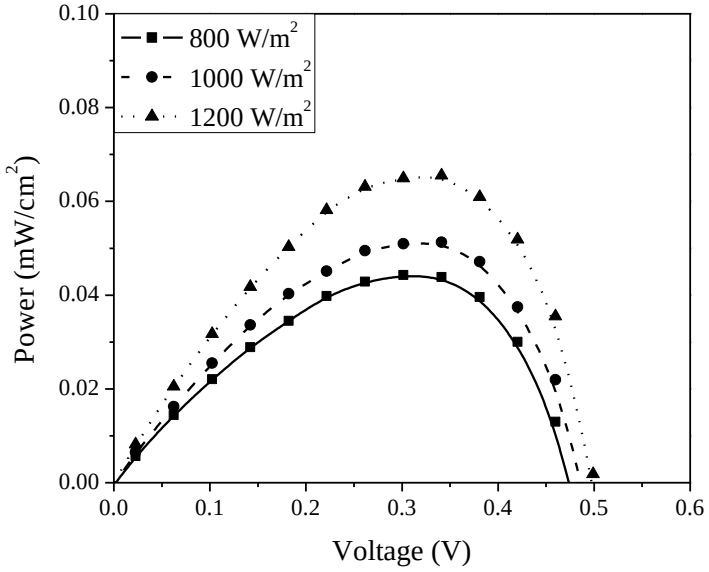

Fig. 4.44. Power versus voltage of the DSSC sensitized with Henna (ND10) at three different light intensities.

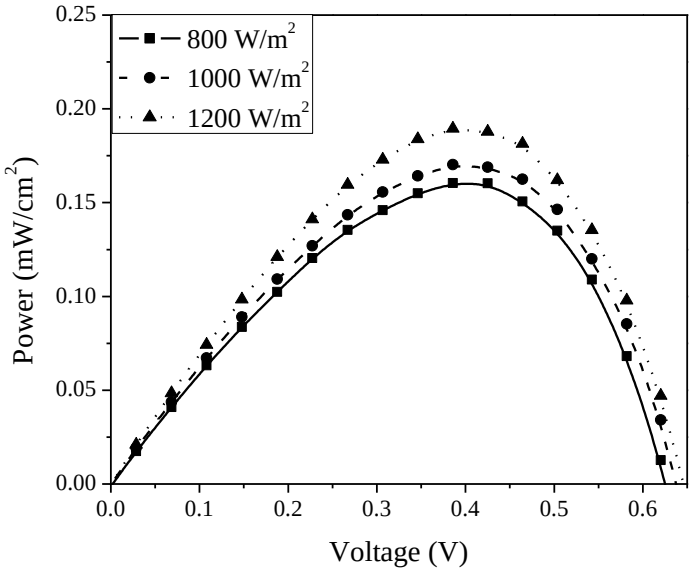

Fig. 4.45. Power versus voltage of the DSSC sensitized with Passion peel (ND11) at three different light intensities.

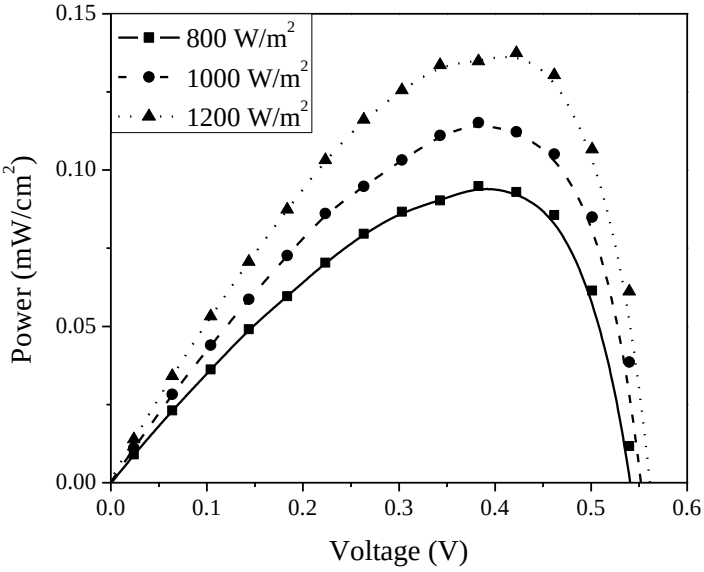

Fig. 4.46. Power versus voltage of the DSSC sensitized with Onion peel (ND12) at three different light intensities.

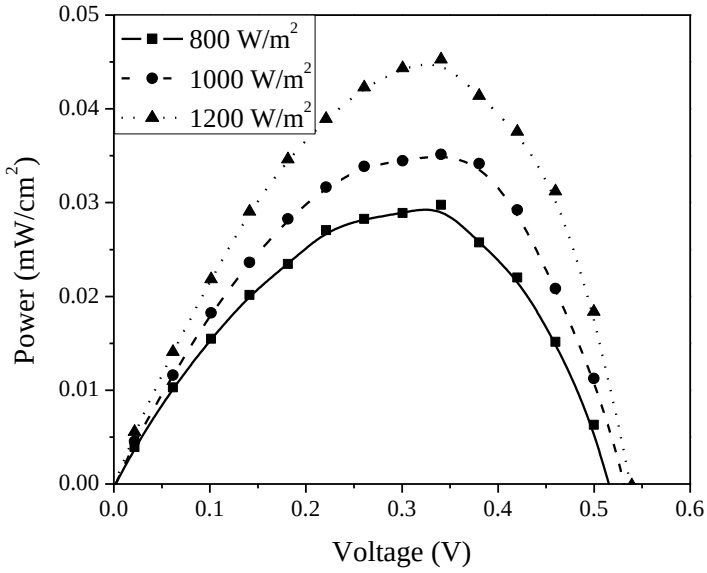

Fig. 4.47. Power versus voltage of the DSSC sensitized with Eggplant peel (ND13) at three different light intensities.

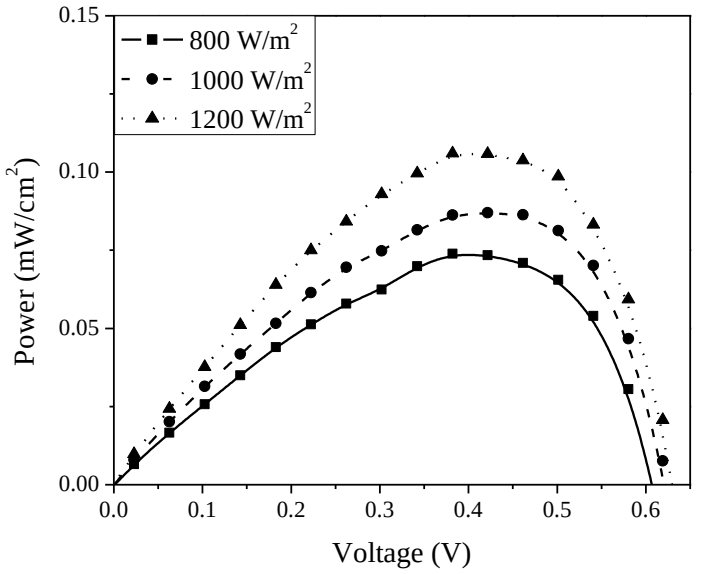

Fig. 4.48. Power versus voltage of the DSSC sensitized with Eggplant pulp (ND14) at three different light intensities.

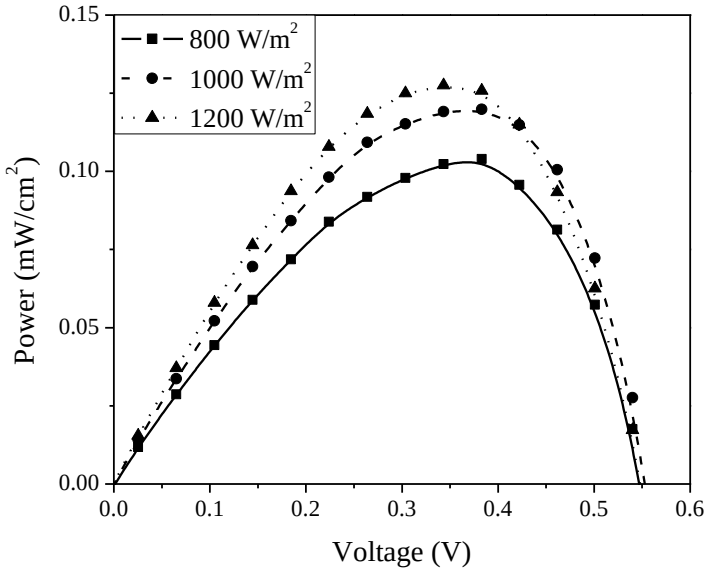

Fig. 4.49. Power versus voltage of the DSSC sensitized with Olive (ND15) at three different light intensities.

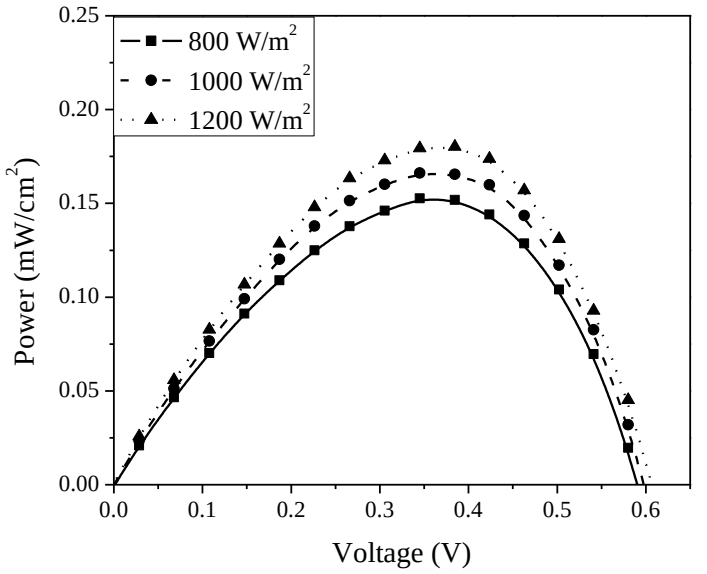

Fig. 4.50. Power versus voltage of the DSSC sensitized with Olive leaves (ND16) at three different light intensities.

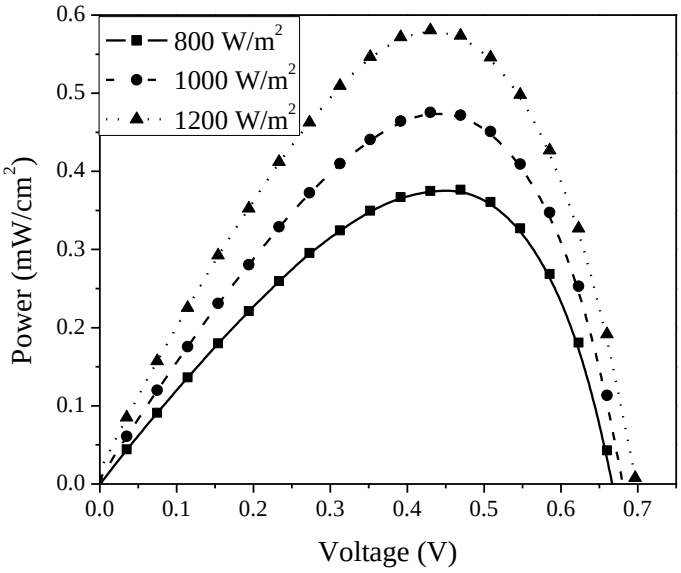

Fig. 4.51. Power versus voltage of the DSSC sensitized with Fig leaves (ND17) at three different light intensities.

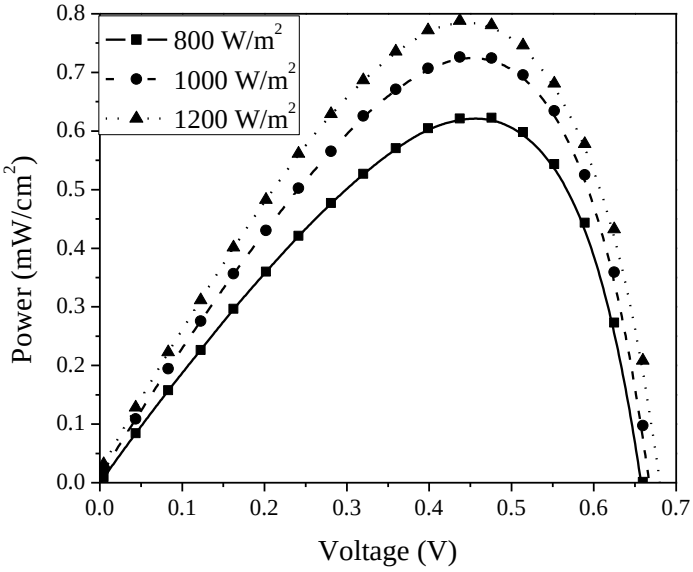

Fig. 4.52. Power versus voltage of the DSSC sensitized with Schinus terebinthifolius (ND18) at three different light intensities.

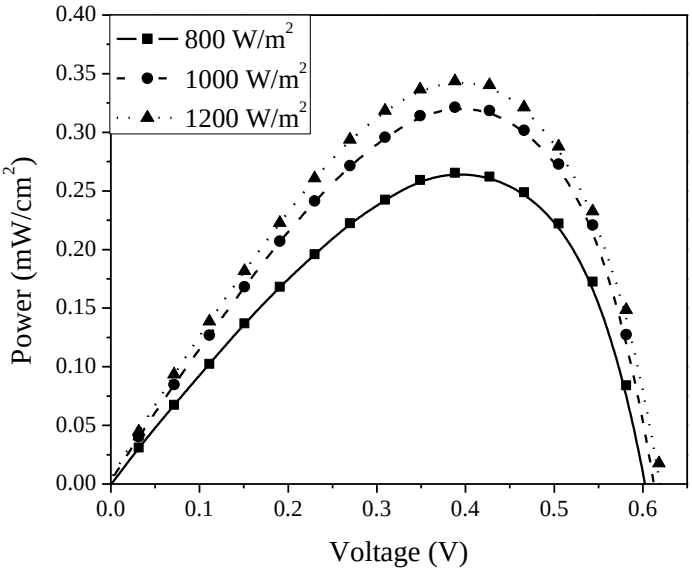

Fig. 4.53. Power versus voltage of the DSSC sensitized with Lycium shawii leaves (ND19) at three different light intensities.

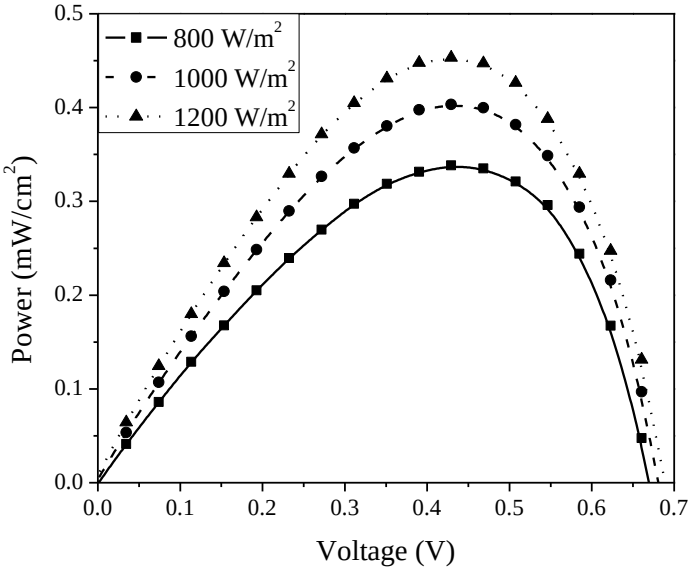

Fig. 4.54. Power versus voltage of the DSSC sensitized with Zizyphus leaves (ND20) at three different light intensities.

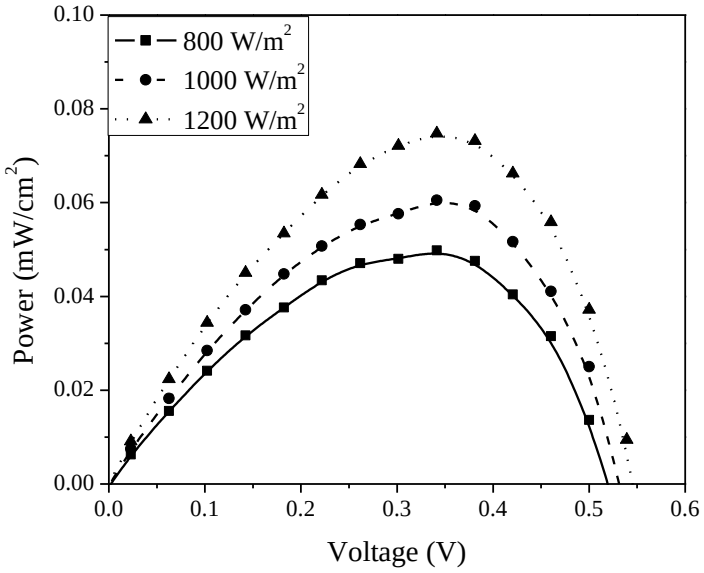

Fig. 4.55. Power versus voltage of the DSSC sensitized with Olive bark (ND21) at three different light intensities.

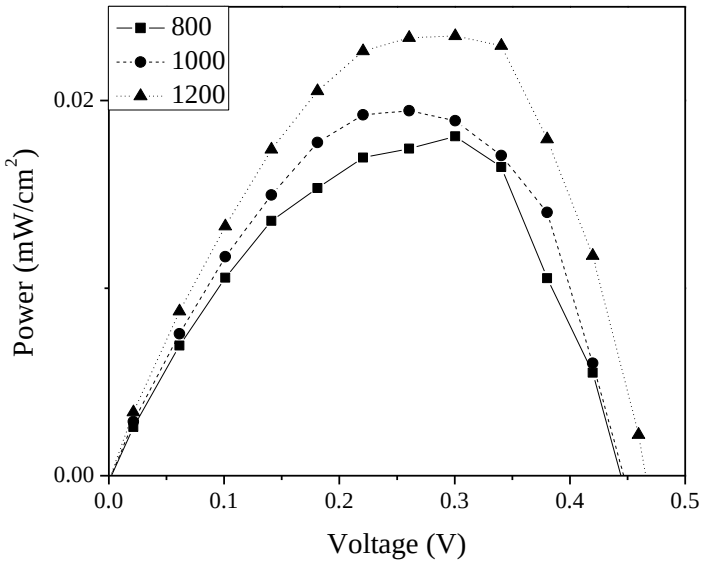

Fig. 4.56. Power versus voltage of the DSSC sensitized with Lycium shawii bark (ND22) at three different light intensities.

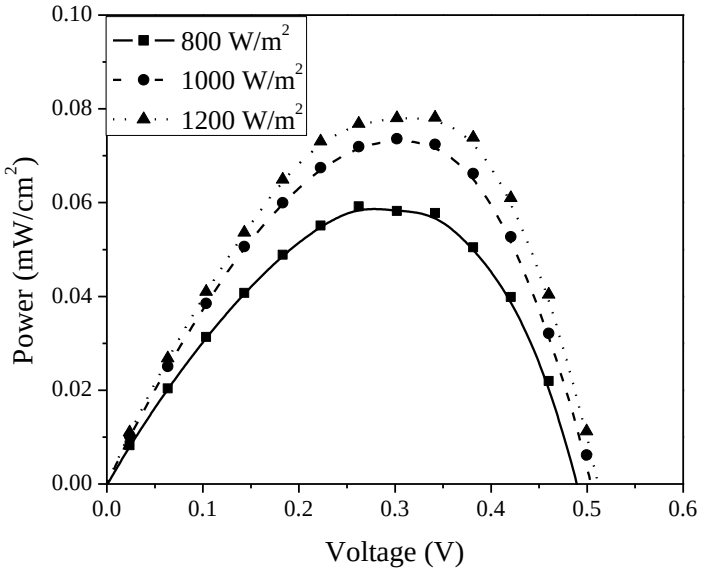

Fig. 4.57. Power versus voltage of the DSSC sensitized with Zizyphus bark (ND23) at three different light intensities.

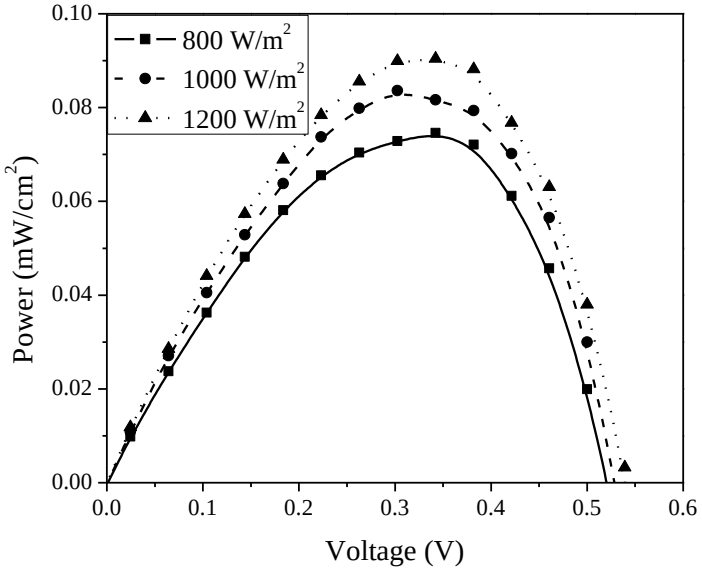

Fig. 4.58. Power versus voltage of the DSSC sensitized with Olive root (ND24) at three different light intensities.

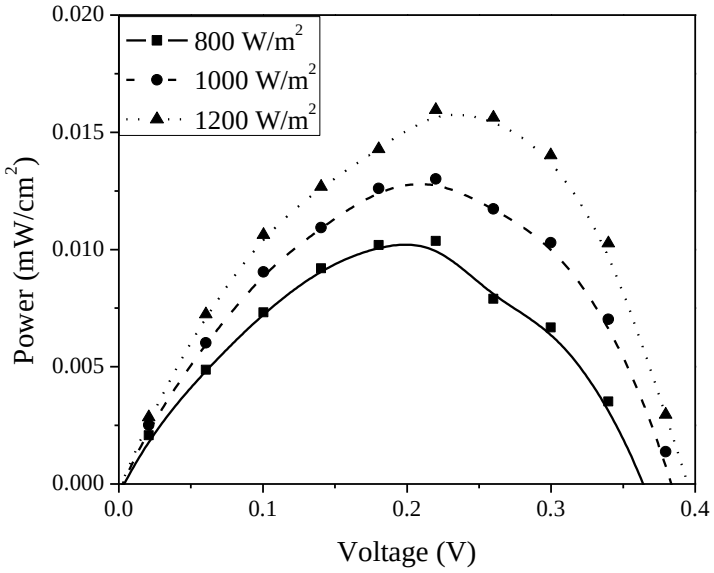

Fig. 4.59. Power versus voltage of the DSSC sensitized with Lycium shawii root (ND25) at three different light intensities.

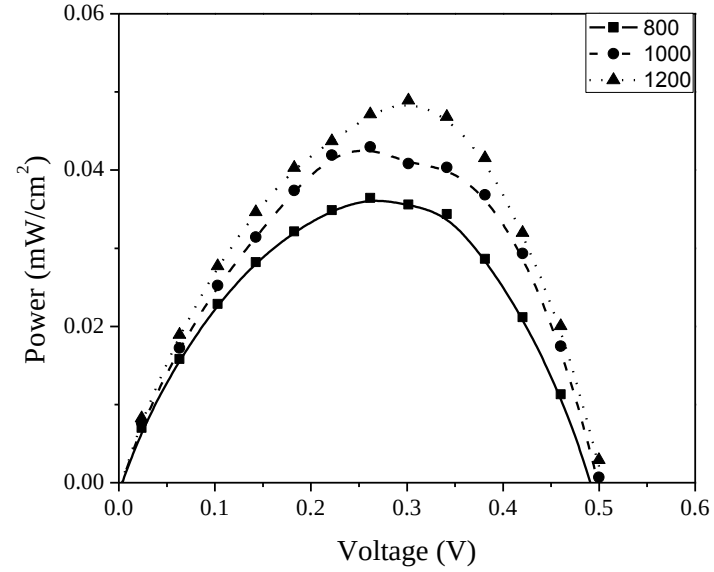

Fig. 4.60. Power versus voltage of the DSSC sensitized with Zizyphus root (ND26) at three different light intensities.

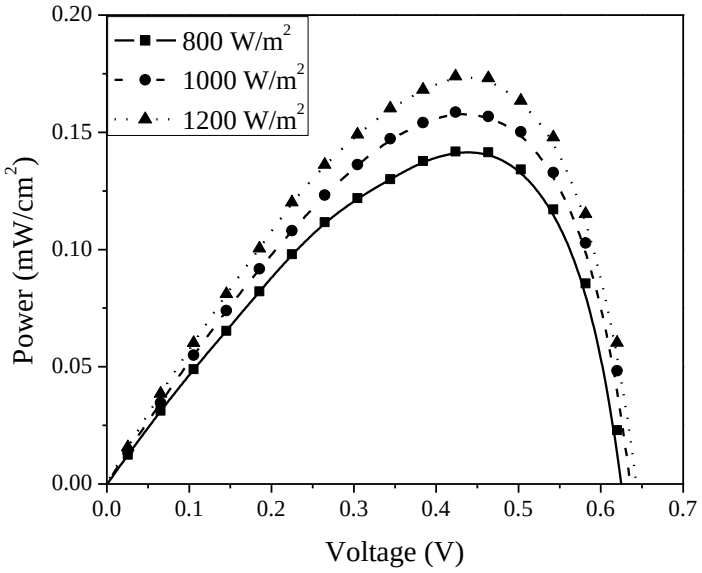

Fig. 4.61. Power versus voltage of the DSSC sensitized with Fig 1: Olive7 (ND27) at three different light intensities.

4.4 The DSSC Parameters

The short circuit current density (J_{SC}) and open circuit voltage (V_{OC}) are obtained from the J-V curves by estimating the J- axis and V- axis intersection, respectively. The maximum power point is determined from the P-V curves from which J_{MP} and V_{MP} can be calculated. The wavelength of maximum absorption of the dyes is determined from absorption spectra curves. The fill factor and efficiency are calculated using Eqs. (2.12) and (2.13), respectively. All these parameters of the fabricated DSSCs are listed in Table 4.1 for the three light intensities considered.

As can be seen from the table, the *FF* varies from 0.23 to 0.45. The highest *FF* is obtained for the DSSC sensitized with Onion peel (ND12) at intensity of 1000 W/m^2 and the lowest *FF* is obtained for the DSSC sensitized with Lycium shawii root (ND25) at intensity of 1200 W/m^2. Generally, the *FF* of the DSSCs increases with the radiation intensity such as dyed with (ND2, ND3, ND4, ND6, ND7, ND10, ND12, ND13, ND16, ND17, ND20, ND21, ND24, ND25, ND26). A increases in *FF* is maybe due to increase in solar irradiance, where the higher number of photons absorbed in the DSSC which

results in enhanced dye excitation and electron transfer into the conduction band of TiO_2 electrode resulting in higher photocurrent. Another decrease the *FF* with the radiation intensity, increases in cell temperature maybe observed because as temperature increases the band gap of the TiO_2 semiconductor layer, the decrease *FF* is the transfer recombination which occurs at the dye-electrode interface, electrolyte-dye interface, and electrolyte-counter electrode interface, These values of *FF* are relatively smaller than those obtained in reference [11], where *FF* has values from 0.52 to 0.67.

The table also shows that η varies from 0.01 to 0.66. The highest η is obtained for the DSSC sensitized with Schinus terebinthifolius (ND18) and the lowest η is obtained for the DSSC sensitized with Lycium shawii root (ND25). As the device temperature increases, negligible increase in η is observed. As a result of increases radiation intensity, increases the cell temperature, higher series resistance appeared resistive power losses and thus reduces its performance by decreases η like with the cells dyed by (ND2, ND3, ND5, ND6, ND8, ND9, ND11, ND14, ND15, ND18, ND19, ND20, ND22, ND23, ND24, ND26, ND27). These values of η can be compared to those obtained in previous work such as reference [28], where η values are from 0.03 to 1.17.

The increases in J_{SC} is attributed to the increased dye-photon interaction and enhanced number of carrier injections from the excited dye molecules to the conduction band of TiO_2 electrode. An exponential dependence of I-V on illumination is observed in the DSSC. This is maybe due to change in the transport recombination magnitude which manages the electron transport process occurring at the TiO_2 nanoparticle interfaces or at the electrode-electrolyte interface. However, the effect of resistive elements starts becoming dominant when the series resistance is getting larger, especially detrimental to the *FF*. The influence of each parameter on the overall conversion η is simulated.

Table 4.1. The parameters of the fabricated DSSCs.

Dye	λ_{Max}	P_{in} (W/m^2)	J_{SC} (mA/cm^2)	V_{OC} (V)	J_{MP} (mA/cm^2)	V_{MP} (V)	P_{Max} (mW/cm^2)	*FF*	**η** %
ND1	666	800	0.60	0.55	0.35	0.38	0.13	0.40	0.16
		1000	0.80	0.57	0.39	0.45	0.18	0.38	0.18
		1200	1.00	0.59	0.39	0.57	0.22	0.37	0.18
ND2	664	800	0.40	0.55	0.38	0.21	0.08	0.37	0.10
		1000	0.45	0.56	0.38	0.25	0.09	0.38	0.09
		1200	0.52	0.57	0.34	0.32	0.11	0.37	0.09
ND3	664	800	1.00	0.59	0.39	0.59	0.23	0.39	0.29
		1000	1.12	0.60	0.39	0.69	0.27	0.40	0.27
		1200	1.30	0.61	0.39	0.80	0.31	0.39	0.26
ND4	448	800	0.53	0.60	0.43	0.29	0.12	0.38	0.15
		1000	0.84	0.63	0.43	0.52	0.22	0.42	0.22
		1200	0.90	0.64	0.43	0.56	0.24	0.41	0.20
ND5	662	800	0.35	0.57	0.38	0.22	0.09	0.43	0.11
		1000	0.42	0.58	0.38	0.27	0.10	0.42	0.10
		1200	0.50	0.59	0.38	0.31	0.12	0.40	0.10
ND6	666	800	0.32	0.54	0.38	0.18	0.07	0.39	0.09
		1000	0.39	0.55	0.38	0.22	0.08	0.40	0.08
		1200	0.45	0.56	0.38	0.27	0.10	0.41	0.08
ND7	410 666	800	0.18	0.45	0.26	0.08	0.02	0.26	0.03
		1000	0.22	0.47	0.26	0.10	0.03	0.26	0.03
		1200	0.24	0.49	0.34	0.10	0.03	0.29	0.03
ND8	662	800	0.36	0.57	0.38	0.23	0.09	0.43	0.11
		1000	0.41	0.58	0.38	0.27	0.10	0.43	0.10
		1200	0.49	0.59	0.38	0.30	0.12	0.40	0.10
ND9	666	800	0.53	0.54	0.42	0.30	0.13	0.44	0.16
		1000	0.60	0.55	0.42	0.33	0.14	0.42	0.14
		1200	0.71	0.57	0.39	0.45	0.17	0.43	0.14

Dye	λ_{Max}	P_{in} (W/m^2)	J_{SC} (mA/cm^2)	V_{OC} (V)	J_{MP} (mA/cm^2)	V_{MP} (V)	P_{Max} (mW/cm^2)	*FF*	**η %**
ND10	410 666	800	0.27	0.48	0.30	0.15	0.04	0.34	0.05
		1000	0.30	0.49	0.34	0.15	0.05	0.35	0.05
		1200	0.36	0.50	0.34	0.19	0.07	0.36	0.06
ND11	666	800	0.65	0.62	0.39	0.42	0.16	0.40	0.20
		1000	0.78	0.63	0.39	0.49	0.19	0.39	0.19
		1200	0.78	0.64	0.39	0.49	0.19	0.38	0.16
ND12		800	0.39	0.54	0.38	0.25	0.09	0.45	0.11
		1000	0.45	0.55	0.38	0.30	0.12	0.47	0.12
		1200	0.55	0.56	0.42	0.32	0.14	0.45	0.12
ND13	416 664	800	0.20	0.52	0.34	0.09	0.03	0.29	0.04
		1000	0.23	0.53	0.34	0.10	0.04	0.29	0.04
		1200	0.26	0.54	0.34	0.13	0.05	0.32	0.04
ND14	668	800	0.30	0.61	0.38	0.19	0.07	0.40	0.09
		1000	0.35	0.63	0.42	0.21	0.09	0.39	0.09
		1200	0.42	0.64	0.38	0.28	0.11	0.39	0.09
ND15	666	800	0.50	0.54	0.38	0.27	0.10	0.39	0.13
		1000	0.58	0.55	0.38	0.31	0.12	0.38	0.12
		1200	0.60	0.56	0.34	0.37	0.13	0.38	0.11
ND16	432 664	800	0.79	0.58	0.35	0.37	0.13	0.28	0.16
		1000	0.85	0.59	0.35	0.48	0.17	0.33	0.17
		1200	0.90	0.60	0.39	0.47	0.18	0.33	0.15
ND17	432 666	800	1.30	0.66	0.48	0.78	0.38	0.44	0.48
		1000	1.60	0.67	0.44	1.11	0.49	0.45	0.49
		1200	2.00	0.69	0.44	1.33	0.58	0.42	0.48
ND18	414 666	800	2.00	0.67	0.48	1.30	0.62	0.46	0.78
		1000	2.40	0.68	0.44	1.64	0.73	0.44	0.73
		1200	2.60	0.69	0.44	1.78	0.79	0.44	0.66
ND19	412 664	800	1.00	0.60	0.39	0.68	0.27	0.44	0.34
		1000	1.20	0.62	0.39	0.82	0.32	0.43	0.32
		1200	1.30	0.63	0.39	0.88	0.34	0.42	0.28

Dye	λ_{Max}	P_{in} (W/m^2)	J_{SC} (mA/cm^2)	V_{OC} (V)	J_{MP} (mA/cm^2)	V_{MP} (V)	P_{Max} (mW/cm^2)	*FF*	**η %**
ND20	416 662	800	1.30	0.67	0.43	0.78	0.34	0.39	0.43
		1000	1.50	0.68	0.43	0.93	0.40	0.40	0.40
		1200	1.70	0.69	0.43	1.05	0.45	0.39	0.38
ND21	662	800	0.30	0.52	0.34	0.15	0.05	0.32	0.06
		1000	0.35	0.54	0.34	0.18	0.06	0.32	0.06
		1200	0.40	0.55	0.34	0.22	0.07	0.34	0.06
ND22	434 662	800	0.14	0.43	0.30	0.06	0.02	0.30	0.03
		1000	0.15	0.44	0.26	0.07	0.02	0.29	0.02
		1200	0.17	0.45	0.26	0.09	0.02	0.31	0.02
ND23	662	800	0.35	0.48	0.26	0.23	0.06	0.35	0.08
		1000	0.42	0.50	0.30	0.24	0.07	0.35	0.07
		1200	0.45	0.51	0.34	0.23	0.08	0.34	0.07
ND24	636	800	0.42	0.52	0.34	0.22	0.07	0.34	0.09
		1000	0.45	0.53	0.30	0.28	0.08	0.35	0.08
		1200	0.50	0.54	0.34	0.26	0.09	0.34	0.08
ND25	662	800	0.12	0.36	0.22	0.05	0.01	0.24	0.01
		1000	0.13	0.38	0.22	0.06	0.01	0.26	0.01
		1200	0.14	0.40	0.22	0.06	0.01	0.23	0.01
ND26	664	800	0.35	0.48	0.26	0.14	0.04	0.22	0.05
		1000	0.37	0.49	0.26	0.16	0.04	0.24	0.04
		1200	0.40	0.50	0.26	0.18	0.05	0.24	0.04
ND27	432 664	800	0.50	0.63	0.42	0.33	0.14	0.45	0.18
		1000	0.55	0.64	0.42	0.37	0.16	0.45	0.16
		1200	0.60	0.65	0.42	0.41	0.17	0.45	0.14

4.5 Electrochemical Impedance Spectroscopy

DSSCs sensitized with fig leaves (ND17), schinus terebinthifolius (ND18), and zizyphus leaves (ND20) have the best performance, so they were investigated using EIS. The following figures show Nyquist Plots, Bode plots, and equivalent circuits of these cells.

Figure 4.62 shows Nyquist Plot, Bode plot, and the equivalent circuit for the DSSC dyed by fig leaves. Figure 4.63 illustrates Nyquist Plot, Bode plot, and the equivalent circuit for the DSSC dyed by Schinus terebinthifolius. Nyquist Plot, Bode plot, and the equivalent circuit for the DSSC dyed by Zizyphus leaves can be seen in fig. 4.64.

Electrochemical Impedance Spectroscopy (EIS) was conducted to investigate the electronic and ionic processes. From the EIS output, it can be seen that increasing the value of the resistance which is in parallel combination with the capacitor, which corresponding to the TiO_2 surface increases the value of impedance. Increasing the value of the series resistance, which representing the diffusion process Nyquist Plot curve intersection with the x- axis is highly affected.

The Nyquist plots exhibit two semicircles including a large semicircle at low frequency and a small one at high frequency. The small semicircle is fitted to a charge transfer resistance and assigned to the charge transfer resistance at the redox electrolyte/Pt counter electrode or TiO_2 interfaces. The large semicircle fitted to a transport resistance is ascribed to the accumulation/ transport of the injected electrons within TiO_2 film and the charge transfer across either the TiO_2/redox electrolyte interface or the TiO_2/FTO interface. The characteristic frequency can be related to the inverse of the electron lifetime in TiO_2 film.

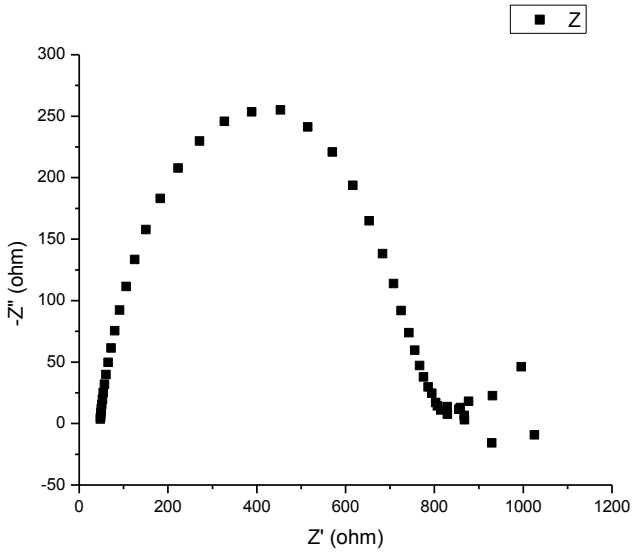

(a)

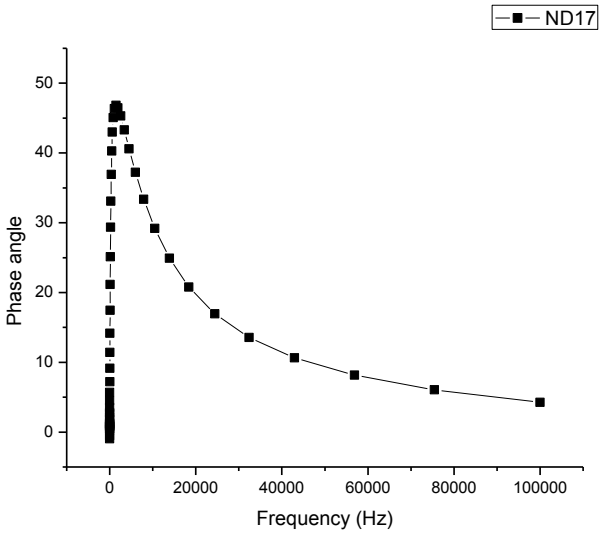

(b)

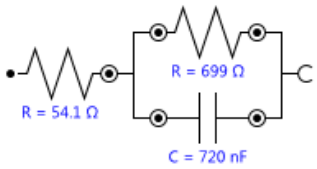

(c)

Fig. 4.62. Output of EIS for the DSSC sensitized with fig leaves (a) Nyquist Plots, (b) Bode plot, and (c) equivalent circuit.

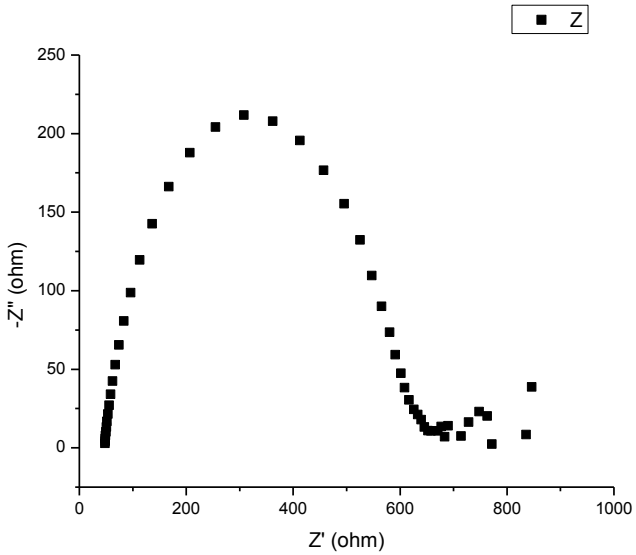

(a)

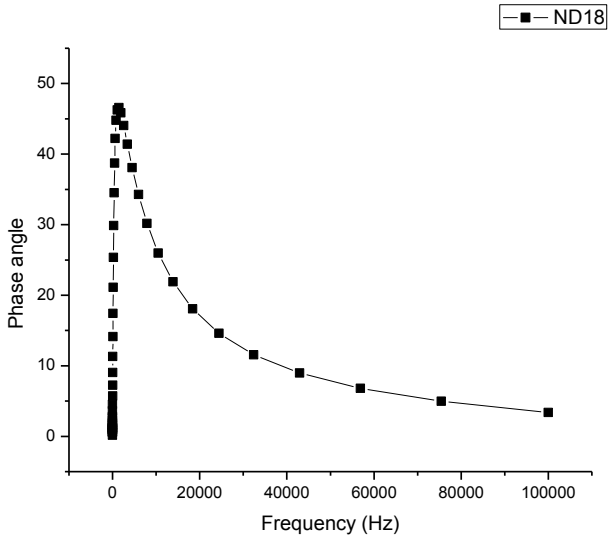

(b)

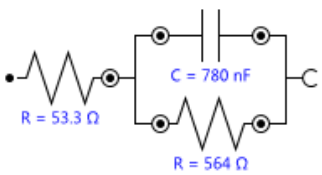

(c)

Fig. 4.63. Output of EIS for the DSSC sensitized with schinus terebinthifolius (a) Nyquist Plots, (b) Bode plot, and (c) equivalent circuit.

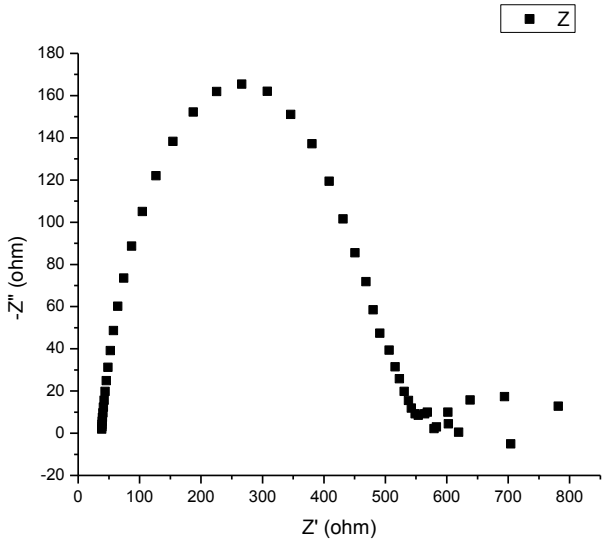

(a)

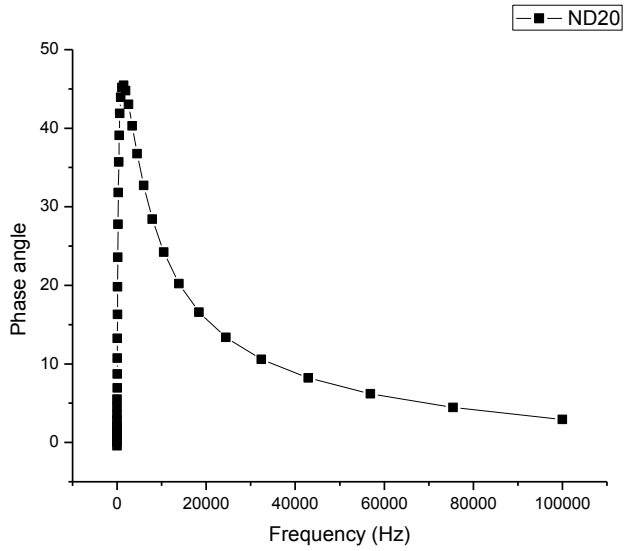

(b)

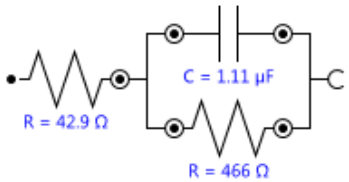

(c)

Fig. 4.64. Output of EIS for the DSSC sensitized with zizyphus leaves (a) Nyquist Plots, (b) Bode plot, and (c) equivalent circuit.

4.6 Mordants

As mentioned in the previous section, DSSCs sensitized with fig leaves (ND17), schinus terebinthifolius (ND18), and zizyphus leaves (ND20) have shown the highest efficiencies. The introduction of mordant will be restricted to DSSCs sensitized with these dyes. Pre-mordanting with $CuSO_4.5H_2O$ and $FeSO_4.7H_2O$ at 90° C for 1hr is first examined with DSSCs dyed with these dyes. The TiO_2 film is first immersed in the mordant solution at 90° C for 1hr and then in the alcoholic solution of the sensitizing dye at 60° C for 24hrs. The J-V characteristic curves of these cells are shown in figure 4.65. and figure 4.66 at illumination of 1000 W/m^2. As can be seen from the figures V_{OC} and J_{SC} were relatively low when compared to the result obtained in the previous section. In figure 4.65. the highest V_{OC} of 0.22 V was obtained for the DSSC sensitized with fig leaves, while the highest J_{SC} of 0.35 mA/cm^2 was obtained for the DSSC sensitized with zizyphus leaves where as in figure 4.66. the highest V_{OC} of 0.18 V and the highest J_{SC} of 0.31 mA/cm^2 was obtained for the DSSC sensitized with fig leaves.

Next, post-mordanting with $CuSO_4.5H_2O$ and $FeSO_4.7H_2O$ was investigated with the DSSCs dyed with these dyes. The TiO_2 film is first immersed in alcoholic solution of the sensitizing dye at 60° C for 24hrs and then in the mordant solution at 90° C for 1hr. The J-V characteristic curves of these cells are shown in figure 4.67. and figure 4.68 at illumination of 1000 W/m^2. The results obtained for V_{OC} and J_{SC} were still low. In figure 4.67. the highest V_{OC} of 0.44 V and the highest J_{SC} of 0.14 mA/cm^2 were obtained for DSSC sensitized with zizyphus leaves where as in figure 4.68. the highest V_{OC} of 0.16 V and the highest J_{SC} of 0.18 mA/cm^2 was obtained for DSSC sensitized with fig leaves.

Pre-mordanting and post-mordanting with $CuSO_4.5H_2O$ was investigatedwith DSSCs dyed with fig leaves. The TiO_2 film is immersed in alcoholic solution of the sensitizing dye at 60° C for 24hrs and in the mordant solution at 60° C for 24hr, first in alcoholic then in mordant for post-mordanting, and first in mordant then in alcoholic for pre-mordanting. The J-V characteristic curves of these cells are shown in figure 4.69 at

illumination of 1000 W/m^2. V_{OC} and J_{SC} were also low. The highest V_{OC} of 0.27 V, and the highest J_{SC} of 0.02 mA/cm^2 was obtained for post-mordanting.

Pre-mordanting and post-mordanting the DSSCs dyed with fig leaves with $CuSO_4.5H_2O$ mordant was examined for different immersion time. The TiO_2 film is first immersed in mordant solution at 60° C for (1, 5, 10, 15, 20, and 30) min and then in the alcoholic solution of the sensitizing dye at 60° C for 24hrs for pre-mordanting, and immersed in alcoholic solution of the sensitizing dye at 60° C for 24hrs and then in the mordant solution at 60° C for (1, 5, 10, 15, 20,and 30)min for post-mordanting. The J-V characteristic curves of these cells are shown in figure 4.70. and figure 4.71 at illumination of 1000 W/m^2. From figure 4.70. the highest V_{OC} of 0.27 V, and the highest J_{SC} of 0.11 mA/cm^2 were obtained for pre-mordanting with 15 min immersion time in mordant, and from figure 4.71. the highest V_{OC} of 0.17 V, and the highest J_{SC} of 0.13 mA/cm^2 was obtained for post-mordanting with 1min immersion time in mordant.

Meta-mordanting with $CuSO_4.5H_2O$ with DSSCs dyed with the three dyes was investigated. The TiO_2 film was immersed in a mixture of the dye extract and $CuSO_4.5H_2O$ at 60° C for 24hr. The J-V characteristic curves of these cells are shown in figure 4.72 at illumination of 1000 W/m^2. V_{OC} and J_{SC} as were low, the highest V_{OC} of 0.16 V was obtained for DSSC sensitized with schinus terebinthifolius, while the highest J_{SC} of 0.07 mA/cm^2 was obtained for the DSSC sensitized with zizyphus leaves.

For evaluating the amount of dye adsorbed on the TiO_2 film, the dye is desorbed in an aqueous NaOH (0.1M) solution [5]. The amount of dye is determined by using a UV-VIS spectrophotometer (Thermoline Genesys 6) in the spectral range from 400 nm to 750 nm. 1mL of the dye solution was added to 5mL of NaOH to be used as a base line to evaluate the amount of dye adsorbed on the DSSCs dyed with fig leaves and fabricated by pre-mordanting and post-mordanting $CuSO_4.5H_2O$. 1 mL of dye

extracted by mordant $CuSO_4.5H_2O$ was added to 5 mL of NaOH to be base line of the amount of dye adsorbed on the DSSCs dyed with fig leaves fabricated by meta-mordanting. Figure 4.73. shows the absorption spectra of 1 mL of mordant $CuSO_4.5H_2O$ added to 5 mL of NaOH, and dye adsorbed from the DSSCs dyed with fig leaves and fabricated by pre-mordanting and post-mordanting. The absorption spectra of dye adsorbed from the DSSCs fabricated by pre-mordanting and post-mordanting dyed with fig leaves are shown in figure 4.74 by using a solution of 1mL of mordant in 5 mL of NaOH as a base line. Figure 4.75 illustrates the absorption spectra of 1 mL of dye extracting with $CuSO_4.5H_2O$ added to 5 mL of NaOH, and meta-mordanting of DSSCs dyed with fig leaves. The results reveal that mordants can be used to increase the stability of the dye adsorbed on the TiO_2 but it reduced the cell response.

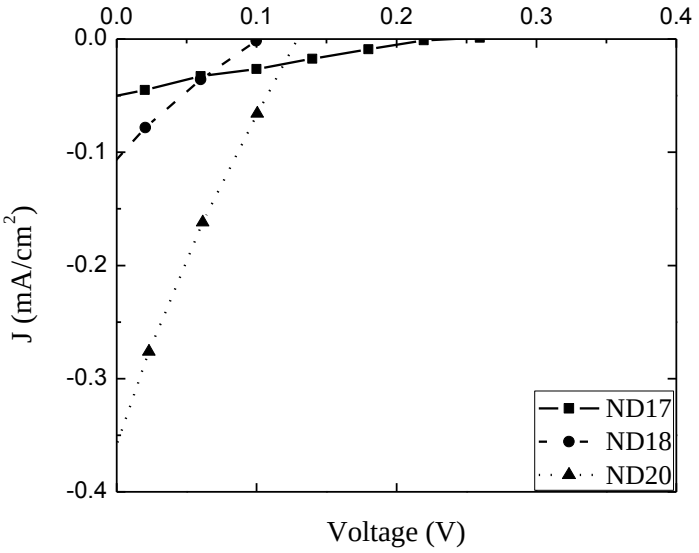

Fig.4.65. J-V curves of Pre-mordanting with $CuSO_4.5H_2O$ for DSSCs sensitized with Fig leaves (ND17), Schinus terebinthifolius (ND18), and Zizyphus leaves (ND20) at illumination of 1000 W/m^2.

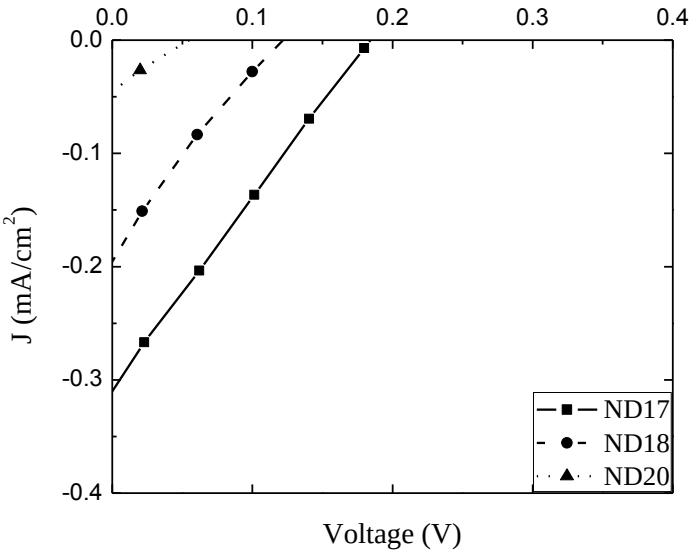

Fig.4.66. J-V curves of Pre-mordanting with $FeSO_4.7H_2O$ for DSSCs sensitized with Fig leaves (ND17), Schinus terebinthifolius (ND18), and Zizyphus leaves (ND20) at illumination of 1000 W/m^2.

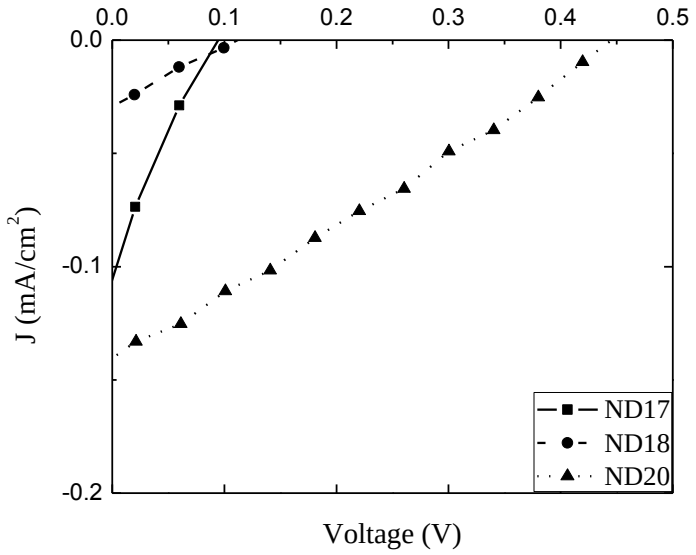

Fig.4.67. J-V curves of Post-mordanting with $CuSO_4.5H_2O$ for DSSCs sensitized with Fig leaves (ND17), Schinus terebinthifolius (ND18), and Zizyphus leaves (ND20) at illumination of 1000 W/m^2.

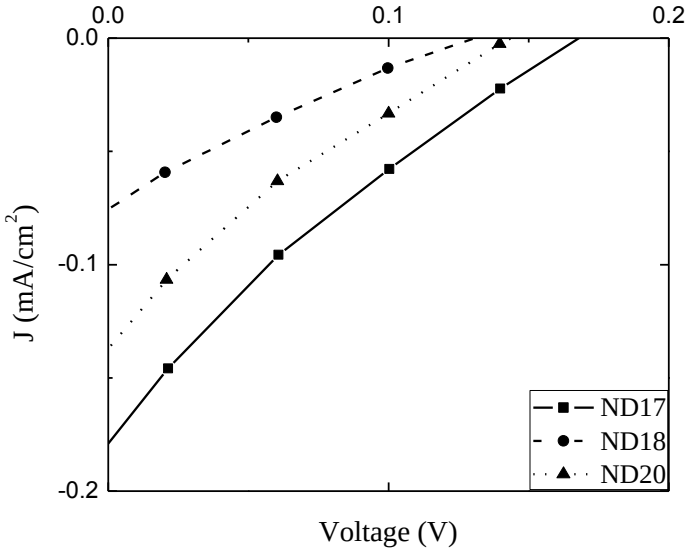

Fig.4.68. J-V curves of Post-mordanting with $FeSO_4.7H_2O$ for DSSCs sensitized with Fig leaves (ND17), Schinus terebinthifolius (ND18), and Zizyphus leaves (ND20) at illumination of 1000 W/m^2.

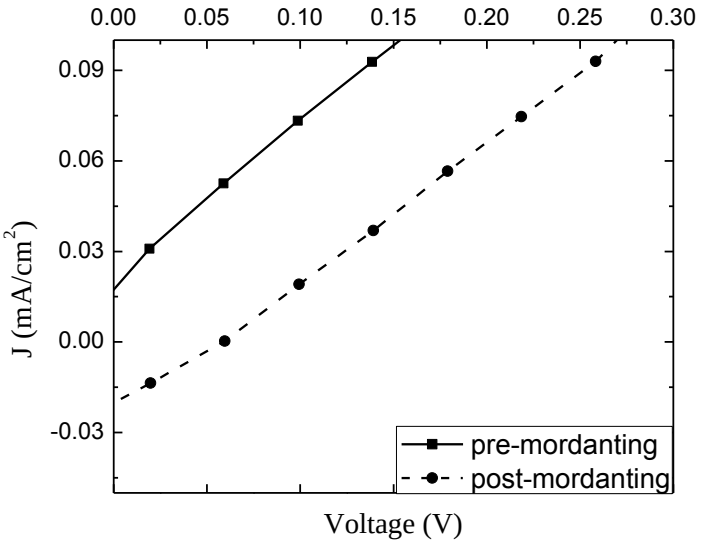

Fig.4.69. J-V curves of Pre- and Post- mordanting with $CuSO_4.5H_2O$ for DSSCs sensitized with Fig leaves (ND17) at 60° C overnight at illumination of 1000 W/m^2.

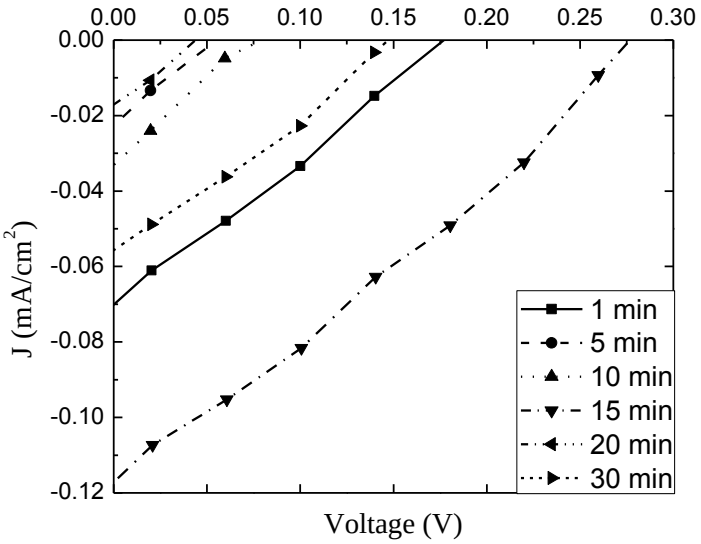

Fig.4.70. J-V curves of Pre-mordanting with $CuSO_4.5H_2O$ for DSSCs sensitized with Fig leaves (ND17) at 60° C for different immersion times at illumination of 1000 W/m^2.

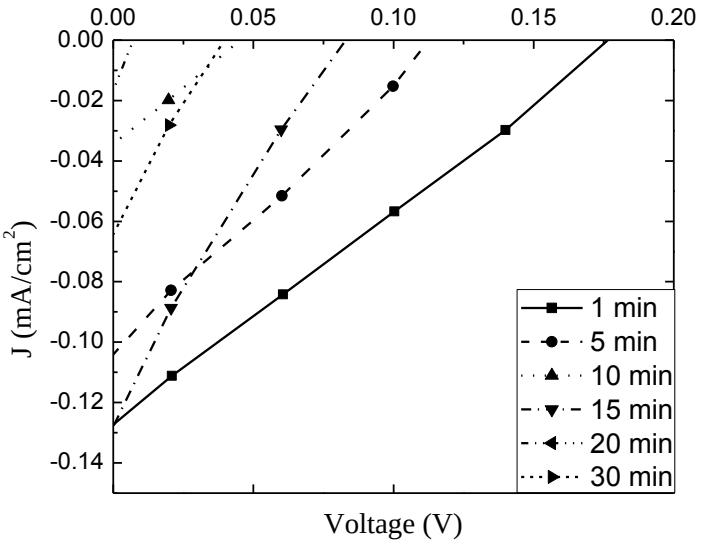

Fig.4.71. J-V curves of Post-mordanting with $CuSO_4.5H_2O$ for DSSCs sensitized with Fig leaves (ND17) at 60° C for different immersion times at illumination of 1000 W/m^2.

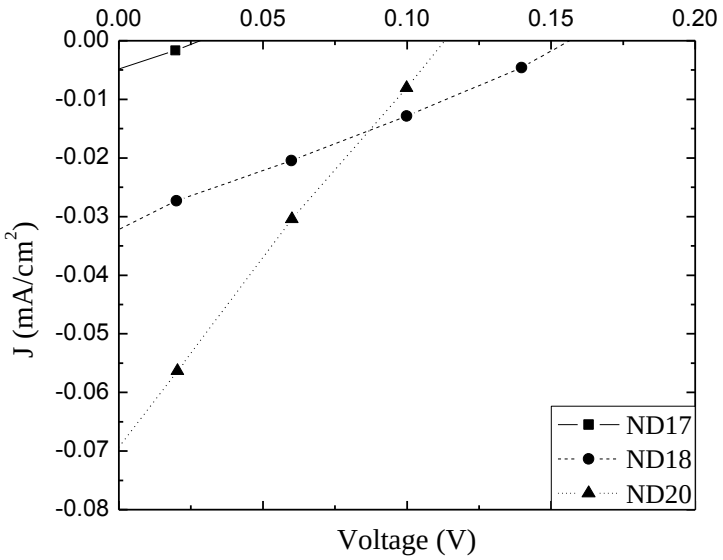

Fig.4.72. J-V curves of meta-mordanting with $CuSO_4.5H_2O$ for DSSCs sensitized with three different dyes at illumination of 1000 W/m^2.

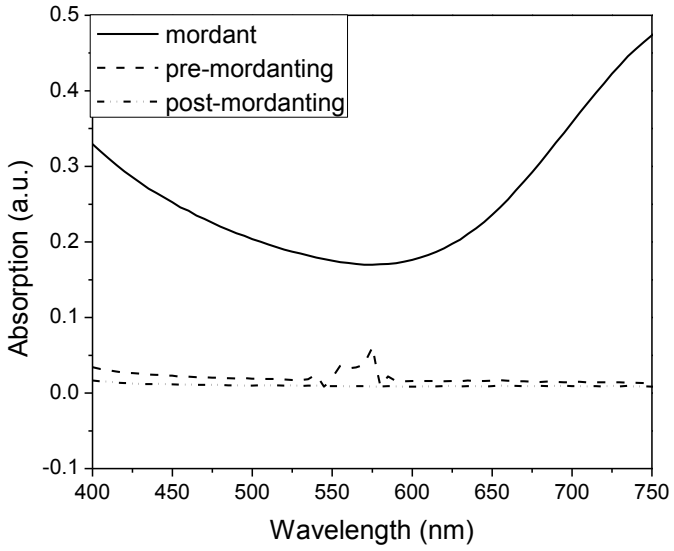

Fig.4.73. The absorption spectra of the dye obtained form the cells dyed with fig leaves (ND17) using NaOH for $CuSO_4.5H_2O$, pre-mordanting and post-mordanting.

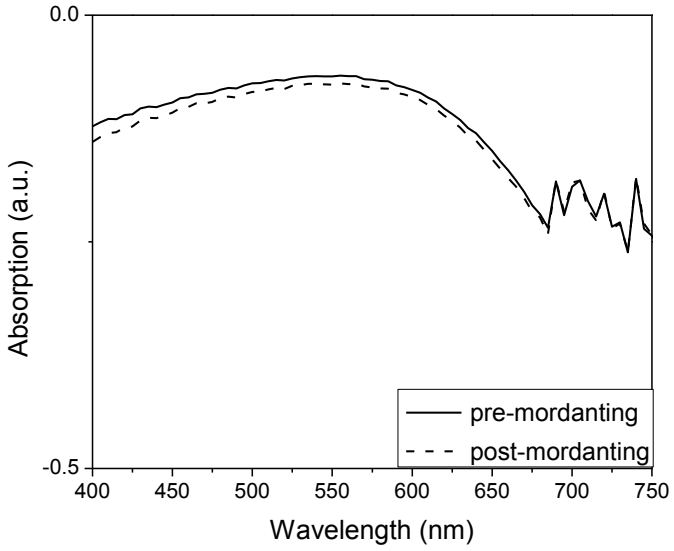

Fig.4.74. The absorption spectra of the dye obtained form the cells dyed with fig leaves (ND17) using NaOH for $CuSO_4.5H_2O$, pre-mordanting and post-mordanting by baseline 1mL $CuSO_4.5H_2O$ and 5 mL NaOH.

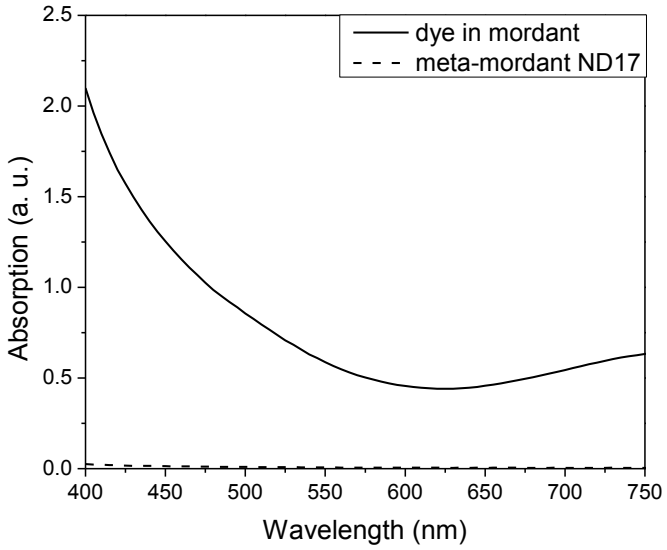

Fig.4.75. The absorption spectra of the dye obtained form the cells dyed with fig leaves (ND17) using NaOH for $CuSO_4.5H_2O$, meta-mordanting.

4.7 DSSCs Fabricated Using a Mixture of TiO_2 and $ZnAl_2O_4$

A mixture of TiO_2 and $ZnAl_2O_4$ is used as a semiconducting material. A ratio of (10, 20, 30, 40, and 50)% of $ZnAl_2O_4$ was added to the TiO_2 powder to form the paste. Fig leaves (ND17), schinus terebinthifolius (ND18), and zizyphus leaves (ND20) were used as dyes. The J-V characteristic curves of these cells are shown in Figs 96-98 at illumination of 1000 W/m^2. Figure 4.76. shows the J-V characteristic curves of DSSCs dyed with fig leaves when using the ratio (10, 20, 30, 40, and 50)%. The highest V_{OC} of 0.46 V and the highest J_{SC} of 0.38 mA/cm^2 were obtained for the DSSC fabricated using a mixture ratio of 10%. The J-V characteristic curves of DSSCs dyed with schinus terebinthifolius fabricated by ratio of weight by (10, 20, 30, 40, and 50)% is shown in Fig. 4.77. The highest V_{OC} of 0.54 V was obtained for the DSSC fabricated using a mixture ratio of 20% and the highest J_{SC} of 0.45 mA/cm^2 was obtained for the DSSC fabricated using a mixture ratio of 10%. In asimilar manner the J-V characteristic curves of the DSSCs dyed with zizyphus leaves fabricated and using the ratios (10, 20, 30, 40, and 50)% are illustrated in figure 4.78. From the figure, the highest V_{OC} of 0.65 V was obtained for the DSSC fabricated using a mixture ratio of 20% and the highest J_{SC} of 1.38 mA/cm^2 was obtained for the DSSC fabricated using the mixture ratio of 10%. DSSCs fabricated by a mixture ratio 10% has almost the highest V_{OC} and J_{SC}.

Then DSSCs are fabricated using mixture ratios of (1, 3, and 5)% by weight. DSSCs were dyed with same dyes mentioned above. The characteristic curves of these cells are shown in Figs 79-81 at illumination of 1000 W/m^2. From figure 4.79, which shows the J-V characteristic curves of the DSSCs dyed with fig leaves and fabricated using a mixture ratio of the (1, 3, and 5)%. The highest V_{OC} of 0.65 V was obtained for the DSSC with the mixture ratio 3% and the highest J_{SC} of 0.70 mA/cm^2 was obtained for the DSSC fabricated using a mixture ratio of 1%. The highest V_{OC} of 0.65 V was obtained for the DSSC dyed with schinus terebinthifolius fabricated using a mixture ratio of 5% and the highest J_{SC} of 0.55 mA/cm^2 was obtained for the DSSC fabricated using a mixture ratio of 1% as seen in Fig. 4.80. Figure 4.81. shows the J-V

characteristic curves of the DSSCs dyed with zizyphus leaves fabricated using a mixture ratio of (1, 3, and 5)%. The highest V_{OC} of 0.69 V was obtained for the DSSC fabricated using the 5% ratio and the highest J_{SC} of 0.90 mA/cm^2 was obtained for the DSSC fabricated using 1% ratio.

So far, the results does not show any enhancement in the cell parameters. DSSCs are now fabricated using the ratios (0, 1, 1.5, 2, 2.5, 3, 3.5, 4, 4.5, 5, 7, and 10)%. The DSSCs were dyed with Ruthenium (Ru) complexcis-dicyano-bis(2,2'-bipyridyl-4,4'-dicarboxylic acid) ruthenium(II), Ruthenizer 505, (Solaronix, Switzerland). The J-V characteristic curves can be shown in figure 4.82 at illumination of 1000 W/m^2. The highest V_{OC} of 0.64 V was obtained for DSSC fabricated using the ratio of 4.5% and the highest J_{SC} of 15.5 mA/cm^2 was obtained for the DSSC fabricated using the ratio of 2%. Figure 4.83 shows the P-V characteristic curves of these cells at illumination of 1000 W/m^2. It shows that the highest output power of 3.5 mW/cm^2 was obtained for the DSSC fabricated using the ratio of 2%. Table 4.2. presents all the parameters of these DSSCs fabricated using the mixture. The highest *FF* of 0.40 was obtained for the DSSC fabricated using the ratio of 1.5%, and the highest η of 2.88% was obtained for the DSSC fabricated using the ratio of 2%. The Figures 84-88 show respectively, J_{SC}, V_{OC}, P_{Max}, *FF*, and η versus the ratio of $ZnAl_2O_4$ in the mixture.

Table 4.2. Parameters of the DSSCs fabricated by a mixture of TiO_2 and $ZnAl_2O_4$

Ratio	J_{SC} **(mA/cm^2)**	V_{OC} **(V)**	P_{Max} **(mW/cm^2)**	V_{MP} **(V)**	J_{MP} **(mA/cm^2)**	*FF*	**η %**
0	6.02	0.60	1.21	0.30	4.06	0.34	1.01
1	4.43	0.61	1.05	0.35	3.03	0.39	0.88
1.5	5.43	0.60	1.31	0.35	3.78	0.40	1.09
2	15.58	0.61	3.45	0.25	13.91	0.37	2.88
2.5	9.20	0.55	1.75	0.25	7.06	0.34	1.46
3	10.96	0.61	1.93	0.25	7.78	0.29	1.61
3.5	12.38	0.60	2.83	0.25	11.41	0.38	2.36
4	5.52	0.60	0.92	0.35	2.65	0.28	0.77
4.5	7.20	0.64	1.77	0.40	4.48	0.38	1.48
5	6.26	0.59	1.37	0.35	3.95	0.37	1.14
7	4.69	0.64	0.82	0.35	2.36	0.27	0.68
10	5.90	0.60	0.97	0.35	2.80	0.27	0.81

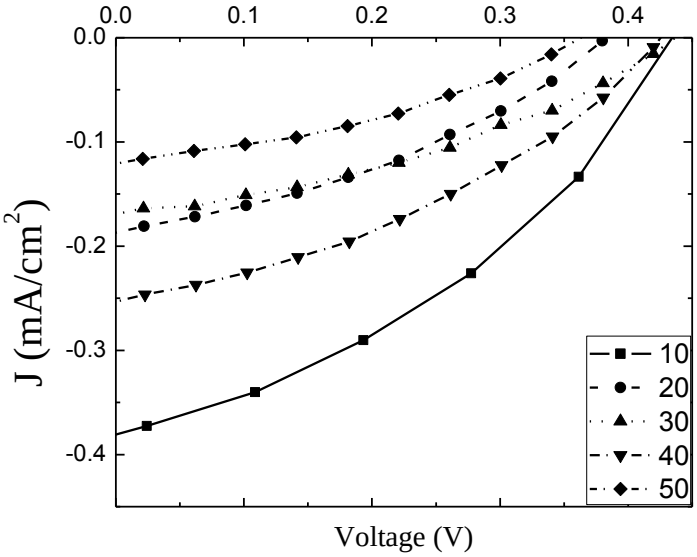

Fig. 4.76. J-V curves of the DSSC dyed with fig leaves using TiO_2 and $ZnAl_2O_4$ with mixture of ratios (10, 20, 30, 40, and 50) % at illumination of 1000 W/m^2.

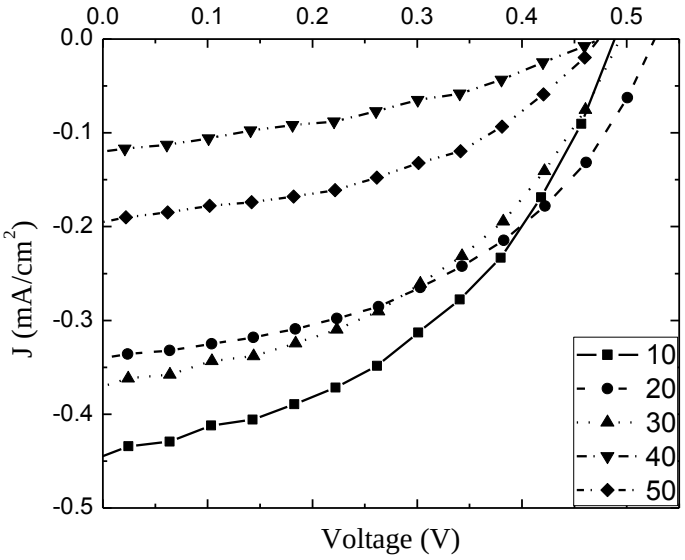

Fig. 4.77. J-V curves of the DSSC dyed with schinus terebinthifolius using TiO_2 and $ZnAl_2O_4$ with mixture of ratios (10, 20, 30, 40, and 50) % at illumination of 1000 W/m^2.

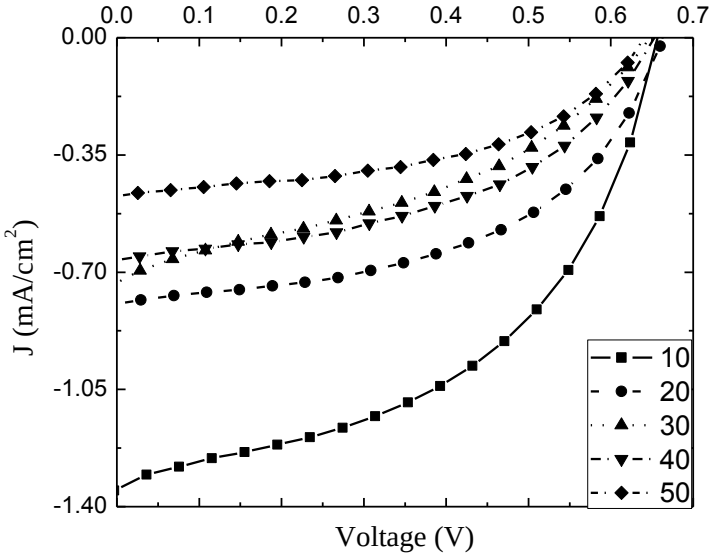

Fig. 4.78. J-V curves of the DSSC dyed with zizyphus leaves using TiO_2 and $ZnAl_2O_4$ with mixture of ratios (10, 20, 30, 40, and 50) % at illumination of 1000 W/m^2.

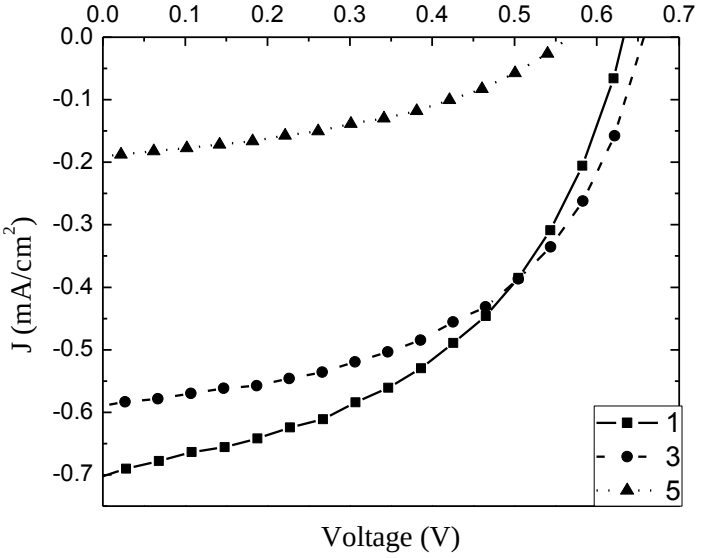

Fig. 4.79. J-V curves of the DSSC dyed with fig leaves using TiO_2 and $ZnAl_2O_4$ with mixture of ratios (1, 3, and 5) % at illumination of 1000 W/m^2.

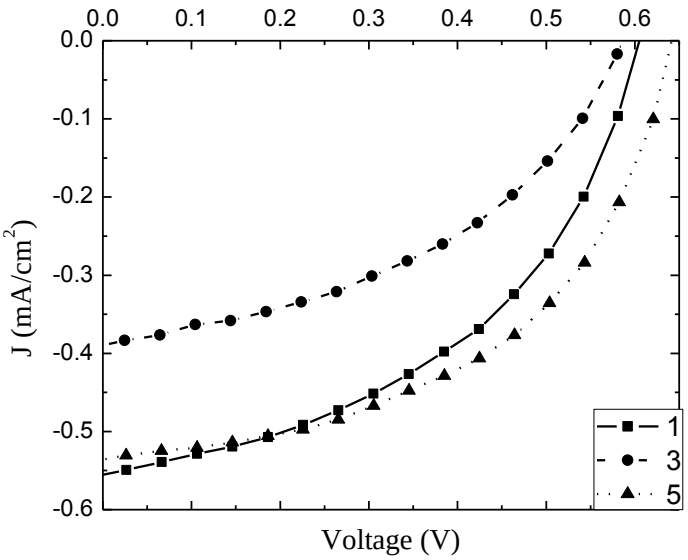

Fig. 4.80. J-V curves of the DSSC dyed with schinus terebinthifolius using TiO_2 and $ZnAl_2O_4$ with mixture of ratios (1 ,3 ,and 5) % at illumination of 1000 W/m^2.

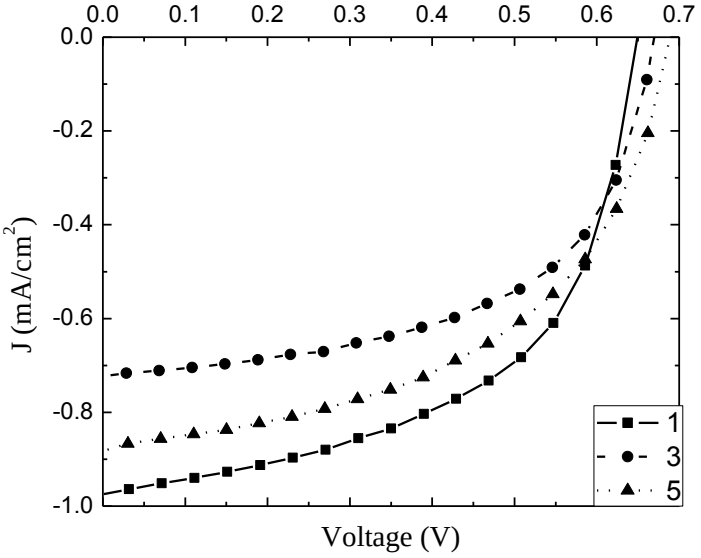

Fig. 4.81. J-V curves of the DSSC dyed with zizyphus leaves using TiO_2 and $ZnAl_2O_4$ with mixture of ratios (1, 3, and 5) % at illumination of 1000 W/m^2.

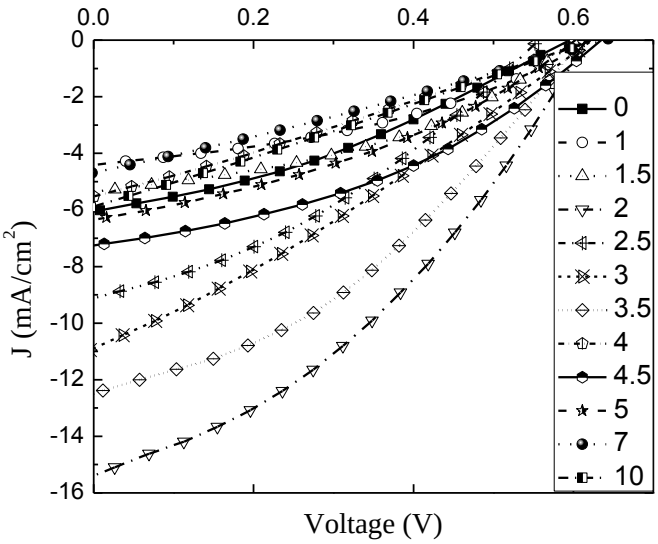

Fig. 4.82. J-V curves of the DSSC dyed with Ru using TiO_2 and $ZnAl_2O_4$ with mixture of ratios (0, 1, 1.5, 2, 2.5, 3, 3.5, 4, 4.5, 5, 7, and 10) % at illumination of 1000 W/m^2.

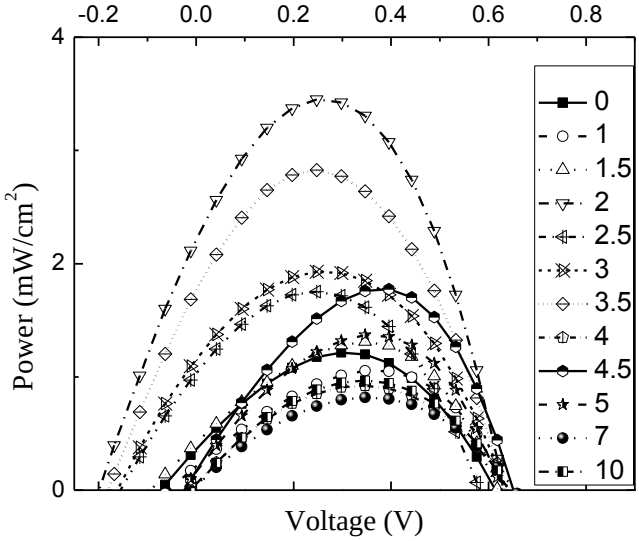

Fig. 4.83. P-V curves of the DSSC dyed with Ru using TiO_2 and $ZnAl_2O_4$ with mixture of ratios (0, 1, 1.5, 2, 2.5, 3, 3.5, 4, 4.5, 5, 7, and 10) % at illumination of 1000 W/m^2.

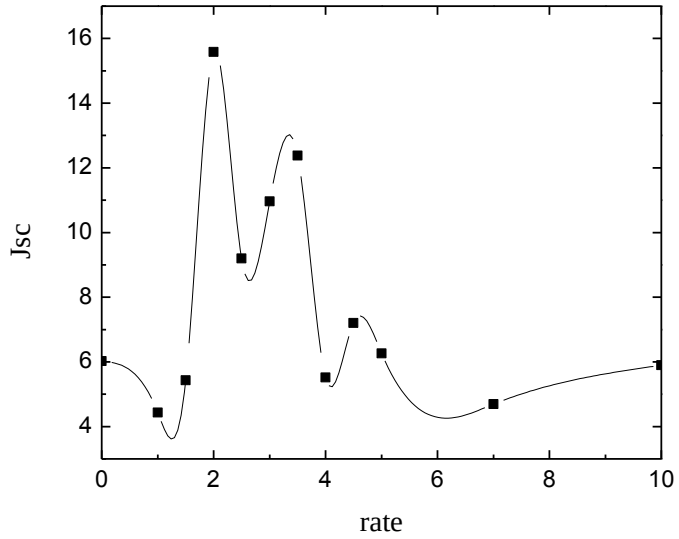

Fig.4.84. The short circuit current versus the ratio of $ZnAl_2O_4$ in the mixture of TiO_2 and $ZnAl_2O_4$ at illumination of 1000 W/m^2.

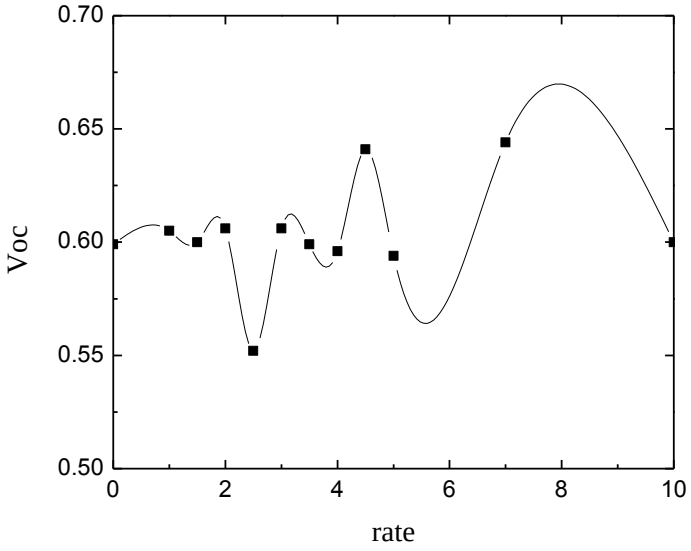

Fig.4.85. The open circuit voltage versus the ratio of $ZnAl_2O_4$ in the mixture of TiO_2 and $ZnAl_2O_4$ at illumination of 1000 W/m^2.

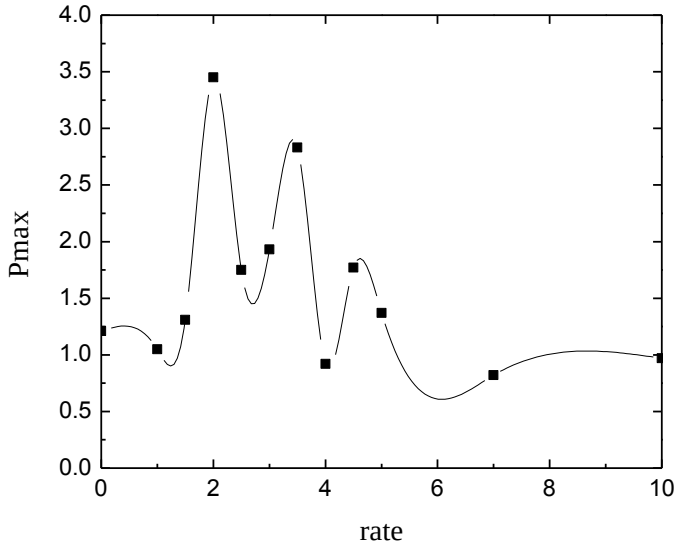

Fig.4.86. The maximum output power versus the ratio of $ZnAl_2O_4$ in the mixture of TiO_2 and $ZnAl_2O_4$ at illumination of 1000 W/m^2.

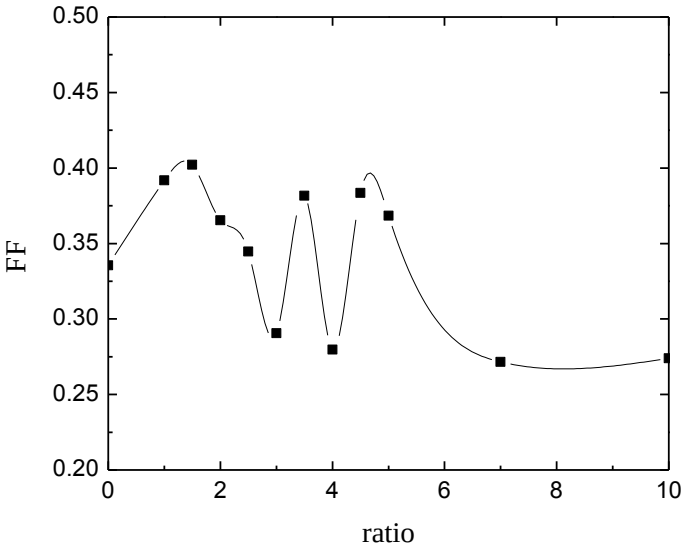

Fig.4.87. The fill factor versus the ratio of $ZnAl_2O_4$ in the mixture of TiO_2 and $ZnAl_2O_4$ at illumination of 1000 W/m^2.

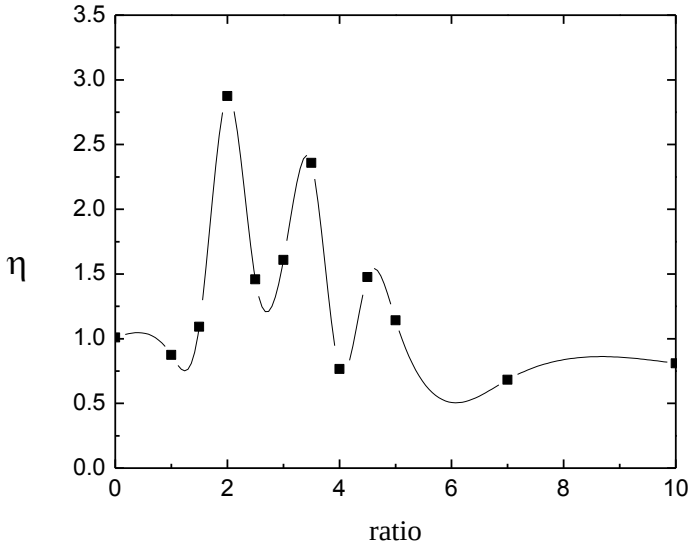

Fig.4.88. The efficiency versus the ratio of $ZnAl_2O_4$ in the mixture of TiO_2 and $ZnAl_2O_4$ at illumination of 1000 W/m^2.

Conclusion

In this work, twenty seven natural dyes were used on photosensitizers of DSSCs fabricated by TiO_2 as semiconductor layer. These dyes include plant's leaves, flowers, fruits, barks, and roots. Plant leaves showed higher efficiency than other parts of trees, due to the presence of chlorophyll which concentration effected in value of absorption. The plant roots have shown the lowest values of efficiency, due to it have not any color pigments. The increases in J_{SC} is attributed to the increased dye-photon interaction and enhanced number of carrier injections from the excited dye molecules to the conduction band of TiO_2 electrode. An exponential dependence of I-V on illumination is observed in the DSSC. This is maybe due to change in the transport recombination magnitude which manages the electron transport process occurring at the TiO_2 nanoparticle interfaces or at the electrode-electrolyte interface. However, the effect of resistive elements starts becoming dominant when the series resistance is getting larger, especially detrimental to the *FF*. The influence of each parameter on the overall conversion η is simulated.

Using mordants reduces the short circuit current density and open circuit voltage values, it can be attributed to make surface to decreases porosity of TiO_2, but increases the stability of dye in the cell.

$ZnAl_2O_4$ can not be used alone as semiconductor layer, but can be mix with another semiconductor to increases it stability on FTO. In this work, the mixture of $ZnAl_2O_4$ and TiO_2 was studied and the results show that some of ratio of mixture got efficiency higher than the efficiency of using TiO_2 alone as semiconductor layer by three-fold.

References

[1] J. Perlin, "From Space to Earth", Aatec Publications, Ann Arbor, Michigan (1999).

[2] C. Julian Chen, "Physics of Solar Energy", John Wiley & Sons, Inc (2011).

[3] B. O'Regan, and M.Grätzel, "low-cost, high-efficiency solar cell based on dye-sensitized colloidal TiO_2 films", Nature, Vol. 353, pp. 737-740 (1991).

[4] Y. Chiba, A. Islam, Y. Watanabe, R. Komiya, N. Koide, and L. Han, "Dye-sensitized solar cells with conversion efficiency of 11.1%", Jpn. J. Appl. Phys., Vol. 45, pp. 638-640, (2006).

[5] A. Tolvanen, "Characterization and manufacturing techniques of dye-senitized solar cells", Master's Thesis, Espoo, Swedish (2003).

[6] K. Wongcharee, V. Meeyoo, and S. Chavadej, "Dye-sensitized solar cell using natural dyes extracted from rosella and blue pea flowers", Sol. Energ, Mat. Sol. C, Vol. 91, pp. 566-571, (2007).

[7] G. Calogero, and G. Marco, "Red Sicilian orange and purple eggplant fruits as natural sensitizers for dye-sensitized solar cells", Sol. Energ. Mat. Sol. C, Vol. 92, pp. 1341–1346 (2008).

[8] P. Luo, H. Niu, G. Zheng, X. Bai, M. Zhang, and W. Wang, "From salmon pink to blue natural sensitizers for solar cells: Canna indica L., Salvia splendens, cowberry and Solanum nigrum L.", Spectrochim. Acta Part A, Vol. 74, pp. 936-942, (2009).

[9] C. Henry, "Limiting efficiencies of ideal single and multiple energy-gap terrestrial solar-cells", J Appl Phys, Vol. 51, pp. 4494–4500, (1980).

[10] P.M. Sirimanne, M.K.I. Senevirathna, E.V.A. Premalal, P.K.D.D.P. Pitigala, V. Sivakumar, and K. Tennakone, "Utilization of natural pigment extracted from pomegranate fruits as sensitizer in solid-state solar cells", J. Photochem. Photobiol. A, Vol. 177, pp. 324–327, (2006).

[11] S. Hao, J.Wu,Y. Huang, and J. Lin, "Natural dyes as photosensitizers for dye-sensitized solar cell", Solar Energy, Vol. 80, pp. 209–214, (2006).

[12] A.S. Polo, and N.Y. Murakami Iha, "Blue sensitizers for solar cells: natural dyes from Calafate and Jaboticaba", Sol. Energ. Mat. Sol. Cell, Vol. 90, pp.1936–1944, (2006).

[13] K. Tennakone, A.R. Kumarasinghe, G.R.R.A. Kumara, K.G.U. Wijayantha, and P.M. Sirimanne, "Nanoporous TiO2 photoanode sensitized with the flower pigment cyaniding", J. Photochem. Photobiol. A, Vol. 108, pp. 193–195, (1997).

[14] D. Zhang, S.M. Lanier, J.A. Downing, J.L. Avent, J. Lumc, and J.L. McHale, "Betalain pigments for dye-sensitized solar cells", J. Photochem. Photobiol. A, Vol. 195, pp. 72–80, (2008).

[15] M.S. Roy, P. Balraju, M. Kumar, and G.D. Sharma, “Dye-sensitized solar cell based on Rose Bengal dye and nanocrystalline TiO2”, Sol. Energ. Mat. Sol. C, Vol. 92, pp. 909–913, (2008).

[16] J.M.R.C. Fernando, and G.K.R. Senadeera, “Natural anthocyanins as photosensitizers for dye-sensitized solar devices”, Curr. Sci., Vol. 95, pp. 663–666, (2008).

[17] Q. Dai, and J. Rabani, “Photosensitization of nanocrystalline TiO2 films by anthocyanin dyes”, J. Photochem. Photobiol. A, Vol. 148, pp. 17–24, (2002).

[18] N.J. Cherepy, G.P. Smestad, M. Gratzel, and J.Z. Zhang, “Ultrafast electron injection: implications for a photoelectrochemical cell utilizing an anthocyanin dye-sensitized tio2 nanocrystalline electrode”, J. Phys. Chem. B, Vol. 101, pp. 9342–9351, (1997).

[19] S. Furukawa, H. Iino, T. Iwamoto, K. Kukita, and S. Yamauchi, “Characteristics of dyesensitized solar cells using natural dye”, Thin Solid Films. Vol. 518, pp. 526–529, (2009).

[20] N.M. Gomez-Ortiz, I.A. Vazquez-Maldonado, A.R. Perez-Espadas, G.J. Mena- Rejon, J.A. Azamar-Barrios, and G. Oskam, “Dye-sensitized solar cells with natural dyes extracted from achiote seeds”, Sol. Energ. Mat. Sol. C, Vol. 94, pp. 40–44, (2010).

[21] E. Yamazaki, M. Murayama, N. Nishikawa, N. Hashimoto, M. Shoyama, and O. Kurita, “Utilization of natural carotenoids as photosensitizers for dye-sensitized solar cells”, Sol. Energy, Vol. 81, pp. 512–516, (2007).

[22] R. Espinosa, I. Zumeta, J.L. Santana, F. Martı_nez-Luzardo, B. Gonza_lez, S. Docteur, and E. Vigil, “Nanocrystalline TiO2 photosensitized with natural polymers with enhanced efficiency from 400 to 600 nm”, Sol. Energ. Mat. Sol. C, Vol. 85, pp. 359–369, (2005).

[23] G.R.A. Kumara, S. Kaneko, M. Okuya, B. Onwona-Agyeman, A. Konno, and K. Tennakone, “Shiso leaf pigments for dye-sensitized solid-state solar cell”, Sol. Energ. Mat. Sol. C, Vol. 90, pp. 1220–1226, (2006).

[24] Z.-S. Wang, K. Hara, Y. Dan-oh, C. Kasada, A. Shinpo, S. Suga, H. Arakawa, and H. Sugihara, “Photophysical and (photo)electrochemical properties of a coumarin Dye”, J. Phys. Chem. B, Vol. 109, pp. 3907-3914 (2005).

[25] Z.-S. Wang, Y. Cui, K. Hara, Y. Dan-oh, C. Kasada, and A. Shinpo, “A high-lightharvesting- efficiency coumarin dye for stable dye-sensitized solar cells”, Adv. Mater., Vol. 19, pp. 1138–1141, (2007).

[26] Z.-S. Wang, Y. Cui, Y. Dan-oh, C. Kasada, A. Shinpo, and K. Hara, “Thiophenefunctionalized coumarin dye for efficient dye-sensitized solar cells: electron lifetime improved by coadsorption of deoxycholic acid”, J. Phys. Chem. C, Vol. 111, pp. 7224–7230, (2007).

[27] Z.-S. Wang, Y. Cui, Y. Dan-oh, C. Kasada, A. Shinpo, and K. Hara, “Molecular design of coumarin dyes for stable and efficient organic dye-sensitized solar cells”, J. Phys. Chem. C, Vol. 112, pp. 17011–17017, (2008).

[28] Z. Huizhi, W. Liqiong, G. Yurong, and M. Tingli, “Dye-sensitized solar cells using 20 natural dyes as sensitizers", Journal of Photochemistry and Photobiology A: Chemistry, Vol. 219, pp. 188–194, (2011).

[29] H. S. El-Ghamri, “DYE-SENSITIZED SOLAR CELLS USING ZnO AS A SEMICONDUCTING LAYER”, Master’s Thesis, IU-Gaza, Gaza (2012).

[30] K. S. ElRefi, “Dye-sensitized solar cell using TiO2 as a semiconducting layer”, Master’s Thesis, IU-Gaza, Gaza (2013).

[31] Y. Zhao, J.S. Tan, L. Wang, L. Jiang, and D. Zhul, “TiO_2 micro/nano-composite structured electrodes for quasi-solid-state dye-sensitized solar cells”, Nanotechnology, Vol. 17, pp. 2090 (2006).

[32] J.A. Anta, F. Casanueva, and G. Oskam, “A Numerical Model for Charge Transport and Recombination in Dye-Sensitized Solar Cells” J. Phys. Chem. B, Vol. 110, pp. 5372-5378 (2006).

[33] M. Kaneko, and I. Okura, “Photocatalysis Science and Technology”, Springer, Berlin (1981).

[34] P. Persson and S. Lunell, "Binding of bi-isonicotinic acid to anatase TiO_2 (101)." Sol. Energy Mat. Sol. C, Vol. 63, pp. 139-148 (2000).

[35] M.K. Nazeeruddin, A. Kay , I. Rodicio, R. Humphry-Baker, E. Mueller , P. Liska, N. Vlachopoulos, and M. Grätzel, “Conversion of light to electricity by cis-X2bis(2,2'-bipyridyl-4,4'-dicarboxylate)ruthenium(II) charge-transfer sensitizers (X = Cl-, Br-, I-, CN-, and SCN-) on nanocrystalline titanium dioxide electrodes”, J. Am. Chem. Soc., Vol. 115, pp. 6382-6390 (1993).

[36] S M Sze, and K. Ng. Kwok, “Physics of Semiconductor Devices”, John Wiley & sons, new jersey (2007).

[37] P. Wang, B. Wenger, R. Humphry-Baker, Jacques-E. Moser, J. Teuscher, W. Kantlehner, J. Mezger, E. V. Stoyanov, S. M. Zakeeruddin, and M. Grätzel, “Charge separation and efficient light energy conversion in sensitized mesoscopic solar cells based on binary ionic liquids”, J. Am. Chem. Soc., Vol. 127, pp. 6850–6856 (2005).

[38] N. Papageorgiou, W. F. Maier, and M. Grätzel, “An iodine/triiodide reduction electrocatalyst for aqueous and organic media.”, J. Electrochem Soc., Vol. 144, No. 3, pp. 876-884, (1997).

[39] M. Law, L.E. Greene, J.C. Johnson, R. Saykally, and P.D. Yang, “Nanowire dye-sensitized solar cells”, Nature Materials, Vol. 4, No. 6, pp. 455-459. (2005).

[40] L. Han, N. Koide, Y. Chiba, and T. Mitate, “Modeling of an equivalent circuit for dye-sensitized solar cells”, Appl. Phys. Lett., Vol. 84, No. 13, pp. 2433-2435. (2004).

[41] L. Han, N. Koide, Y. Chiba, T. Mitate, and A. Islam, "Modeling of equivalent circuit for dye sensitized solar cells: improvement of efficiency of dye-sensitized solar cell by reducing internal resistance". Comptes. Rendus. Chime., Vol. 9, pp. 645-651. (2006).

[42] K.-i. Ishibashi, Y. Kimura, and M. Niwana, "An extensively valid and stable method for derivation of all parameters of a solar cell from a single current-voltage characteristics", J. Appl. Phys., Vol. 103, pp. 094507, (2008).

[43] R. Kern, R. Sastrawan, J. Ferber, R. Stagnl, and J. Luther, "Modeling and interpretation of electrical impedance spectra of dye solar cell under open circuit conditions", Electrochimica Acta, Vol. 47, pp. 4213-4225.(2002).

[44] H. J. Snaith, M. Schmidt-Mende, and M. Gratzel, "Light intensity, temperature, and thickness dependence of the open-circuit voltage in solid-state dye-sensitized solar cells", Phys, Rev. B, Vol. 74, No. 045306, pp. 1-6. (2006).

[45] A. Usami, S. Seki, Y. Mita, H. Kobyashi, H. Miyashiro, and N. Terada, "Temperature dependence of open circuit voltage in dyesensitized solar cells", Sol. Energy Mat. Sol. C, Vol. 93, pp. 840-842. (2009).

[46] M. Ni, M.K.H. Leung, and D.Y.C. Leung, "Theoretical modeling f the electrode thickness effect on maximum power point of dyesensitized solar cell". Can. J. Chem. Eng., Vol. 86, pp. 35-42. (2008).

[47] B. Shin, J. Won, T. Son, Y.S. Kang, and C.K. Kim, "Barrier effect of dendrons on TiO2 particles in dye sensitized solar cells". Chem. Commun., Vol. 47, pp. 1734-1736. (2011).

[48] U. Bach, "Solid-state dye-sensitized mesoprrous TiO2 solar cells", PhD Thesis, ÉCOLE POLYTECHNIQUE FÉDÉRALE DE LAUSANNE, Lausanne, Switzerland, (2000).

[49] J. Nelson, "The Physics of Solar Cells", Imperial College Press, (2003).

[50] American Chemical Society, "Ultrathin, Dye-sensitized Solar Cells Called Most Efficient To Date", ScienceDaily, (2006).

[51] F. Kremer, A. Schonhals, and W. Luck, "Broadband Dielectric Spectroscopy", Springe, Verlag, (2003).

[52] E. Phipps, "Cochineal Red: The Art History of a Color", Yale University Press, New Haven and London (2010).

[53] Q. Wang, Jacques-E. Moser, and M. Grätzel, "Electrochemical impedance spectroscopic analysis of dye-sensitized solar cells", J. Phys. Chem. B, Vol. 109, No. 31, pp. 14945–14953 (2005).

[54] H.St.C. O'Neill, and W.A. Dollase, "Crystal structures and cation distribution in simple spinels from powder XRD structural refinements: MgCr2O4, ZnCr2O4, Fe3O4, and the temperature dependence of the cation distribution in ZnAl2O4", Physics and Chemistry of Minerals, Vol. 20, No. 8, pp. 541-555, (1994).

[55] H. Dixit, N. Tandon, S. Cottenier, R. Saniz, D. Lamoen, B. Partoens, V. Van Speybroeck, and M. Waroquier, "Electronic structure and band gap of zinc spinel oxides beyond LDA: $ZnAl_2O_4$, $ZnGa_2O_4$ and $ZnIn_2O_4$", New J. Phys., Vol. 13, No. 6**,** pp. 063002 ,(2011).